

2017

Performance of a Novel Sustainable Binder Under Extreme Dynamic Loading Conditions

Paul David Schmidt
University of Rhode Island, schmidt.paul.david@gmail.com

Follow this and additional works at: <https://digitalcommons.uri.edu/theses>

Terms of Use

All rights reserved under copyright.

Recommended Citation

Schmidt, Paul David, "Performance of a Novel Sustainable Binder Under Extreme Dynamic Loading Conditions" (2017). *Open Access Master's Theses*. Paper 1049.
<https://digitalcommons.uri.edu/theses/1049>

This Thesis is brought to you by the University of Rhode Island. It has been accepted for inclusion in Open Access Master's Theses by an authorized administrator of DigitalCommons@URI. For more information, please contact digitalcommons-group@uri.edu. For permission to reuse copyrighted content, contact the author directly.

PERFORMANCE OF A NOVEL SUSTAINABLE BINDER
UNDER EXTREME DYNAMIC LOADING CONDITIONS

BY

PAUL DAVID SCHMIDT

A THESIS SUBMITTED IN PARTIAL FULFILLMENT OF THE
REQUIREMENTS FOR THE DEGREE OF
MASTER OF SCIENCE
IN
CIVIL AND ENVIRONMENTAL ENGINEERING

UNIVERSITY OF RHODE ISLAND

2017

MASTER OF SCIENCE
OF
PAUL DAVID SCHMIDT

APPROVED:

Thesis Committee:

Major Professor Sumanta Das

George Tsiatas

Arun Shukla

Nasser H. Zawia
DEAN OF THE GRADUATE SCHOOL

UNIVERSITY OF RHODE ISLAND
2017

ABSTRACT

Iron Carbonate is a novel carbon-negative sustainable binder that is made from metallic iron powder waste and utilizes the chemistry of iron carbonation. To produce the binder, usually landfilled iron powder and other constituents (fly ash, limestone powder, metakaolin, sodium carbonate, sodium bicarbonate, powdered organic reducing agent, and water) are mixed together and exposed to a pressurized CO₂ regime that leads to slow external diffusion. The carbonation of iron particles results in the formation of complex iron carbonates that have binding capabilities and mechanical properties similar or better compared to ordinary Portland cement (OPC)-based binders. The metallic particulate phase incorporated in the novel binders' microstructure increases the toughness of Iron Carbonate because of the energy dissipation by plastic deformation of the unreacted and elongated iron particles which are strong and ductile. In addition, the matrix contains other additives including harder fly ash particles, softer limestone particles, and ductile clayey phases which significantly influence the overall fracture performance of the novel sustainable binder.

Understanding the behavior of Iron Carbonate at high strain rates is important for a wide range of both military and civilian applications. The material behavior under highly dynamic conditions is significantly different from the material response under quasi-static conditions. The split Hopkinson (Kolsky) pressure bar (SHPB) system is used to test dynamic compressive mechanical response and failure behavior of Iron Carbonate under high strain rates to establish exceptional dynamic load

mitigation characteristics for the carbon-negative sustainable binder under extreme combined environments.

Dynamic tests are conducted on cylindrical Iron Carbonate specimens using a conventional SHPB set-up. The experimental arrangement includes a gas gun and three steel bars (a striker bar, an incident bar, and a transmitted bar), aligned along a single axis. The Iron Carbonate specimen is placed between the incident and transmitted bar and the striker projectile is fired toward the face of the incident bar. Due to the impact of the striker bar an incident pulse, a reflected pulse and a transmitted pulse are generated that build up the stress level in the specimen and compress it. Objective of the carried out dynamic compression tests on Iron Carbonate specimen is the determination of the stress equilibrium, true stress-strain plots and strain-rate.

Analysis of the obtained pulses revealed that the transmitted pulses of the tested Iron Carbonate specimens were of much smaller magnitude than the incident and reflected pulses. As a result, achievement of stress equilibrium and homogeneous deformation of the Iron Carbonate samples was prevented. The small amplitude of the transmitted pulses is due to the possibly low mechanical impedance of Iron Carbonate. Testing specimens made of material with low mechanical impedance allows the incident bar-specimen interface to nearly move freely under stress wave loading, so that most of the incident pulse is reflected backward into the incident bar. Only a small portion of the loading pulse is transmitted through the specimen into the transmission bar.

Therefore, the conventionally used experimental standard set-up of the SHPB system using steel bars has to be modified in order to determine accurate dynamic stress-strain responses for Iron Carbonate. To increase the magnitude of the transmitted pulses a softer material, such as aluminum, should be used as transmitted bar material instead of common steel. Furthermore, a hollow transmitted bar instead of a solid bar should be used. The lower Young's modulus of an aluminum alloy and the smaller cross-section of the hollow bar increase the amplitude of the transmitted strain signals by at least an order of magnitude as compared to a conventional steel bar.

ACKNOWLEDGMENTS

The author sincerely acknowledges the support from Dr. Arun Shukla and the Dynamic Photomechanics Laboratory of the University of Rhode Island towards the conduct of this study and for the use their facilities. Especially the author would like to thank Koray Senol, Prathmesh Parrikar and Shyamal Kishore for dedicating their time to help setting up the split Hopkinson pressure bar (SHPB) experiment in their laboratory. Furthermore, the author thanks the URI technical staff assistants David Ferreira and Kevin Broccolo. They were extremely helpful in solving issues concerning the cutting of samples, building up the SHPB, and manufacturing missing parts for the experiment.

The author acknowledges his advisor and major professor Dr. Sumanta Das and – once again – Dr. Arun Shukla, as well as Dr. George Tsiatas and Dr. Mayrai Gindy for agreeing to serve as members on the authors Master’s Program Committee. Also, the author would like to thank Dr. David Taggart for agreeing to serve as defense committee chair.

Samples of the novel binder material were manufactured and provided by Dr. David Stone and his company Iron Shell LLC, which is sincerely acknowledged.

TABLE OF CONTENTS

ABSTRACT	ii
ACKNOWLEDGMENTS.....	v
1 Introduction	12
2 Approaches to improve sustainability in cement manufacture	14
2.1 Ordinary Portland Cement	14
2.1.1 Importance of OPC	14
2.1.2 History and discovery of Portland Cement	15
2.1.3 Manufacture of OPC	16
2.1.4 Carbon Footprint and environmental issues of OPC	21
2.1.5 Durability of OPC	25
2.1.6 OPC market and future development.....	27
2.2 General approaches to improve sustainability of cement manufacture ...	29
2.2.1 Definition of sustainable development	29
2.2.2 CO ₂ reduction plan of the IEA for the cement industry	29
2.2.2.1 <i>Energy efficiency</i>	30
2.2.2.2 <i>Utilization of industrial process wastes</i>	32
2.2.2.3 <i>Carbon Capture</i>	35
2.2.3 Other approaches to reduce the carbon footprint of the cement industry	37

2.2.3.1	<i>Nanoengineering</i>	37
2.2.3.2	<i>Chemical Admixtures</i>	40
2.2.3.3	<i>Recycling concrete</i>	40
2.3	Modification of cement for improved sustainability	41
2.3.1	Blended OPC-based cements (Supplementary Cementitious Materials).....	41
2.3.1.1	<i>Fly ash and pulverized fuel ash (PFA)</i>	42
2.3.1.2	<i>Ground granulated blast furnace slag (GGBS)</i>	43
2.3.1.3	<i>Ground limestone</i>	44
2.3.1.4	<i>Silica fume</i>	45
2.3.1.5	<i>Calcined clay (Metakaolin)</i>	46
2.3.1.6	<i>Rice husk ash</i>	47
2.3.1.7	<i>Other types of supplementary cementitious materials</i>	47
2.3.2	Alternative cements	48
2.3.2.1	<i>Calcium aluminate cement (CAC)</i>	48
2.3.2.2	<i>Calcium sulfoaluminate cement (CSA)</i>	50
2.3.2.3	<i>Alkali-activated cement (AAC)</i>	56
2.3.2.4	<i>Supersulfated cement</i>	64
2.3.2.5	<i>Magnesia cement</i>	66
2.3.2.6	<i>Sequestrated carbon cement</i>	69
2.3.2.7	<i>Carbonate binders</i>	70
2.3.2.8	<i>Other types of cementitious systems</i>	74

2.4	Specifying alternative binders.....	76
2.5	Preliminary Summary and Conclusion.....	77
3	Iron Carbonate	83
3.1	Introduction.....	83
3.2	Composition and carbonation reaction.....	84
3.3	Microstructure.....	86
3.4	Material properties	87
3.5	Preliminary summary.....	91
4	Dynamic concrete tests using split Hopkinson bar systems	92
4.1	Importance of understanding dynamic strain-rate effects on concrete	92
4.2	History of split Hopkinson pressure bar system	94
4.3	Basic principle for split Hopkinson (Kolsky) bar.....	95
4.3.1	Strain-rate definition.....	99
4.3.2	Pulse shaping technique.....	100
4.3.3	Dynamic compression tests	103
4.3.3.1	<i>Inertia effects and slenderness ratio</i>	<i>104</i>
4.3.3.2	<i>Friction effect.....</i>	<i>105</i>
4.3.3.3	<i>Compressive strength and dynamic increase factor (DIF).....</i>	<i>106</i>
4.3.3.4	<i>Lateral confinement.....</i>	<i>107</i>
4.3.3.5	<i>Elastic modulus.....</i>	<i>108</i>

4.3.4	Dynamic tension tests	108
4.3.5	Split Hopkinson (Kolsky) bar experiments on brittle materials	110
4.3.5.1	<i>Stress-strain behavior and toughness</i>	113
4.3.6	Failure mode	113
4.3.7	Calibration of SHPB systems	114
4.3.8	Analysis of SHPB test	116
4.4	Preliminary Summary	118
5	Testing of Iron Carbonate with SHPB system	120
5.1	Iron Carbonate sample preparation	120
5.2	Experimental set-up	124
5.2.1	Mechanical system.....	125
5.2.2	Measurement system.....	129
5.2.2.1	<i>Settings of the digital oscilloscope</i>	130
5.2.2.2	<i>Settings of the amplifier and half bridge</i>	130
5.2.3	Video recording system	132
5.2.4	Challenges.....	132
5.3	Experimental procedure.....	138
5.4	Data analysis.....	140
5.4.1	Digital Image Correlation	144

6 Results.....	145
6.1 Verification of results.....	145
6.1.1 Single-bar experiment.....	145
6.1.2 Bar-to-bar experiment.....	146
6.1.3 Testing of aluminum specimen.....	149
6.2 Expected results.....	155
6.3 Results and Discussion.....	160
6.4 Implications for future research.....	178
7 Conclusive Summary	181
8 Bibliography.....	184

LIST OF FIGURES

Figure	
1. Cement production process [9]	20
2. Global monthly mean CO ₂ since 2012 [13]	22
3. World cement production in 2014, by region and main countries [%] [23]	28
4. Computed C-S-H fracture toughness with respect to Ca/Si molar ratio as a function of number of atomic constraints [28].....	39
5. Schematic of conversion process and approximate temperature ranges for the formation of metastable and stable hydration products [18].....	49
6. Phase development of a CSA cement (w/c = 0.8) as a function of hydration time (calculated by thermodynamic modeling) [34].....	53
7. Schematic alkali-activation reaction process [35].....	57
8. Phase composition of supersulfated slag as a function of slag dissolved [39].....	65
9. Particle size distribution of metallic iron powder, OPC, fly ash, metakaolin, and limestone powder [47].....	85
10. Microstructure of iron-based binder:	86
11. Compressive strengths of the iron carbonate mixtures (exposure condition: 3 days in CO ₂ and 2 days in air) [49].....	88
12. Comparison between OPC and iron carbonate binder (control and fiber reinf.): (a) tensile strength, (b) ultimate strain; (c) tensile modulus [47].....	89
13. Comparison of flexural strength of 6-day carbonated iron carbonate sample and OPC paste after 28 days for different fiber dosage (the error bars represent one standard deviation of flexural strength obtained from four replicate specimens) [48]	90

14. Split Hopkinson pressure bar test system [53].....	95
15. SHPB system; x-t diagram of stress wave propagation in SHPB and typical strain gage signals [61].....	96
16. Typical pulse profiles [61]	97
17. SHPB system (0.5 in. diameter) at the Dynamic Photomechanics Laboratory	99
18. Clay as pulse shaper on an 0.5 in. incident bar at the Dynamic Photomechanics Laboratory	101
19. Loading pulses produced by pulse shapers of different materials [64].....	102
20. Stress-strain curve of cement mortar with and without pulse shaping [53].....	102
21. Split Hopkinson tension bar: first arrangement [61].....	109
22. Split Hopkinson tension bar: second arrangement [61]	110
23. Split Hopkinson tension bar: third arrangement [61].....	110
24. Brittle specimen configurations [52].....	112
25. Schematic failure patterns of concrete at different strain rates [53]	114
26. Stress wave in the bars in good alignment [52]	115
27. Stress wave in the bars in misalignment [52].....	115
28. Data analysis for an SHPB experiment; (a) measured strain gage signals, (b) computed stress and strain rate histories, (c) computed strain history, and (d) stress-strain relationship [51].....	116
29. Samples provided by Iron Shells LLC. P-series contains polypropylene fibers; S-series contains steel fibers	120
30. Cut and smoothed samples from „P1“-cylinder	123

31. Steel fiber containing samples („S1“-series) cut with a diamond saw blade (left) and with a steel saw blade (right).....	123
32. 2 in.-diameter SHPB system at the Dynamic Photomechanics Laboratory.....	124
33. Aluminum striker with mounted O-rings.....	125
34. Aluminum striker centered within gas gun by O-rings.....	126
35. KWIK-STAK portable elevating truck to support the overhanging part of the SHPB system.....	127
36. compressed gas mechanism with gas tank, automatic gas launcher, and solenoid valve control box	128
37. Settings of the oscilloscope (red box)	130
38. Settings of the amplifier	131
39. Settings of the half bridge	131
40. Gap between incident bar (left) and transmitted bar (right) indicating misalignment	134
41. Opening of the SHPB gun barrel that had to be closed off.....	135
42. Repositioned pressure regulator with short connector mounted on the SHPB stand	136
43. 120 Ω - strain gage (top) with terminal installed by the author	137
44. Incident and reflected pulse (left) and transmitted pulse (right) created by the MATLAB code [60].....	141
45. Force applied on the specimen over time; matching incident and reflected pulses [60]	142

46. Force applied on the specimen over time; incident and reflected pulses do not match [60]	142
47. True strain over time diagram [60]	143
48. Incident and reflected pulse obtained in a SHPB single-bar test	145
49. Original pulses of SHPB bar-to-bar experiment (300 psi gas pressure)	146
50. Misalignment between incident (left) and transmitted (right) bar	147
51. Force equilibrium	148
52. Strain vs. time of incident-, reflected-, and transmitted pulses	148
53. Aluminum 6061 specimen(1.5 in. diameter, 0.6 in. thickness) tested to verify future results	149
54. Original pulses obtained by testing a cylindrical aluminum 6061 specimen	150
55. Force applied on the aluminum 6061 specimen	151
56. Initial engineering stress vs. engineering strain of aluminium 6061	152
57. Dynamic stress-strain curves of Al-6061-T6 alloys showing (inset) material constants (m) and hardening coefficients (n) under the impacts at various strain rates [83]	153
58. Initial part of the dynamic stress-strain curve of aluminum [82]	154
59. True strain vs. time of aluminum 6061	154
60. Strain-rate vs. time of aluminum 6061	155
61. Dynamic compressive strength of paste, mortar and concrete [53]	156
62. Comparison of stress-strain curves of specimens determined by experiments and model [53]	157
63. Clay as pulse shaper on one face of the incident bar	161

64. Misalignment of Iron Carbonate specimen P1-2	161
65. Undeformed and deformed Iron Carbonate specimens.....	163
66. Strain time records for(low impedance) RTV630 silicone rubber specimen using a conventional SHPB [84]	166
67. Original pulses of specimen P1-1	167
68. Original pulses of specimen (a) P1-1, (b) P1-2, and (c) P1-4	169
69. Incident-, reflected-, and transmitted pulses of specimen (a) P1-1, (b) P1-2, and (c) P1-4.....	170
70. Forces applied on specimen (a) P1-1, (b) P1-2, and (c) P1-4	172
71. Eng. stress vs. eng. strain of specimen (a) P1-1, (b) P1-2, and (c) P1-4.....	173
72. True strain vs. time of specimen (a) P1-1, (b) P1-2, and (c) P1-4	174
73. Strain-rate vs. time of specimen (a) P1-1, (b) P1-2, and (c) P1-4.....	175
74. Modified SHPB set-up using a hollow transmitted bar [61].....	178
75. Typical pulse signals of a solid and hollow bar transmitted bar [61]	180

LIST OF TABLES

Table

1. Primary constituents of a modern Portland cement finished clinker [1].....	18
2. Main types of Portland cement (ASTM) and their general features [10]	20
3. Iron Carbonate standard dry mixture composition.....	121
4. SHPB experiments on mortar carried out by Grote et al. [51].....	158
5. Values used in Eq.(1) to estimate stress in specimen during SHPB tests	159
6. Diameter \emptyset and thickness t of cylindrical Iron Carbonate specimens before (undeformed) and after (deformed) dynamic compression test in SHPB	164
7. Incident pulse starting and end time, reflected pulse starting time and transmitted pulse starting time used in the MATLAB-codes.....	165
8. Strain-rates of specimen P1-1, P1-2, and P1-4 obtained with the MATLAB- code	171
9. Magnifications in the transmitted signal for different incident and transmitted bar materials and area ratios [61].....	179

1 Introduction

Portland cement is the primary constituent of concrete and has established itself as the mainstay of the modern construction industry and crucial material for civilization. Even though cement only comprises around 10-15% of the mass of concrete, its production is responsible for roughly 3% of the global anthropogenic greenhouse gas emissions and 5-7% of all anthropogenic CO₂ emissions, making the cement industry a heavy polluter. Manufacture of 1 ton of Portland cement results in emitting about the same amount of CO₂. Due to a growing world population, demand for housing and infrastructure and therefore concrete respectively cement as building material is increasing, especially in developing countries like China or India.

To avoid potential climate change and to protect our resources and surrounding environment, CO₂ emissions during production of Portland cement have to be drastically reduced. One way to reduce carbon emissions could be the use of novel carbon-negative sustainable binder developed by Dr. Das and his colleagues that utilizes the chemistry of iron carbonation. Iron carbonated binders made from metallic iron powder waste could potentially replace cementitious binders and thus reduce the overall production of Portland cement, resulting in a significant reduction of the carbon footprint of the cement and building industry. Iron Carbonate has strong environmental benefits because it consumes and sequesters CO₂ from Greenhouse gas-emitting industries. At the same time, iron carbonated binders have good mechanical properties similar or even better compared to Portland cement-based binders.

This thesis gives a general overview of different approaches to improve sustainability and to reduce the carbon footprint of the cement production. It focuses

on the description of alternative cementitious materials, especially on a novel carbon-negative sustainable binder called Iron Carbonate. However, the report also gives background about the carbon footprint and manufacture of ordinary Portland cement. The author tried to show the big picture of cement manufacturing and its many approaches to make it more sustainable.

To facilitate acceptance of Iron Carbonate as a replacement for ordinary Portland cement, more research on specific material properties is needed. The characterization of Iron Carbonate behavior under impact and impulse loading is a prerequisite for the design of concrete structures. The material behavior under highly dynamic conditions is significantly different from material response under quasi-static conditions.

Main objective of the present paper is to carry out a traditional analysis of a split Hopkinson pressure bar (SHPB) experiment on Iron Carbonate specimens. Analysis of Strain gage output signals using a MATLAB program will eventually provide stress, strain-rate and strain in the tested specimen under dynamic compression.

The performance of novel concrete, made from industrial iron powder waste, under extreme dynamic loading conditions, will potentially establish exceptional dynamic load mitigation characteristics for the carbon-negative sustainable binder under extreme combined environments. Enhanced durability of the novel sustainable concrete through better resistance against dynamic loading would prolong its lifetime and make it even more sustainable.

2 Approaches to improve sustainability in cement manufacture

2.1 Ordinary Portland Cement

2.1.1 Importance of OPC

Ordinary Portland cement (OPC) is a vital construction material as the dominant precursor of concrete, a widely-used mixture comprising coarse and fine aggregates, cement powder, water and, if applicable, performance-enhancing admixtures [1]. Portland cement consists of finely ground calcium silicate minerals that are hydraulically active [2]. It is considered one of the most important technological advances in the history of humanity, as OPC played and still plays a major role in the reconstruction and redefinition of many of the worlds' major cities [3]. In addition, the scientific studies of cement have contributed significantly to progress in material sciences as a whole. OPC has become the centerpiece of the modern construction industry [2].

OPC is the most common form of cement [4] and has dominated concrete production for the past 150 years [2], being the most important component to the hardening reaction of the initial fluid phase of the mixture to form artificial rock. Concrete is formed when powdered cement creates a paste with water that binds and encapsulates sand, gravel and rocks and hardens with time. Portland cement and other hydraulic binders are used almost exclusively to make concrete [5] and other binding pastes, such as mortars, screeds, stucco, coatings, soil stabilizations and other applications [1].

Main reasons for the immense popularity in usage of concrete are good structural properties such as strength, acceptable durability, and fire resistance.

Furthermore, OPC-based concrete is widely available in almost every part of the world, easy to make off and on site, technologically simple and inexpensive to produce [5].

Although cement is a minor constituent comprising only 10-15% of the mass of concrete, it makes up a significant portion of the overall cost of concrete and its properties of the fresh and hardened cement paste [2]. Nonetheless, Portland cements' popularity is due to its relatively low price compared to other construction materials. At the same time, cement has low margins for generating profit – cement prices have dropped in the U.S. since 2006 [1] – and profit generally can only be achieved by high-production turnover [2].

Cement, especially OPC, has become a crucial raw material for civilization [4] and represents the second most consumed material on the planet after water [1].

2.1.2 History and discovery of Portland Cement

Cementitious materials played an important role throughout history in creating buildings and structures and were used widely in the ancient world [6]. First, the Egyptians used calcined gypsum as cement, followed by the Greeks and Romans using lime – made by heating limestone – together with sand and coarse aggregates for making mortar respectively concrete. The Romans were the first who systematically manipulated the properties of cementitious materials to fit specific applications. They discovered cement that sets under water and used it for building harbors. This cement was made by adding crushed volcanic ash to lime and named “pozzolanic cement” after the village of Pozzuoli near the volcano Mount Vesuvius.

In 1824, a British stone mason from Leeds named Joseph Aspdin, obtained a patent (No. 5022, issued 21 Oct 1824 [7]) for cement he produced in his kitchen stove. Aspdin heated finely ground limestone and clay until the limestone was calcined and afterwards ground the mixture into a powder, creating hydraulic cement, meaning that the cement hardened with the addition of water. He named it Portland cement because the concrete made from it looked like Portland stone, a widely-used building stone in England [6] quarried on the British Isle of Portland [8].

Even though history usually regards Aspdin as the inventor of Portland cement, Aspdin's cement was not produced at a high-enough temperature to be the real precursor of modern Portland cement [6]. Nevertheless, Joseph Aspdin laid the foundation for today's Portland cement industry with his invention.

In 1845, Isaac Johnson finally produced the first modern Portland cement by heating a mixture of chalk and clay at much higher temperatures (1400-1500°C), at which the formation of the so-called clinker occurs [6]. Three important developments in the manufacturing process lead to modern Portland cement: development of rotary kilns, addition of gypsum to control the setting of cement and the use of ball mills to grind clinker and other raw materials.

In 1868, the first recorded shipment of Portland cement to the U.S. took place [8]. The first Portland cement manufactured in the U.S. was produced at a plant in Coplay, Pennsylvania in 1871.

2.1.3 Manufacture of OPC

Ordinary Portland cement (OPC) is a complex multiphase material [5] consisting of compounds produced by burning limestone and clay together in a rotary

kiln. It is an artificial building material which – on a human time scale – does not return to its original form when it has reacted with water [5]; Portland cement is a hydraulic, meaning water-resistant material.

The basic cement is produced through the calcination process in which calcium carbonate (limestone) is decomposed respectively decarbonated to calcium oxide (lime); calcium carbonate and silicon oxides (clay) are combined at temperatures around 1,450°C to form calcine, also called clinker [1]. The calcination reaction (in this case for Alite) is as follows:



calcium carbonate + silica $\xrightarrow{\text{Heat}}$ calcium silicate (clinker) + carbon dioxide

Alite (Ca_3SiO_5) and Belite (Ca_2SiO_4) are primary minerals in the clinker that emerge through chemical and mineralogical transformations of lime and silica in the clinkering zone [5]. In cement chemist notation Alite and Belite can also be written as C_3S respectively C_2S .

The calcination process produces lumps of clinker that contain silicon, iron, aluminum, and calcium oxides; the latter form when heat drives CO_2 out of the limestone's calcium carbonate [4]. After the clinker has cooled to fix C_3S and C_2S in their highly hydraulic forms (“quenching”) [5], it is combined with gypsum and ground into a powder that can react with water and change from a paste respectively liquid solution into a solid phase [1]. The finer the cement clinker is ground, the faster the hardening reaction will be, due to an increased surface area of the cement powder that is in contact with water. The gypsum thereby controls how fast the cement will set [4]. *Table 1* shows the main chemical compounds of a modern Portland cement finished clinker.

Table 1 - Primary constituents of a modern Portland cement finished clinker [1]

Constituent	Proportion	Chemical Formula	CCN
Tricalcium silicate	50%	Ca_3SiO_5 or $3\text{CaO}\cdot\text{SiO}_2$	C_3S
Dicalcium silicate	25%	Ca_2SiO_4 or $2\text{CaO}\cdot\text{SiO}_2$	C_2S
Tricalcium aluminate	10%	$\text{Ca}_3\text{Al}_2\text{O}_6$ or $3\text{CaO}\cdot\text{Al}_2\text{O}_3$	C_3A
Tetracalcium aluminoferrite	10%	$\text{Ca}_4\text{Al}_2\text{Fe}_2\text{O}_{10}$ $4\text{CaO}\cdot\text{Al}_2\text{O}_3\cdot\text{Fe}_2\text{O}_3$	or C_4AF
Gypsum	5%	$\text{CaSO}_4\cdot 2\text{H}_2\text{O}$	$\text{C}\bar{\text{S}}\text{H}_2$

Portland cement sets through a series of simultaneous chemical reactions that produce products leading to a hardening process [4]. The so-called hydration reaction is most important to the final solid phase. Hydration is the chemical reaction of the cement with water. Chemical components of the clinker, such as C_3S , C_2S and C_3A , react with water and form new compounds. The hydration produces a stable, amorphous solid hydrate called calcium silicate hydrate [1], also written as C-S-H ($\text{CaO}\text{-SiO}_2\text{-H}_2\text{O}$). This C-S-H gel continues to grow and expand in the presence of water and encapsulates other materials, such as coarse and fine aggregates within its matrix of hydrate solid. The chemical reaction in cement saturates water with calcium (Ca) and hydroxide (OH) ions, leading to the formation of solid calcium hydroxide and calcium silica hydrate (C-S-H) precipitating from the solution into pore spaces; a process that produces heat and is therefore exothermic. The negative hydroxide ions raise the alkalinity of the cement paste and make it an alkaline substance ($\text{pH} > 12$). It is important to note that the reaction products depend on many different factors, such as the initial ingredients, amount of water, ratio of calcium to silicon, additives, contaminants, temperature, and humidity [4].

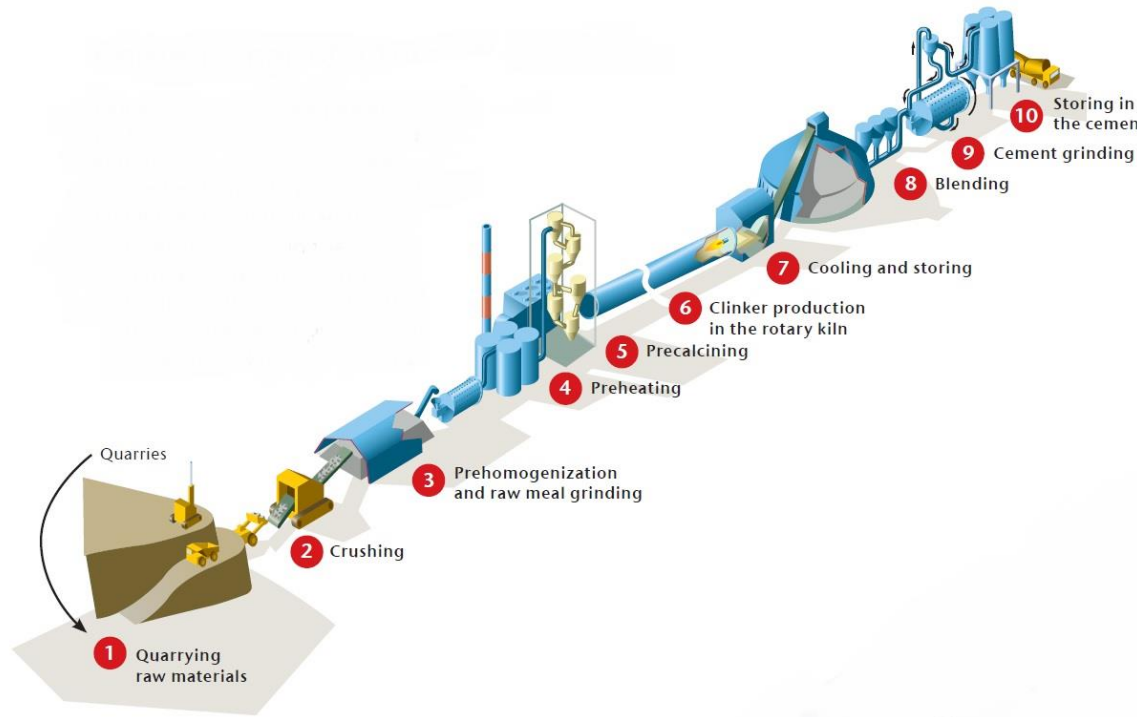
Within the hydration reaction, Alite (C_3S) and Belite (C_2S) give rise to the C-S-H gel; Alite is more reactive than Belite and begins to cure within hours after the

addition of water [4]. Therefore, it gives the forming concrete its initial strength. Belite is ultimately stronger but takes days or even months to begin hardening. However, Belite already forms at temperatures around 1,200°C, whereas Alite requires significantly higher temperatures of 1500°C.

The overall manufacture process of Portland cement can be divided into 3 major steps, the first one being the quarrying and milling together of the raw materials limestone and clay [1]. This is followed by pyroprocessing in the kiln: the raw meal, in form of finely divided particles, is exposed to high temperatures (1,400-1,500°C) to transform lime and silica into cement clinker (C_3S , C_2S , C_3A and C_4AF) through the calcination process. In the final step, the lumps of clinker are interground with gypsum (calcium sulfate dehydrate); gypsum controls the setting time and rate of hardening.

Figure 1 shows the cement manufacture process in detail.

Figure 1 - Cement production process [9]



The American Society for Testing and Materials (ASTM) has specified five types of Portland Cement, named Types I-V (see *Table 2*) [10]. Physically and chemically the cement types differ primarily in their content of C_3A and in fineness. In terms of performance, they differentiate in the rate of early hydration and in the ability to resist sulfate attack. **Table 2** lists the types of Portland cement.

Table 2 - Main types of Portland cement (ASTM) and their general features [10]

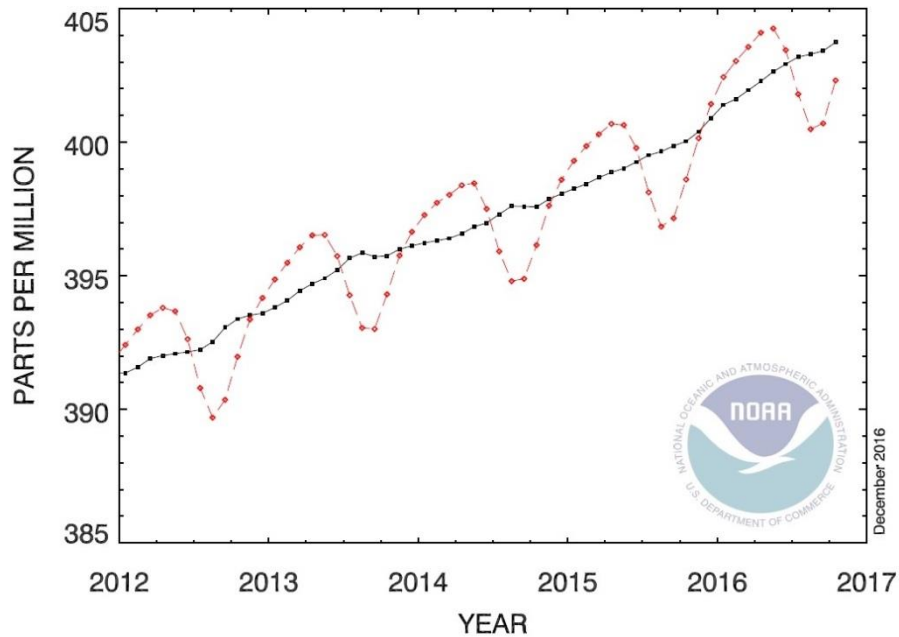
	Classification	Characteristics
Type I	General purpose	Fairly high C_3S content for early strength development
Type II	Moderate sulfate resistance	Low C_3A content (<8%)
Type III	High early strength	Ground more finely, may have slightly more C_3S
Type IV	Low heat of hydration (slow reacting)	Low content of C_3S (<50%) and C_3A
Type V	High sulfate resistance	Very low C_3A content (<5%)
White	White color	No C_4AF , low MgO

2.1.4 Carbon Footprint and environmental issues of OPC

Many chemical compounds found in the Earth's atmosphere act as so-called greenhouse gases [11]. These gases allow sunlight to enter the atmosphere freely but absorb from the Earth's surface reflected infrared radiation and trap heat in the atmosphere.

The release of greenhouse gases, such as carbon dioxide (CO₂), methane (CH₄) and nitrous oxide (N₂O), into the atmosphere possibly causes a change in global climate and is a threat to future life and prosperity on the planet. CO₂ thereby is the primary greenhouse gas emitted through human activities [12], for example, the production of cement. In the past decades, emission of greenhouse gases has been increasing due to population growth and increased industrialization and economic activity in developing countries [1]. At the beginning of the industrial revolution in the mid-eighteenth century, CO₂ concentration in the air was approximately 280 ppm, increasing to 310 ppm in the 1950s [3]; currently (October 2016) the CO₂ concentration is at about 402 ppm [13], meaning that there has been a significant increase in the rate of increase of CO₂ concentration over the past years. *Figure 2* shows the global monthly mean atmospheric CO₂ averaged over marine surfaces; the red line represents the monthly mean values. The black line represents the monthly mean values after correction of the average seasonal cycle. The average CO₂ concentration has to remain below 450 ppm to limit the overall temperature increase to +3°C [14].

Figure 2 - Global monthly mean CO₂ since 2012 [13]



Roughly 3% of the global anthropogenic (man-made) greenhouse gas emissions [15] and 5-7% of all anthropogenic carbon emissions are due to the manufacture of vast quantities of cement [1] [3] [14] making the industry a heavy polluter. Every ton of OPC produced releases – on average – a similar amount of CO₂ into the atmosphere [1] [5]. One ton of CO₂ is approximately the amount of carbon dioxide that a tree absorbs over 100 years [16]. The cement production is a highly energy-intensive process: manufacture of cement is the third most energy intensive process, after the production of aluminum and steel [17], and accounts for approximately 2% of the total global primary energy consumption (representing 10-11 EJ of energy annually [18]) respectively for 5% of the total global industrial energy consumption [19].

The emission of CO₂ during the production of cement has three major sources: burning fossil fuel to heat the kiln, the calcination process itself and indirect sources,

such as grinding the raw materials, transportation, or the production of necessary electricity.

Approximately 40% of the cement plant CO₂ emissions result from the combustion fuel to heat the raw materials – interground limestone and clay – to sintering temperatures around 1500°C [1] [20]. Cement kilns are usually fired using coal, fuel oil, natural gas, petroleum coke, biomass, waste-derived alternative fuels, or mixtures of these fuels. Each tonne of OPC produced requires about 60-130 kg of – usually fossil – fuel, depending on the cement variety and process used.

The main source of carbon emissions is the calcination process of calcium carbonate (CaCO₃) to calcium oxide (CaO), also called lime, in order to produce the basic clinker (C-S-H). The high heat of 1500°C drives CO₂ out of the limestone's calcium carbonate [4]. Such temperatures are needed for the formation of the primary clinker mineral Alite (C₃S), that gives concrete its initial strength. Alite is the main constituent of the Portland cement finished clinker, accounting for a share of about 50%. (see *Table 1*). At the same time, Alite (C₃S) has the highest carbon footprint of all individual clinker phases, followed by C₃A, Belite (C₂S) and C₄AF with the lowest carbon footprint [14]. The decarbonation of limestone in the rotary kiln accounts for roughly 50% of the cement plant CO₂ emissions [1]. The overall production of cement consumes large amounts of non-renewable raw materials: one ton of OPC starts from 1.7 tons of raw materials.

The remaining 10% cement plant CO₂ emissions are due to indirect sources [1]. Operating of machinery for grinding the raw meal and transportation of unground and ground material causes carbon emissions, as well as the production of electricity

being used in the overall cement production process. Each ton of OPC produced requires approximately 110 KWh of electricity [1] [20].

Conservative estimates assume an annual CO₂ emission of 3.24 billion tons as a by-product of the cement production [1]. The reason behind the large carbon footprint is simply the large quantity of worldwide produced and consumed concrete. The growing demand for cement will further increase carbon emissions. Assuming an exponential trend, the cement industry emissions in the year 2050 could rise to an alarming 32.7 billion tons of CO₂ per year, representing 33 times the cement industry emissions from 1990.

Besides CO₂ emissions and the consumption of large amounts of non-renewable raw-materials, the cement industry emits persistent organic pollutants (POPs), such as PCDD and PCDF [20]. These toxic chemicals have a negative impact on the environment and human health [21]. They persist for long periods of time in the environment and can accumulate and pass from one species to the next through the food chain. Furthermore, some of the nitrogen in the air is transformed into NO_x (during the combustion of fuel) and some of the Sulphur into SO₃ [5]. In addition, the manufacture process emits solid particles, also referred to as cement kiln dust (CKD), that can be collected in electrostatic precipitators and reintroduced into the kiln. However, if the alkali content of the CKD is too high, the particles have to be stockpiled, possibly contaminating the groundwater through leaching processes.

It is important to notice that cement is always used in connection with many other materials [20], that themselves have a carbon footprint and influence on the environment. The large share of OPC-based concrete used worldwide is reinforced

with steel bars to increase the tensile strength of concrete structures. The production of steel also emits vast amounts of carbon dioxide and requires even more energy as the production of cement [22]; the contribution of steel to the environmental load of reinforced concrete is greater than the one of the aggregates but much less than the one of cement [15].

The expected increase in output of cement due to a growing population and construction boom under way in developing nations, such as China and India [4], calls for actions to reduce the environmental impact of the cement production. Especially, because developing countries only have a subordinate environmental awareness; economic growth is taking top priority.

2.1.5 Durability of OPC

Its many good structural properties – and its relatively low cost – make OPC-based concrete the most popular construction material on the planet. However, OPC-based concrete is not a material of endless durability and occurrence of structural and material degradation is quite common [2]. Given the immense environmental impact the cement production has, especially in terms of greenhouse gas emissions, it is concerning that its durability is limited. The main reasons for the poor durability of OPC-based concrete are the brittleness of the material, a low strength to weight ratio, high permeability, low tensile strength and ductility, shrinkage, and a weak resistance to acid. Over the past decades common OPC composition has supposedly changed from a Alite (C_3S)/ Belite (C_2S) ratio of 1.2 to 3.0, resulting in higher early age strengths but also in higher heat of hydration and less later age strength after 28 days.

Limited durability and degradation problems of OPC result from its microstructure and chemical composition consisting of unnatural compounds, such as C-S-H, CH, CA, and calcium sulfoaluminates, being prone to degradation in certain environments [2]. Calcium hydroxide (CH), also called portlandite, is the most soluble of the hydration products [10], meaning that CH dissolves when exposed to water; CH is highly mobile and reactive [2]. Thus, CH increases the porosity of the paste, making it more vulnerable to chemical attacks [10], such as sulfate attacks [2]. Therefore, CH represents a weak link from a durability point of view [10].

The major shortcoming of C-S-H (calcium silicate hydrate), the main and most important hydration product, is, that it is thermodynamically unstable [2]. It tends to deform to silica gel and calcium carbonate. In addition, the 2-dimensional bonding structure or network of C-S-H is not as strong as a 3-dimensional. Durability and material performance, such as tensile strength, toughness, crack resistance, and permeability to fluids, are restricted through a discontinuous and inhomogeneous nanostructure respectively microstructure. Structural reinforcements and admixtures can overcome most of the issues mentioned above. However, new alternative cements could help to improve durability and structural performance at the microstructural respectively chemical level.

Sustainable cement depends on durability and lifetime of the cement [2]. Durability in turn is strongly linked to the permeability respectively porosity of the microstructure. A more compact hardened cement matrix would reduce permeability and ultimately extend the service life respectively life cycle of concrete structures [5]. Thus, it would reduce the ecological impact. High performance concrete (HPC) and

reactive powder concrete (RPC) are just two examples of approaches that improve compactness of the cement matrix. In addition, an adjusted Alite (C_3S)/ Belite (C_2S) ratio would improve later age strength.

Furthermore, it is necessary to pay attention to the quality of the placing and curing of the concrete, which also have a significant impact on the durability. Aïtcin [5] calls for the establishment of precise specifications and the payment of contractors to specifically improve the quality of the placing and curing. The city of Montreal is one of the few cities that have realized that this low initial investment will eventually result in great monetary long-term savings [5]: durable concrete decreases the frequency at which a structure will have to be repaired or replaced.

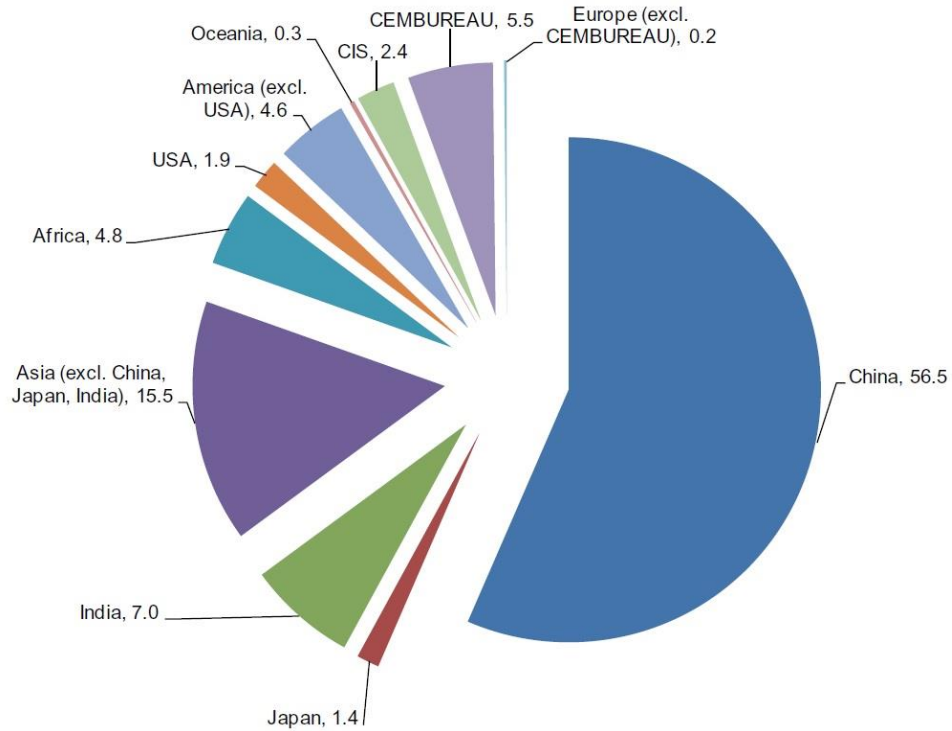
It should be pointed out, that concrete is still specified only on the basis of its compressive strength. The – sometimes harsh – environmental and placing conditions, in which concrete has to fulfil its structural functions, are usually not considered [5]. In this respect, one should appreciate OPC-based concrete's versatility and ability to generally withstand environmental impacts with an acceptable durability. Nonetheless, with rising environmental awareness, the ecological impact of the cement and concrete production must be drastically reduced.

2.1.6 OPC market and future development

Nearly 3.6 billion metric tonnes of OPC worldwide were produced annually (2012) with a predicted rise in volume to more than 5 billion metric tons by 2030 [1]. In 2014, cement production already reached 4.3 billion tons [23]. *Figure 3* shows that China dominates the global cement market by far with a production share of 56.5%, followed by Asia (15.5%), India (7.0%) and the USA (1.9%). The global cement

production is increasing constantly, particularly in developing countries, such as China and India, that have a high demand for infrastructure and housing [1].

Figure 3 - World cement production in 2014, by region and main countries [%] [23]



2015 domestic production of cement in the U.S. was about 80.4 million metric tons of Portland cement and 2.4 million tons of masonry cement, which was well below the record level of 99 million tons in the year 2005 [24]. The sales of cement have been increasing in 2015 with an overall value of \$9.8 billion. Most of the increased sale was accounted for by imports and 70% of the sales were to make concrete. 99 plants in 34 States, as well as 2 plants in Puerto Rico, produced cement. The 5-leading cement-producing States, that accounted for nearly 50% of the U.S. production, were Texas, California, Missouri, Florida, and Alabama (descending order).

2.2 General approaches to improve sustainability of cement manufacture

2.2.1 Definition of sustainable development

1987 the UN-Brundtland Commission defined sustainable development as “development that meets the needs of the present without compromising the ability of future generations to meet their own needs” [25]. In addition, sustainable concrete structures were described as follows: “An environmentally sustainable concrete structure is a structure that is constructed so the total environmental impact during the entire life cycle, including use of the structures, is reduced to a minimum. [...] the concrete and its constituents shall be extracted and produced in an environmentally sound manner.”

2.2.2 CO₂ reduction plan of the IEA for the cement industry

The International Energy Agency (IEA) [9] has realized the need and urgency of drastically reducing the CO₂ emissions of the cement production. To do so, the IEA has developed a so-called technology roadmap for the cement industry, outlining different growth scenarios and actions to reduce carbon dioxide emissions of the industry.

The technology roadmap outlines major actions for the CO₂ reduction [9]: improved thermal and electric efficiency of the cement plant (see section 2.2.2.1), use of industrial process wastes (see section 2.2.2.2), i.e. use of alternative, less carbon intensive fuels in the production process (see section 2.2.2.2.1) and substitution of carbon-intensive clinker with low-carbon materials having cementitious properties (see section 2.2.2.2.2), and carbon capture and storage, short CCS (see section 2.2.2.3).

The IEA plans to reduce CO₂ emissions from 2 Gt (2007) to 1.55 Gt (2050) [14]. At the same time, it is predicted that the cement production will drastically increase. The existing technologies (fuel efficiency, alternative fuels, clinker substitution) would enable reaching only half of the reduction goal. To fulfil the other half of the reduction, new CCS-technologies, capturing and storing CO₂ emissions from the production process, are necessary. By now, those technologies are relatively unproven and could result in significant additional costs for society if implemented. The most powerful approach – in the opinion of the IEA – is the use of alternative fuels to produce heat for decarbonating limestone.

However, it must be pointed out, that IEA's assumptions and plans were developed in 2009 and are therefore somewhat dated. IEA assumed a high growth scenario with a 2050 production at 4.4 billion tons [9], which has been almost reached already in 2014 (4.3 billion tonnes [23]).

2.2.2.1 Energy efficiency

One approach to reduce the vast amount CO₂ emissions of the cement industry is to improve the – thermal and electric – energy efficiency of the cement plant and cement production processes. Over the past decades many cement plants improved their energy efficiency and energy flexibility [14]. As already mentioned, cement has low margins for generating profit – cement prices have dropped in the U.S. since 2006 [1] – and profit generally can only be achieved by a high-production turnover [2]. Therefore, improved production efficiency is a logical step for a cement producer to reduce production costs through lower energy costs. For instance, the so-called dry production process (low moisture content manufacture) replaced the insufficient so-called wet production process of clinker. Even less efficient long dry kilns are phased

out by the industry [26]. The five-stage preheater with precalciner is currently considered “Best Available Technology” (BAT); the most recently developed technologies are typically the most energy efficient [14]. In 1990 the specific thermal energy consumption, using the mentioned preheater with precalciner as kiln type, was 3,605 MJ/t clinker. In 2006, consumption was down to 3,382 MJ/t clinker, indicating a 6% reduction (220 MJ/t) over 16 years [26]; the 2006 world average energy consumption was estimated at 4.2 GJ/t of clinker [14]. Currently, the BAT-kiln consumes 3.0-3.1 GJ/t clinker, which represents about half of the energy consumption of the old wet process.

The theoretical minimum primary energy consumption (heat) for the clinker production reactions taking place is approximately 1.6-1.85 GJ/t [26]. However, there are limits and restrictions that keep energy efficiency from increasing above a certain point, for example unavoidable conductive heat loss through kiln surfaces. Furthermore, strengthened environmental requirements can increase power consumption, for instance due to more needed power for dust separation. Demand for higher cement performances or the use of clinker substitutes, such as fly ash or slag, require more energy for grinding cement finely. Nevertheless, improving plant efficiency is an ongoing process and not yet possible further improvement may be achieved through future developments.

Efficiency is a function of initial and following cement plant investments, which are usually dictated by local energy prices [9]. It is the only approach to reduce carbon emissions that is managed by the cement industry itself; policy and legal framework mainly influence other approaches.

2.2.2.2 Utilization of industrial process wastes

Waste production of industrialized societies, mostly associated with mineral processing, energy production, individual consumption and disposal of non-renewable resources, is increasing [2]. The majority of global industrial processes relied upon daily produce waste that is usually disposed in landfills by incineration. Due to the large and increasing amounts of industrial waste, it becomes less socially, environmentally and practically acceptable to simply landfill waste. Integrated waste management options include waste prevention and reduction, composting, incinerating with energy recovery, recycling and re-use of waste products.

There are many industrial process wastes that are suitable for re-utilization in cement and concrete production [2]. Waste-derived fuels as a substitute for fossil fuel can be used in the burning process of the cement clinker. Supplementary cementitious materials (SCMs) can be used as a filler to replace Portland cement, for example combustion ashes, slags, kiln dust, foundry sand and other inorganic residues. Even organic materials like rice hull ashes (see section 2.3.1.6) can be used as a source of silica [20]. Mining wastes, such as tailings, brines, slags and residues from processing materials can also be re-used [2]. Discarded concrete can be recycled as aggregate in making new concrete.

The following sections 2.2.2.2.1 and 2.2.2.2.2 give a more detailed summary about the use of alternative fuels and cement replacement materials.

2.2.2.2.1 *Alternative fuels*

Alternative fuels can partly replace conventional fuels, mainly coal and petroleum coke, that heat the cement kiln and thus lower CO₂ emissions of the combustion. Cement kilns are well-suited for alternative fuels because the energy

component is used as substitute for fossil fuels and the inorganic components, such as ashes, can be integrated into the final clinker product [26]. Typical alternative fuels that are used by the cement industry, are pre-treated industrial and municipal solid wastes, discarded tires, waste oil and biomass. Alternative fuels derived from biomass and used as a fossil fuel substitute, can reduce CO₂ emissions by 20-25% [1]. Sources for fuels from biomass are animal meal, scrap wood, agricultural residues, sewage sludge and biomass crops [26]. The use of waste-derived alternative fuels and biomass in clinker manufacturing is expected to be the most powerful approach to reduce the carbon footprint of cement [14].

Furthermore, it seems reasonable to use natural gas instead of coal or petroleum coal to fire the kiln because carbon and fuel prices are predicted to further increase in the future [26]. Natural gas has a significantly lower carbon content than conventional fossil fuels. Switching to natural gas would reduce CO₂ emissions more significantly than the effect of increased use of alternative fuels.

However, there are practical limitations for the use of waste-derived alternative fuels, even though cement kilns could technically use up to 100% of alternative fuels [26]. Some of the fossil fuel substitutes mentioned above have a low calorific value, high moisture content or high concentrations of harmful and hazardous substances. Alternative fuels burn differently compared to traditional fossil fuels and can therefore influence cement clinker properties and cement performance, for example decrease early strength and extend setting times [1]. This is due to the introduction of different inorganic components (ashes) into the kiln.

The IEA's technology roadmap (see section 2.2.2) assumes that alternative fuel costs will increase with increasing costs for emitting carbon emissions into the atmosphere, making it difficult for the cement industry to source sufficient quantities of biomass at acceptable prices [26]. The assumption further states, that it will only be economically viable for the cement industry to use alternative fuels until 2030; until then prices of alternative fuels will reach about 30% of the conventional fuel costs. By the year 2050, IEA presumes an increase up to 70% of the conventional fuel costs.

2.2.2.2.2 Clinker substitution

Clinker is the main component in cement. After its production in the cement kiln through the calcination process, it is ground and mixed with up to 5% gypsum. The clinker then reacts with water and hardens through the hydration process. Other mineral components also have hydraulic properties, meaning that they harden with the addition of water, when they are ground and mixed with clinker and gypsum. Thus, these alternative hydraulic components, so-called supplementary cementitious materials (SCMs), can be used to partially substitute clinker in cement, reducing the volume of used clinker and – to some extent – process-, fuel- and power-related CO₂ emissions [26].

The clinker content in cement can vary. OPC can contain up to 95% clinker, the 5% balance being the added gypsum. The global average clinker to cement ratio in 2006 was 78% [26]. It should be pointed out, that different national industry structures exist: in some regions (e.g. China and Latin America) the clinker ratio can be below 75% [14] and there are differences about when adding clinker substitutes to the clinker. In most European countries clinker substitutes are added in the plant, reducing

the clinker to cement ratio, whereas in the U.S. and Canada, substitutes are typically added when producing the actual concrete [26].

Cement replacement materials are fly ash, ground blast furnace slag, natural pozzolans (e.g. silica fume, volcanic ash, rice husk ash), artificial pozzolans (e.g. calcined clay) and limestone [26]. A more detailed analysis of the different SCMs will be carried out in section 2.3.1.

However, there are limitations to the implementation of substituting clinker with alternative hydraulic materials [26]: regional availability of good quality SCMs, increasing prices of SCMs, properties of SCMs, national standards for OPCs and composite cements, and common practice of construction contractors.

The main challenge, according to IEA's technology roadmap [9], will be the scarcity of good quality SCMs. Besides, clinker substitution does not play a big role in the IEA's proposed approaches to improve the carbon footprint of the cement production. In their opinion, carbon capture and storage (CCS) technologies will have to reduce the major part of cement CO₂ emissions [26]. However, Imbabi et al. [1] state that carbon-reducing cements will be the safest, most economical and elegant CCS technology, but in order to be successfully implemented, new concrete design guidelines, that allow an increased SCM use, have to be developed.

2.2.2.3 Carbon Capture

Carbon Capture and Storage (CCS) is a new technology that captures emitted CO₂, compresses it into a liquid and transports it in pipelines to a permanent storage deep underground; the storage process is also called CO₂ sequestration [26]. As already outlined in section 2.1.4, the cement industry emits large amounts of CO₂ through fuel combustion and limestone calcination in the kiln. That makes it

interesting to implement capture technologies in cement production plants. Two different, general CO₂ capture technologies are considered appropriate for the cement production: post-combustion technologies and oxyfuel technology [26].

Post-combustion technologies are so-called end-of-pipe mechanisms that can be implemented without changing the clinker-burning process [26]. Therefore, those technologies could be suitable for both new kilns and retrofits. Post-combustion technologies include chemical absorption using chemical solutions (e.g. potassium, amines) and membrane technologies to capture CO₂. Furthermore, an adsorption process, called carbonate looping, is applicable: calcium oxide is put into contact with CO₂ containing combustion gas to produce calcium carbonate.

Oxyfuel technology uses oxygen instead of air in cement kilns, resulting in a pure CO₂ stream [26].

However, CCS technologies are not yet proven at the industrial scale in cement production and require a high initial investment [26]. Due to higher specific costs, smaller kilns (capacity less than 4000-5000 tons per day) will probably not be equipped with CCS technology. Retrofits will not be common either. The IEA also predicts that carbon capture technologies will not be commercially available before 2020. In addition, CCS essentially requires a CO₂ transport infrastructure (e.g. pipelines) and access to safe and long-term storage sites, as well as a supporting political and economic framework.

CCS technologies could be used to provide CO₂ as a constituent to produce alternative cements, such as sequestered carbon cement, like Calera cement (see

section 2.3.2.6), or carbonate binders (see section 2.3.2.7) that are exposed to a pressurized CO₂ curing regime.

2.2.3 Other approaches to reduce the carbon footprint of the cement industry

2.2.3.1 Nanoengineering

Nanoengineering could help to create green concrete by nanoengineering higher strength and toughness from first principles [27]. Based on Galileo's Strength of Materials Theory, the CO₂ impact of cement is driven by volume: increasing the strength of a cement-based concrete would therefore result in a decrease of its environmental impact [16]. Theoretically, an increase in the material strength by 100% would result in halving the environmental impact. Thus, the size of concrete columns and beams could be reduced because of the higher concrete strength, at the same time reducing the carbon footprint.

Increasing the strength of a concrete by a factor of λ could reduce the environmental footprint for pure compressive members, such as columns and perfect arches and shells, by λ^{-1} [27]. The environmental footprint for beams in bending and slabs could be reduced by a factor of $\lambda^{-2/3}$ respectively $\lambda^{-1/2}$.

Mechanics could help to develop a sustainable concrete. The nanoengineering approach starts at the electron and atomic scale and upscales strength, fracture and stiffness properties from nanoscales to macroscales [27]. Nanoindentation analysis of heterogeneous composites combined with micromechanics-based scaling relations and atomistic simulations, could link the atomic structure of the main OPC-hydration product C-S-H with its nanomechanical morphology and macroscopic performance.

C-S-H phases exist in three structurally different forms: Low Density (LD), High Density (HD) and Ultra-High-Density (UHD). Increasing the packing density of C-S-H respectively reducing the C-S-H gel porosity would result in an overall higher strength of the concrete. A “dry concrete”, meaning a very low water-cement ratio (w/c) in concrete, would favor almost exclusively the formation of strong UHD C-S-H [27], creating a so-called high-performance concrete (HPC) [5]. A w/c of 0.15 results in a hydration degree of around 60%, a 50% C-S-H solid volume formation and a 10% gel porosity [27]. But at the same time a low water content worsens workability of the cement paste, as a low w/c means that the concrete mix is less flowable. Using admixtures (see section 2.2.3.2), such as superplasticizers, can help making the paste workable again.

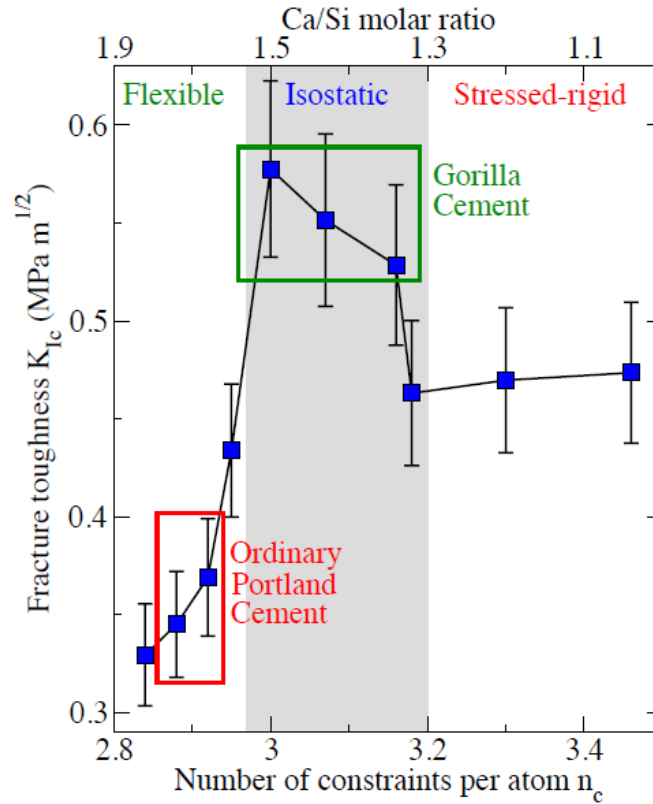
2.2.3.1.1 Gorilla cement

Gorilla cement also orientates on the nanoengineering approach (see previous section 2.2.3.1) and on the idea that tougher cement would allow using less material while having comparable mechanical properties [28]. An increased resistance of the binding phase C-S-H (calcium-silicate-hydrates) to fracture would make cement more durable and increase sustainability even more. Therefore, it is important to understand the influence of the cement composition on the fracture resistance of C-S-H.

Rigidity theory focuses on the atomic topology and how it affects macroscopic properties [28]. In glass science, the development of so-called Gorilla glass by Corning was based on rigidity theory. Complex molecular networks were reduced to simple mechanical trusses, creating a flexible, stressed-rigid, or isostatic network as requested. The characteristics of the network depend on the number of chemical

constraints in comparison to the number of degrees of freedom of the atoms: lower (flexible), higher (stressed-rigid), or equal (isostatic).

Figure 4 - Computed C-S-H fracture toughness with respect to Ca/Si molar ratio as a function of number of atomic constraints [28]



Rigidity analysis of C-S-H molecular models shows that isostatic compositions achieve the highest fracture toughness of C-S-H grains, at a Ca/Si molar ratio of 1.5 [28]. Isostatic systems are able to deform and show relatively high surface energy. In comparison, stressed-rigid compositions tend to break in a brittle way because a high number of constraints completely lock the systems. Flexible systems, on the other hand, can deform and have some ductility, but the surface energy is low. *Figure 4* shows the fracture toughness of C-S-H with respect to composition as a function of the number of constraints. OPC typically has a Ca/Si molar ratio of 1.7.

By replacing OPC-based clinker with silica-rich by-products, such as fly ash (see section 2.3.1.1), the relative amount of calcium (Ca) in cement can be reduced [28]. Decreasing the Ca/Si molar ratio of C-S-H from 1.7 to 1.5 would significantly increase C-S-H toughness by 70%. Less material with still comparable performance could be used, reducing the carbon footprint of cement.

2.2.3.2 Chemical Admixtures

Concrete usually consists of roughly 8-15% cement, 80% coarse and fine aggregates and 2-5% water [15]. Chemical admixtures are added to the concrete mix right before or during mixing [29] and can reduce the water and cement dosage consumed for a given strength [15]. Nanoengineering (see section 2.2.3.1) shows that a low w/c ratio in concrete favors the formation of UHD C-S-H. Furthermore, admixtures could make concrete more durable. Therefore, use of admixtures could help to reduce the carbon footprint of cement and concrete. However, use of advanced admixtures can be expensive.

Chemical admixtures can be classified in five categories: air-entraining, water-reducing, retarding, accelerating, and plasticizers (superplasticizers) [29]. In addition, there are other special admixtures with the following functions: corrosion inhibition, shrinkage reduction, alkali-silica reactivity reduction, workability enhancement, bonding, damp proofing, and coloring. Effectiveness of an admixture depends on type and amount of cement, water content, mixing time, slump, and temperatures of the concrete and air.

2.2.3.3 Recycling concrete

Recycling concrete construction waste to produce aggregate that in turn can be used for the production of new concrete could reduce energy consumption and CO₂

emissions [5]. Coarse and fine aggregates represent between 70 to 75% of the concrete's mass. Especially concrete with a high packing density, namely high-performance concrete (HPC) has great potential for recycling. That is, because each time a material is recycled, it results in a decrease in performance of the new material. Initially selected materials lose some of their original properties when recycled. Also, it should be noted that grinding concrete construction waste into usable aggregates requires energy. The processing of construction debris creates macro- and micro-cracking in the solid [20] reducing durability.

2.3 Modification of cement for improved sustainability

2.3.1 Blended OPC-based cements (Supplementary Cementitious Materials)

Blended Portland cements are hydraulic cements consisting of a homogeneous mixture of Portland cement and a replacement material [2], such as fly ash, ground granulated blast furnace slag, ground limestone, silica fume and others. Blended OPC-based cement is produced by intergrinding the replacement material with Portland cement clinker or by mixing both during concrete mix proportioning. Replacement materials, also referred to as supplementary cementitious materials (SCMs), can be natural pozzolans or waste-derived materials, mainly industrial by-products. Those silica- or alumino-silicate-rich materials react with calcium hydroxide (CH) from OPC to form C-S-H phases. SCM particles usually hydrate in the same way as OPC does [1]. However, SCMs supply more silicate in the mixture which then reacts with excess hydrated lime and alkalis released during OPC hydration.

Advantages of the use of blended OPC-based cement are a lower heat of hydration, better workability of the fresh paste, higher resistance to alkali-aggregate

reaction, reduction of permeability of the material [2] and higher ultimate strength [19]. In addition, the carbon footprint of blended cement is much lower than of pure OPC. CO₂ emission reduction of the total CO₂ emissions from the cement industry could reach 5-20% through common production and use of blended cements [19].

Drawbacks are lower early age strength and higher CaO content that restricts use in certain aggressive environments [2].

The following sections 2.3.1.1 to 2.3.1.6 introduce some common SCMs used for blending Portland cement.

2.3.1.1 Fly ash and pulverized fuel ash (PFA)

Fly ash and PFA are produced during coal and lignite combustion of power plants [5]. Fly ash and PFA are essentially the same but collected at different stages of combustion [1]: fine grained fly ash is carried with combustion fuel gases and collected by electrostatic precipitation, whereas fuel ash is left in the region of combustion.

Generally, the term fly ash describes a large family of powders having the same grain-size distribution as Portland cement and containing vitreous particles [5]. It is chemically composed of silicon oxides (SiO₂), aluminum oxides (AlO₃) and iron oxides (Fe₂O₃, Fe₃O₄) [1]. Two different types of fly ash can be differentiated, even though ASTM does not use the classification: calcium rich Class-C fly ash and aluminosilicate rich, truly pozzolanic, Class-F fly ash. However, the fly ashes recovered in the dedusting system have varying chemical and phase composition depended on the fuel and combustion type and contained impurities [5]. They are composed of all fused and unfused residues present in the coal or lignite being burned. Leaving the flame, some particles are quenched and solidify in the shape of vitreous

glass spheres. Other impurities are not fused because they rapidly pass through the flame. Therefore, fly ashes usually contain a certain amount ($< 6\%$) of unburned carbon that varies depending on the energy production of the power plant. The carbon content is important because some admixtures can be absorbed by carbon particles.

OPC blended with fly ash hardens by calcium hydroxides, produced during Portland cement hydration, reacting with fly ash particles [1]. Reactivity can be increased by grinding the fly ash and thus creating freshly fractured surfaces [5].

Fly ash can typically replace up to 30% of the mass of OPC in a concrete mix [1]. Its pozzolanic properties are used to lower permeability and heat of hydration. The spherical particle shape improves workability of the paste. Also, use of fly ash lowers the carbon footprint of cement.

The American company CeraTech produces cement containing 95 percent fly ash [4] [30]. It uses supposedly half as much water as the Portland cement it replaces and has better durability. CeraTech cement is made through a chemical reaction with several liquid additives [4] instead of being baked in a kiln. Another company, the Sefa Group, has developed a process for making concrete with fly ash taken from the ground in addition to what can be captured from coal-fired power plants [30]. This technique could help clean up landfills filled with ash that has been sitting for years.

2.3.1.2 Ground granulated blast furnace slag (GGBS)

Ground granulated blast furnace slag (GGBS) is an industrial by-product of the iron and steel production. Slag is left-over while extracting pig iron from the melted raw iron ore, consisting of calcium and magnesium aluminosilicates [1]. Its pozzolanic properties depend on the cooling method used to quench the material. There are 3

main types of blast furnace slag: air cooled slag, granulated slag, and expanded slag. All slags can be used as raw feed materials for cement clinker production.

Granulated slag is formed by quickly quenching melted slag with water, resulting in a glassy sand-like material [1]. Ground into a fine powder, this material develops strong hydraulic cementation properties when reacting with alkali. Air cooled slag and expanded slag can also be used as supplementary cementitious material (SCM) in Portland cement. But mainly those slags are used as aggregates in concrete and bitumen applications.

GGBS hydrates similar to Portland cement when mixed with water [31]. Typical blends with OPC range from 60% Portland cement and 40% GGBS to 30% Portland cement and 70% GGBS.

OPC blended with GGBS sets more slowly than pure OPC, depending on the amount of GGBS in the cement mix [31]. However, the GGBS blend continues to gain strength over a longer period resulting in improved durability extended service life. Another advantage of the use of GGBS is the reduction of CO₂ emissions due to significantly less required energy to perform calcination in the kiln [1].

2.3.1.3 Ground limestone

Limestones are sedimentary rocks primarily containing calcium carbonate [17]. Limestone powder can either be interground with OPC clinker in the cement manufacturing process or blended with cement during concrete batching [32]. ASTM standard allows for up to 15% of limestone powder in Portland cement.

Blending OPC with limestone powder, thus creating Portland Limestone Cement (PLC), densifies the microstructure of the paste [1] because limestone chemically combines with aluminate phases in OPC [32]. Intergrinding limestone with

cement improves particle packing [1]. Also, fine limestone particles act as nucleation sites that enhance the rate of hydration of the OPC phases [32].

Due to increased hydration, limestone powder improves early age strength. However, it can reduce later age strength because of a dilution effect [22]. Besides improving cement properties, limestone is a low-cost material that is readily available [1]. Furthermore, it is easier to grind than Portland cement clinker and therefore reduces energy consumption during cement manufacturing. The use of limestone also improves workability and reduces bleeding of the concrete mix. Besides, it has a synergetic chemical effect with alumina-bearing SCMs, such as fly ash or metakaolin, improving properties of the mix [32].

Another advantage of limestone powder is that it reduces CO₂ emissions of cement. PLC containing 20% limestone can reduce CO₂ emissions by 10% compared to pure OPC, having a similar performance [1].

2.3.1.4 Silica fume

Silica fume, also called microsilica, is a by-product of the fabrication of silicon, silicon metals and ferrosilicon alloys. It is collected in the dedusting system of electric arc furnaces during the metal and alloy production [5]. Silica fumes are very reactive fine pozzolans that can also have a filler effect. They can be blended with Portland cement in binary, ternary or quaternary blended cements.

For producing silicon, the raw material quartz (SiO₂) is reduced to the metallic state Si in the electric arc furnace [5]. During the silicon production process SiO vapors form within the arc. In contact with air, SiO vapors oxidize and form very small SiO₂ vitreous particles that are collected in a dedusting system together with some impurities, such as untransformed quartz particles, carbon particles and graphite

particles. SiO_2 particles are a hundred times finer than Portland cement particles. Silica fumes have a constant chemical composition because the raw materials for producing silicon or ferrosilicon themselves have a constant chemical composition.

During the hydration of silica-fume blended cement, portlandite (calcium hydroxide, $\text{Ca}(\text{OH})_2$) is present at the beginning and reacts in the course of the hydration with silica-fume particles to form C-S-H phases [5].

Advantage of the use of silica fume is decreased bleeding of the concrete mix [5]. Furthermore, silica fume modifies the microstructure of the hydrated cement paste to be denser. Therefore, silica fumes reduce the permeability of the concrete and increase protection of steel reinforcement [1]. The transition zone around coarse aggregates is much more compact compared to pure Portland cement [5].

Also, use of silica fume reduces CO_2 emissions. Approximately 0.432 kg of CO_2 is avoided for every kg of silica fume substituted in cement [1].

Major drawback of silica fume is the high cost because of limited availability of the raw materials [5]. In addition, use of silica fume greatly increases water demand of a mix, which makes it hard to use, especially because many building codes limit water addition to around 6% [1].

2.3.1.5 Calcined clay (Metakaolin)

Calcined clays were used in the earliest produced concretes. Clay or shale is calcined at relatively low temperatures (700-750°C), being dehydrated and its crystalline structure getting disorganized [5]. Active silicon tetrahedra reacts with liberated lime from Portland cement hydration of C_3S and C_2S . Metakaolin ($2\text{SiO}_2 \cdot \text{Al}_2\text{O}_3$) is produced by calcination of kaolin which is a particular clay mineral ($2\text{SiO}_2 \cdot \text{Al}_2\text{O}_3 \cdot 2\text{H}_2\text{O}$).

Metakaolin increases strength, durability and workability, but it also increases the water demand in concrete [5].

2.3.1.6 Rice husk ash

The protecting husk of rice grains against rain represents about 20% of a grain's mass and has a siliceous skeleton [5]. Rice husks can be burned at relatively low temperatures (700-750°C). The resulting rice-husk ashes are essentially composed of vitreous silica but they can also contain unburned carbon. The vitreous silica from rice-husk ashes has excellent pozzolanic properties.

Major drawback of rice-husk ashes is an increased water demand of the fresh concrete mix [5].

2.3.1.7 Other types of supplementary cementitious materials

Natural pozzolans are ancient binders containing a sufficient amount of reactive silica (> 25%), alumina and iron oxide [5]. They are of volcanic origin or sedimentary rocks and harden in the presence of water and lime from Portland cement hydration. Silica reacts with lime to form C-S-H. Use of natural pozzolans decreases the carbon footprint of the cement clinker production.

Another type of SCM is *diatomaceous earth*, also called Tripoli or kiselghur [5]. It is composed of siliceous skeleton of Microalgae and therefore contains very reactive silica. However, use of diatomaceous earth increases water demand due to higher porosity. It is not suitable for blending cement.

Perlite is produced by heating rhyolitic rock, a volcanic silica-rich rock, which is then transformed into a spongy, water absorbing mass [5]. It is used as ultra-lightweight aggregate for production of thermal and acoustic insulating concrete. Drawback of perlite is its high absorptivity that limits use as SCM in concrete.

2.3.2 Alternative cements

2.3.2.1 Calcium aluminate cement (CAC)

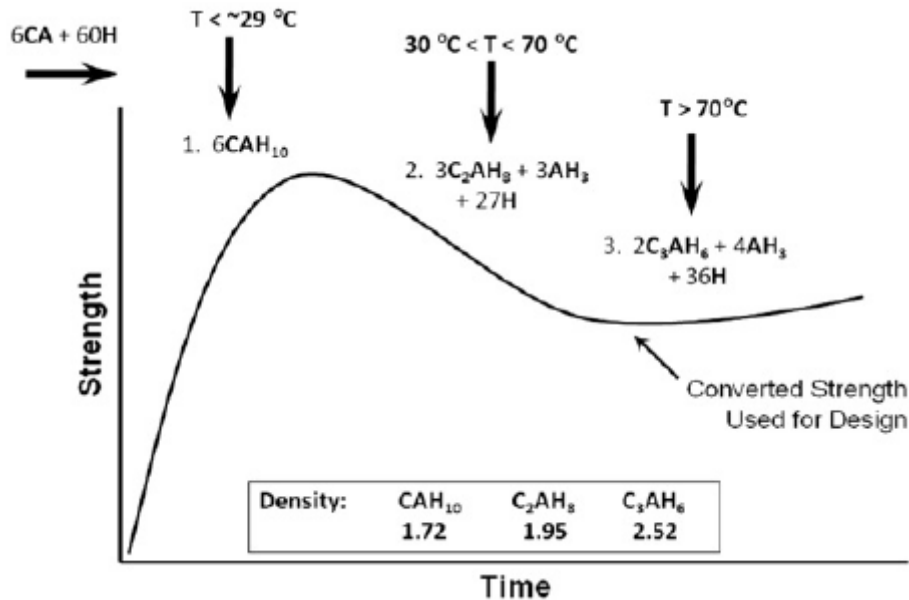
Calcium aluminate cements (CACs) were initially developed to resist sulfate attack and are mainly used in refractory and building chemistry applications nowadays, for example as rapid hardening mortars and floor screeds [18]. They contain primarily monocalcium aluminate (CA) and sometimes small amounts of $C_{12}A_7$, CA_2 , Silica (C_2S , C_2AS) and ferrite.

Like Portland cement, CAC is made in a rotary kiln [1] [5]. But instead of the typical calcium silicates found in clay, bauxite (aluminum ore) is used for mixing with limestone. Afterwards, the mixture is fused into a cement clinker in the same way as Portland cement.

In CAC, the temperature during hydration impacts not only the rate of reaction (as it does during Portland cement hydration), but also the phases that form and the conversion process of those phases, meaning the rate of transition from metastable to stable hydrates [18]. Metastable hydrates CAH_{10} and C_2AH_8 form at low curing temperatures; CAH_{10} being the dominant metastable hydrate that forms at temperatures below $15^\circ C$. As the curing temperature increases to $30^\circ C$, metastable hydrates C_2AH_8 are also formed. The conversion of the metastable hydrates CAH_{10} and C_2AH_8 to stable C_3AH_6 phases is a thermodynamically inevitable process and results in the additional formation of AH_3 gel and release of water. Stable C_3AH_6 hydrates are predominantly formed at higher curing temperatures above $70^\circ C$. *Figure 5* illustrates the conversion process and approximate temperature ranges for the formation of metastable and stable hydrates. It also shows that metastable phases have higher strength than stable phases. During the conversion process, hydrates are

densified and the paste increases porosity, consistently leading to a decrease in strength of the material.

Figure 5 - Schematic of conversion process and approximate temperature ranges for the formation of metastable and stable hydration products [18]



A CAC microconcrete, that is isothermally cured at 20°C in a laboratory, has a relatively dense microstructure filled with CAH₁₀-hydration products [18]. At the same time, large amounts of unreacted CA are present. Nevertheless, the porosity of the CAC microstructure is similar to a high-performance Portland cement. CAC microconcrete, that is cured at higher temperatures (38°C), shows little unreacted CA and high amounts of porosity, consequently resulting in a lower strength for 38°C isothermal curing in comparison to 20°C isothermal curing of CAC-concrete.

Besides influencing the formation of metastable and/or stable phases, the curing temperature also effects early-age volume changes [33]. Under isothermal curing, the formation of metastable CAH₁₀ hydrates resulted in shrinkage of the material, whereas the formation of stable C₃AH₆ phases was linked to expansion.

CAC has many advantages over Portland Cement (PC) [18]: rapid hardening respectively strength gain and enhanced durability through better resistance to sulfate attack, alkali-silica reaction and abrasion (denser microstructure). In addition, CAC production has a lower carbon footprint than PC production.

The major drawback and challenge of CAC is the inevitable conversion process that occurs in hydrated CAC over time [18]: metastable hydrates convert to stable hydrates, increasing the porosity of the microstructure, and consistently reduce strength of the material. Another challenge, that limits widespread use of CACs, is high costs of bauxite, main source of alumina in CAC, due to limited supply. Both of these challenges need to be solved, if CAC should be considered as a viable alternative to Portland cement. Currently the use of pure CACs is limited to refractory applications [1] [5]. The combination of common SCMS, such as GGBS [1], and use of admixtures (chemical accelerators) with CACs, lowers costs and results in no formation of metastable hydrates [18]. Therefore, a conversion process over time does not take place. Nevertheless, more research on the understanding of the CAC hydration reaction kinetics is needed.

2.3.2.2 Calcium sulfoaluminate cement (CSA)

Calcium sulfoaluminate cement (CSA) has been produced and used on an industrial scale in China since the late 1970s [1]. Called the “third cement series”, they are used in China as binders for various applications, for example for concrete in bridges, concrete pipes, precast concrete and low temperature constructions [18]. In Europe and the U.S. however, they are not commonly used.

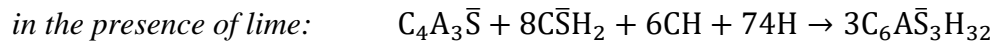
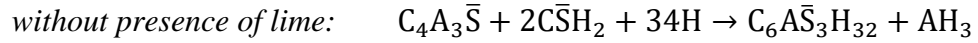
CSAs contain ye’eliminte ($C_4A_3\bar{S}$) as major component (30-70%) that was discovered in the 1960s as a cementitious phase [18]. Furthermore, CSAs contain 30%

Belite (C_2S) and 10-30% ferrite (Calcium Ferro Aluminate). CSA clinkers are produced from using limestone, bauxite and calcium sulfate as raw materials. The clinkers are interground with different levels of calcium sulfate (anhydrite or gypsum) to form different types of CSA, such as rapid-hardening, high strength, expansive or self-stressing and shrinkage compensated cements.

CSA clinkers can be manufactured in conventional Portland cement plants using dry rotary kilns [1]. However, manufacturing CSA requires less heat and therefore less energy because CSA calcination needs lower temperatures (between 1,250-1,350°C) compared to Portland cement.

Two types of CSA clinker can be distinguished [18]: sulfoaluminate belite clinker (containing mainly $C_4A_3\bar{S}$ and C_2S) and ferrialuminate clinker (containing mainly $C_4A_3\bar{S}$, C_4AF and C_2S).

In Portland cement, hydration of C_3S and C_2S result in formation of C-S-H and CH (portlandite); the hydration of C_3A and C_4AF result in formation of ettringite and/or calcium monosulfoaluminate [5]. In CSA cement the hydration of ye'eliminte ($C_4A_3\bar{S}$) and product development are influenced by adding calcium sulfate or calcium hydroxide; the w/c ratio needed for complete hydration is determined by the amount of added calcium sulfate, the maximum being 30% [18]. This is higher compared to Portland cement, where usually 5% of gypsum is added [1]. The addition of gypsum or anhydrite accelerates hydration kinetics [18] and eventually results in the formation of ettringite ($C_6A_3\bar{S}_3H_{32}$) according to the following two reactions (with and without presence of lime) [5]:

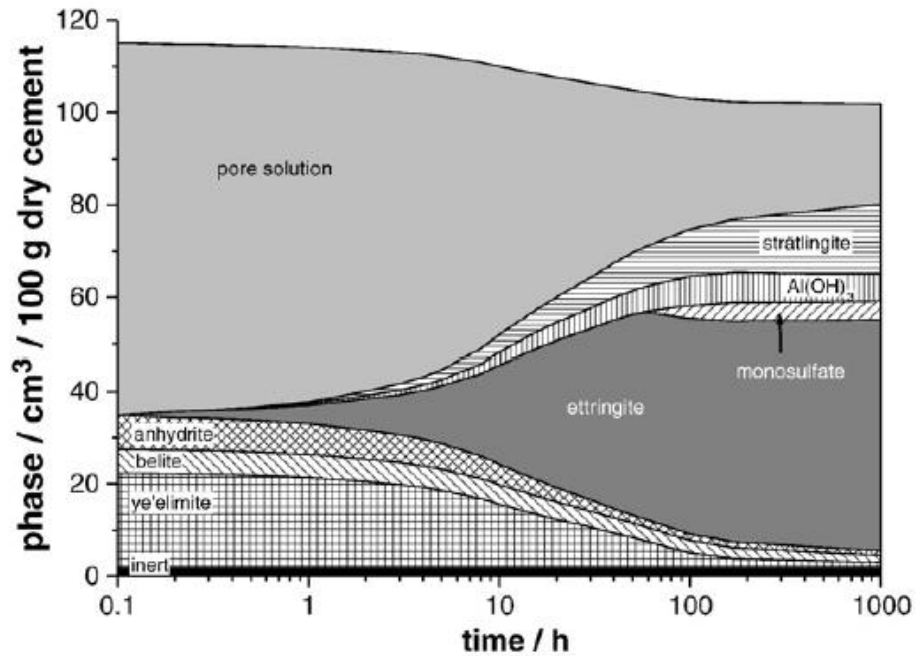


The microstructure of the formed ettringite depends on the presence of lime. Ettringite produced without presence of lime is not expansive and generally has a high early strength [5]. Therefore, it is suitable for shrinkage-resistant and self-stressing cements [3]. On the other hand, ettringite forming in the presence of lime, is expansive [5] and raises the early age strength of cement significantly [3]. This expansion is being used in expansive or shrinkage compensating cements [5].

CSA cements usually contain several hydraulic phases and similar reactions take place [18]. Generally, ye'elimite ($C_4A_3\bar{S}$) is more reactive than accessory phases, such as C_2S , C_4AF and CA . Additional hydration products can form depending on the clinker composition, for example strätlingite (C_2ASH_8), calcium silicate hydrates or CAH_{10} . *Figure 6* shows the phase development of CSA cement – containing C_2S – as a function of hydration time (calculated by thermodynamic modeling).

CSA cements react faster than Portland cement and most of hydration heat evolution occurs between 2-24 h of hydration [18]. The space-filling ettringite needles in combination with the occurrence of monosulfate, aluminum hydroxide, calcium silicate hydrates and/or strätlingite, create a dense microstructure with low porosity.

Figure 6 - Phase development of a CSA cement (w/c = 0.8) as a function of hydration time (calculated by thermodynamic modeling) [34]



The main advantage of CSA is that these cements use the same production process as Portland cement, meaning that CSA clinkers can be manufactured in conventional Portland cement plants using dry rotary kilns [1]. In addition, manufacturing CSA requires a lower firing temperature of 1,250-1,350°C, which is approximately 200°C lower than for Portland cement [18]. Therefore, CSA calcination requires 25% less energy compared to Portland cement manufacturing [1]. Furthermore, CSA clinker is easier to grind, saving even more energy [18].

The CSA clinker itself further reduces the carbon footprint of the material due to a release of only 0.216 g of CO₂ per g of cementing phase when made from limestone, alumina and anhydrite [18]. That is significantly lower compared to Portland cement; Alite (C₃S) releases 0.578 g of CO₂ per g of cementing phase when made from calcite and silica. Overall reduction of CO₂ emissions using CSA cement is about 20% compared to OPC [1].

Other advantages are: high early and late strengths, low pH (low alkalinity) leading to better protection of steel reinforcement from corrosion, low porosity and therefore high impermeability, high resistance to freeze-thaw and against chemical attacks, and durability comparable to OPC [18]. Good strength development and acceptable setting times are achieved by rapid formation of ettringite and variable quantities of amorphous gel phase [1]. Also, ettringite and AFm phases are able to bind heavy metals and are therefore of interest for encapsulating hazardous wastes [18].

Major drawbacks of CSA cement are high costs of bauxite (as for CAC, see section 2.3.2.1) and higher tendency of shrinkage [18]. The theoretical chemical shrinkage of CSA cement is about $11 \text{ cm}^3/\text{g}$ cement after 28 days, whereas Portland cement experiences only $4\text{-}5 \text{ cm}^3/\text{g}$ cement. Furthermore, CSA is very sensitive to the water/cement (w/c) ratio and temperature [3]. It needs a relatively high w/c ratio of typically 0.60 for complete hydration [18]. However, generally a lower w/c of 0.30-0.45 is used, leading to self-desiccation of the cement. Carbonation also depends on the w/c ratio and tends to be more rapid than in Portland cement. Consequence of carbonation is the decomposition of ettringite, causing moderate strength loss.

Even though, production of CSA emits fewer CO_2 emissions due to a lower limestone content and reduced fuel consumption, SO_2 emissions actually increase and are significantly higher compared to Portland cement [3].

Pure CSA cement can be blended with other industrial by-products, such as fly ash, blast furnace slag, phosphogypsum, and others, to reduce the impact of high bauxite costs [1]. Cement manufacturer Lafarge has developed a class of cement

clinkers called Belite-Calcium Sulfoaluminate Ferrite (BCSAF) clinker. BCSAF can also be mixed with gypsum and produced in the same way as Portland cement. Due to the reactivity of the CSA phase, BCSAF cements can have greater early strength compared to Portland-slag cement; they are an intermediate between Portland cements and CSA cements and have the potential to be produced in large volumes.

Nevertheless, high bauxite costs may become less important in the future, if costs for emitting CO₂ into the atmosphere in form of taxes increase [1]. Still, new codes and standards need to be establishment to use greater amounts of CSA cements. Although, use of CSA seems promising, Shi et al. [3] think that CSA cements do not have the potential to lead the transition to the cements of the future.

2.3.2.3 Alkali-activated cement (AAC)

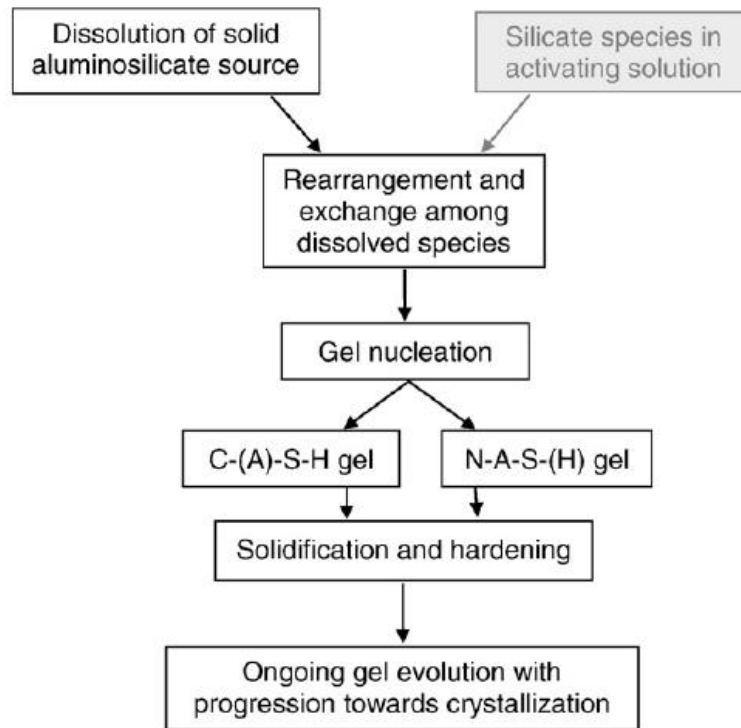
Alkali-activated cements (AACs) are not based on limestone or calcium silicate; instead their chemistry is based on an aluminum-silicon system [1]. The two main components of AAC are a cementitious component and an alkaline activator [3]. AAC cements are composed of sand, water, natural or synthetic pozzolans and the mentioned alkali activator, such as caustic alkalis or alkaline salts. The activators are usually mixed into the water before further mixing to create an alkaline activating solution [1]. Different industrial by-products and waste materials can be used as the cementitious respectively aluminosilicate component. The solid aluminosilicate component can be entirely waste-stream materials which can be used with limited further processing [18]. Materials being used include granulated blast furnace slag, granulated phosphorous slag, steel slag, coal fly ash, volcanic glass, zeolite, metakaolin, silica fume and non-ferrous slag [3].

Alkali activation is the key element of this kind of cement. It is the process of cement particles being initiated to react after the addition of an alkaline solution in the early stages of mixing [2]. This leads to the release of chemical constituents forming a new binding phase and prepares the surface of the particles for bonding. The alkaline solution decomposes the precursors into silicate and aluminum units which then recombine to produce AAC [1].

The alkali activation of aluminosilicates is completely different from the chemical hydration process in Portland cement. The main reaction product of OPC is a C-S-H-type calcium silicate gel ($\text{CaO} \cdot \text{SiO}_2 \cdot n\text{H}_2\text{O}$), whereas the reaction product of AAC is an alkaline aluminosilicate hydrate, N-A-S-H gel ($\text{Na}_2\text{O} \cdot \text{Al}_2\text{O}_3 \cdot 2\text{SiO}_2 \cdot n\text{H}_2\text{O}$) [3]. The chemical composition of the N-A-S-H gel depends on the starting material

(level of available calcium [18]), type of alkaline activator, and curing conditions [3]. The initial formed gel phase will continue to structurally rearrange through extended curing into a thermodynamically more favorable form with increased density [18]. High-temperature curing is not required for high strength development in AACs; alkali-activated binders can set and harden at room temperatures and below [18]. *Figure 7* shows the schematic alkali-activation process, indicating that one or both gel types will be formed, depending on the system composition [35]. A mixture of both C-(A)-S-H and N-A-S-H gel can be obtained through blending low- and high calcium precursors [18].

Figure 7 - Schematic alkali-activation reaction process [35]



Advantages of AACs are: high strength and durability in aggressive environments as result of alkali-activated phases being more insoluble compared to OPC [2]. Also, the setting process is much faster compared to OPC and AAC has a

good heat and fire resistance. Furthermore, AAC has a low environmental impact. Substituting Portland cement in concrete for alkali-activated binders could reduce CO₂ emissions by roughly 80% [18].

The N-A-S-H gel contains low levels of chemically bound water, which brings both advantages (e.g. fire resistance) and disadvantages in performance [18]. One of the drawbacks of low levels of chemically bound water is high permeability. Other general disadvantages of AAC are: sensitivity of activation conditions to amount of added water, handling of concentrated caustic solutions, high costs of activators [18], as well as rapid setting time, shrinkage crack and efflorescence [36]. In addition, good durability of AAC is strongly dependent on adequate curing regimes and the development of a compact and refined pore structure. Carbonation can also be problematic because there is no reservoir of available calcium to provide a pH buffer. Furthermore, common superplasticizers are often degraded by highly alkaline activators and therefore do not enhance the flow behavior of alkali-activated binders. Shen et al. [36] propose adding reactive magnesia cement (see section 2.3.2.5) to prolong setting time and reduce shrinkage of alkali activated cement.

Phair [2] criticizes a lack of characterization techniques, international standards, processing know-how and field data that constrain growth of AACs. He also argues that it is difficult to produce cement with consistent properties because chemical and physical properties of the waste or secondary material can vary. Therefore, Phair [2] calls for the development of test procedures of the constituents before producing the cement. Materials should be assessed for their reactivity prior to usage to determine the amount of required alkali.

AACs were initially discovered by Glukhovsky in the late 1960s, who developed a binder from calcium-free aluminosilicate (clay) and an alkaline metal solution, calling it “soil cement” [3]. Glukhovsky distinguished two groups of binders depending on the composition of the starting materials: group 1 and group 2.

Group 1 describes so-called alkaline-binding systems ($\text{Me}_2\text{O}-\text{Al}_2\text{O}_3-\text{SiO}_2-\text{H}_2\text{O}$) [3]. Cements of group 1 have recently begun to acquire technological significance, although already in 1982 Davidovits managed to produce binders by mixing alkalis with a burnt mix of kaolinite, limestone, and dolomite. He called those binders geopolymers [3] because of their supposed greater network of inorganic polymers [2] respectively their similar structure as organic thermoset polymers [18]. Known trademarks are: Pyrament, Geopolycem and Geopolymite [3].

Glukhovsky’s second group classifies as alkali-alkaline-earth binding systems ($\text{Me}_2\text{O}-\text{MO}-\text{Al}_2\text{O}_3-\text{SiO}_2-\text{H}_2\text{O}$) [3]. Examples of cements belonging to this group are: Scandinavian F-cements and alkali-activated blended cements.

Alkali activated cements can be separated into five categories based on the composition of their cementitious components [3]. The categories are described in the following sections 2.3.2.3.1 to 2.3.2.3.4.

2.3.2.3.1 Alkali-activated slag-based cement

Alkali-activated slag-based cements were mostly researched in the 1980s and 1990s and can be further distinguished into the following categories respectively cementitious systems [3]:

- Alkali-activated blast furnace slag cement
- Alkali-activated phosphorus slag cement
- Alkali-activated blast furnace slag-fly ash
- Alkali-activated blast furnace slag-steel slag

- Alkali-activated blast furnace slag-MGO
- Alkali-activated blast furnace slag based multiple component cement

The main hydration product formed in all categories is a C-S-H gel containing Al in its structure [3]. There is no free $\text{Ca}(\text{OH})_2$.

Advantages of alkali-activated slag cement are: much higher strength than OPC, increased impermeability to water and chlorides (under moist conditions), more resistance to corrosive media and fire, and acceptable carbonation rates [3].

However, performance is governed by the used slag, the dosage of activators and – not surprisingly – the curing conditions [3].

Drawback of alkali-activated slag cements is that conventional water reducers or superplasticizers designed for Portland cements cannot be used [3]. These commercial admixtures have little or no effect on workability and setting times of AA slag cements.

2.3.2.3.2 Alkali-activated pozzolan cement

As already mentioned, Glukhovskiy developed a hydraulic binder by alkali-activation of aluminosilicate materials, calling it “soil cement”. To highlight similarities in the formation of the binder and natural geological materials, and because of the presence of natural mineral analogues in hydration products of the binder, Krivenko [37] named binders of this category “geocements”. Davidovits [38] called these binders “geopolymers” because of their polymeric structure although Phair [2] points out that the term “geopolymers” describes a wide variety of composite materials with limited restrictions on their composition and Al-Si content. Phair [2] criticizes that geopolymer are not polymers in the chemical sense and that the 3-dimensional Al-Si network is not infinite and homogeneously space filling, as it should

be for a glass or polymeric monolithic solid. Geochemists classify only geologically derived organic resins, amorphous organic matter, macromolecules or asphaltens as geopolymers [2].

Alkali-activated pozzolan cements differ from other pozzolanic cements through low hydrate formation, lower porosity, and usage of aluminosilicates as bonding phase [2].

Alkali-activated pozzolan cements can be classified into the following cementitious systems [3]:

- Alkali-activated fly ash cement
- Alkali-activated natural pozzolan cement
- Alkali-activated metakaolin cement
- Alkali-activated soda lime glass cement

2.3.2.3.3 Alkali-activated lime-pozzolan cement/ slag cement

Lime-pozzolan mortars and concretes were discovered around 7000 BC and were among the earliest building materials [3]. The Romans commonly used lime-pozzolan cements for building aqueducts and bridges. However, the invention of Portland cement drastically reduced use of these cements because OPC sets faster and has higher early age strength.

The main hydration reaction product of alkali-activated lime-pozzolan cements is a C-A-S-H gel, although in highly alkaline environments a mixture of C-S-H and N-A-S-H gel is possible [3]. As alkali activators, only alkali hydroxides and alkali sulphates can be used.

Advantages of lime-pozzolan cements are its low cost and long durability [3]. The addition of alkali activators (alkali sulphates) even improves setting and can

double or triple early age strength. However, those cements may still not be strong enough for structural uses.

Alkali-activated lime-pozzolan cements/ slag cements can be classified into the following cementitious systems [3]:

- Alkali-activated lime-natural pozzolan cement
- Alkali-activated lime-fly ash cement
- Alkali-activated lime-metakaolin cement
- Alkali-activated lime-blast furnace slag cement

2.3.2.3.4 Alkali-activated calcium aluminate blended cement

Recent studies deal with the use of calcium aluminate cement (CAC) as source of reactive alumina in the alkali activation of aluminosilicates [3]. Aluminum is very important for the formation of hydrated N-A-S-H gel. Also, a certain amount of reactive aluminum is essential for strength development in the final product. Generally, materials containing reactive alumina are not as plentiful as materials containing high reactive silica.

Requirements for activating aluminosilicates by alkalis are: high solubility of aluminosilicates in basic media and high availability of Al_2O_3 and SiO_2 in the medium [3]. In the alkali-activation of materials with low reactive alumina but high reactive silica content, proportions of under 30% of CAC can be used as source of reactive Al. In this case, CAC does not undergo normal hydration, although it still forms metastable phases. The Al and Ca present in CAC are taken up into the N-A-S-H gel, which is the primary reaction product. In addition, depending on blend proportions and reaction conditions, small amounts of C-A-S-H gel can be obtained.

Alkali-activated calcium aluminate blended cements can be classified into the following cementitious systems [3]:

- Alkali-activated metakaolin/ CAC
- Alkali-activated pozzolan/ CAC
- Alkali-activated fly ash/ CAC

2.3.2.3.5 *Alkali-activated Portland blended cement (hybrid cements)*

One common solution to reduce the carbon footprint of Portland cement is the use of supplementary cementitious materials (SCMs) as cement replacement [3]. Blast furnace slag, phosphorous slag, coal fly ash and natural pozzolans are widely used as SCMs.

However, the use of SCMs in cement respectively concrete lengthens setting times and lowers early age strength [3]. The addition of alkaline activators can improve properties, such as early age strength, of blended Portland cement. Reason for improvement is the enhanced potential pozzolanicity of the SCMs. The compatibility of C-S-H gel and N-A-S-H gel could be important for future applications. Alkaline activation could serve as a link in transition from Portland cement to alternative cements.

Nevertheless, more research is needed on understanding the effect of alkali activators on silicoaluminous materials and the relationship between reaction mechanisms [3]. Many aspects of the reactive process are still poorly understood.

Alkali-activated Portland blended cements can be classified into the following cementitious systems [3]:

- Alkali-activated Portland blast furnace slag cement
- Alkali-activated Portland phosphorus slag cement
- Alkali-activated Portland Fly ash cement
- Alkali-activated Portland blast furnace slag-steel slag cement
- Alkali-activated Portland blast furnace slag-fly ash cement
- Alkali-activated multiple components blended cements

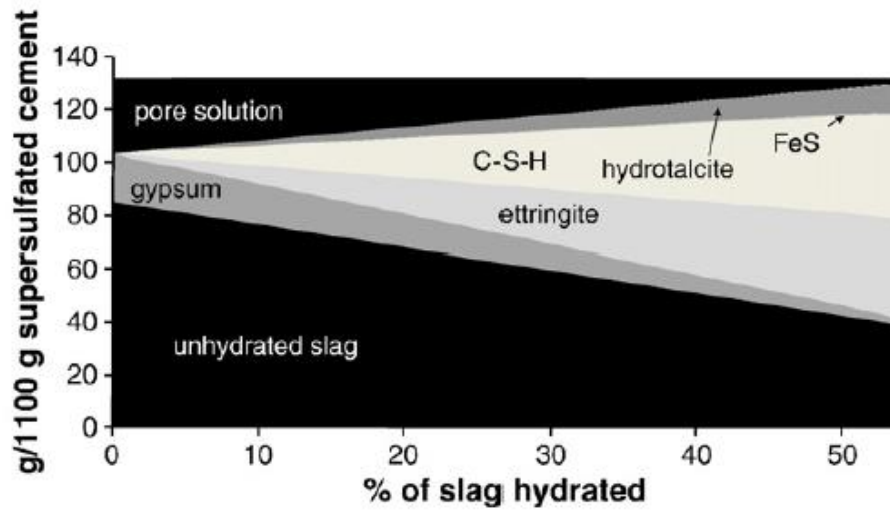
2.3.2.4 Supersulfated cement

Supersulfated cements have promising potential for industrial applications [18]. They can be used for repair mortar applications, such as rendering, injection mortars and masonry mortars. Supersulfated cement binder contains only minor amounts of Portland cement clinker, which mainly functions as alkaline activator. Main constituents are 70-90% ground granulated blast furnace slag, 10-20% calcium sulfate and low quantities (<5%) of an alkaline activator, usually Portland cement clinker. Other possible alkaline activators are calcium hydroxide, potassium hydroxide, and sodium carbonate. Slag used for supersulfated cements should have high CaO, MgO and Al₂O₃ contents.

Hydration of supersulfated cement starts with the dissolution of the slag promoted by the alkaline pore solution [18]. Then, dissolved aluminum, calcium and silicon ions react with the added calcium sulfate to form C-S-H phases, ettringite and minor hydration products, such as AFm phases or hydrotalcite. Generally, the hydration degree of Portland cement is greater than the hydration degree of slags. Samples of hydrated supersulfated cements with blastfurnace slags showed hydration degrees of 15-25% between 28 and 90 days. However, slag chemistry, slag fineness, and the kind and amount of alkaline activator used, strongly influence hydration reaction kinetics. Too high amount of alkaline activator has a significant negative impact on strength development and volume stability of the binder.

Figure 8 shows the phase composition of hydrated supersulfated cement as a function of the hydration degree of the slag; calculated by thermodynamic modeling [39].

Figure 8 - Phase composition of supersulfated slag as a function of slag dissolved [39]



The microstructure of hydrated supersulfated cements is dominated by several μm large ettringite crystals with fibrous or plate-like C-S-H phases in between, occurring on the surface of the slag grains [18]. The ettringite crystals are responsible for setting and early age strength development.

Main advantages of supersulfated cements are their very low heat of hydration and good durability in chemically aggressive environments due to low capillary porosity [18]. They have a good resistance against chlorides, seawater, high sulfate concentrations and frost. In addition, supersulfated cements are made almost entirely from waste materials.

Nevertheless, the mixture composition is very sensitive to the chemical composition of the slag and too high amounts of alkaline activator decrease strength of the binder [18]. Other disadvantages are longer setting times compared to OPC, as well as slow and poor early age strength development. Furthermore, carbonation is an issue, especially in combination with insufficient curing. It causes decomposition of ettringite, leading to an increase in capillary porosity with the result of a dusting of the

concrete skin. Another drawback is the high cost and limited availability of the materials [1].

2.3.2.5 Magnesia cement

Magnesia cement, also referred to as water-activated-magnesium-oxide based cement, reactive magnesium oxide cement or Sorel cement, is widely regarded as a promising low carbon cement [36]. It is considered ancient cement because cement similar to modern magnesia cement was used to build the Great Chinese Wall [1]. Also, it was commonly used in the Soviet Union [5].

Magnesia cement consists of normal hydraulic cement, such as Portland cement, reactive magnesium oxide, and a certain amount of pozzolans, for example fly ash [36]. The key constituent of magnesia cement is reactive magnesium oxide (MgO), also known as caustic calcined magnesia, caustic magnesia or CCM [1]. It is produced by burning magnesite in a kiln at relatively low temperatures below 750°C. Magnesite is an ore composed of 90% MgCO₃ (magnesite), 7% SiO₂ and 3% CaCO₃.

Hydration of reactive magnesia in magnesia cement leads to transformation into the main hydration product brucite (Mg(OH)₂, magnesium hydroxide) [36]. Brucite forms a fibrous layered structure [36] and – when exposed to the atmosphere – carbonates to magnesite (MgCO₃) [1].

Magnesia cement is considered an alternative to Portland cement because magnesium and calcium both belong to the same elemental group and have similar high abundances [36]. Therefore, magnesium-based cement could be a substitute for calcium-based Portland cement.

Main advantage of magnesia cement is its permeability, which makes it useful for heat regulation and control in buildings, especially in warm climates [1]. That is

the reason for magnesia cement also being referred to as “living cement”. Imbabi et al. [1] claim that production of magnesia cement requires 30% less energy compared to OPC production. Therefore, magnesia cement is supposed to have a lower environmental impact due to burning reactive magnesia at lower temperatures and – more importantly – subsequent reabsorption of CO₂ by the main hydration product magnesium hydroxide (brucite) [36].

Disadvantage is that magnesium oxide is not as available as calcium sourced from limestone making production more expensive [1]. Also, the addition of magnesia in Portland cement to produce magnesia cement, create a more complex material system which is more difficult to recycle or reuse [36].

However, Shen et al. [36] carried out a life cycle carbon emission study on magnesia cement in comparison with Portland cement. The results show that magnesia cement is not as environmentally friendly as it is widely believed and actually has a bigger life cycle carbon footprint than Portland cement. According to the authors of the study, magnesia cement production emits 79-395 kg/ton more direct CO₂ than Portland cement production. In addition, thermodynamic analysis concludes that magnesia cement cannot absorb CO₂ from the environment during its service life. On the other hand, Portland cement can absorb more than 250 kg CO₂ per ton. Also, magnesia cement supposedly has a lower performance than OPC: reactive magnesia cement has a 3 times lower strength than Portland cement. Another issue is that the pH value of the magnesia cement paste is too low to protect steel reinforcement in concrete from corrosion.

Although it is true that burning temperatures for calcining magnesite in the kiln are much lower, the energy consumption of reactive magnesia production is even higher than energy consumption of Portland cement clinker [36]. Magnesium carbonate supposedly has a higher loss on ignition than calcium carbonate of Portland cement. This leads to usage of more raw materials and consequently emittance of more raw material CO₂ than OPC. The above-mentioned study lists the following sources of CO₂ emissions for magnesia cement: 1.1 tons of raw material CO₂ and 0.5 tons of fuel-derived CO₂, adding up to 1.6 tons of CO₂ per ton of produced reactive magnesia.

Furthermore, there is no proof that magnesia cement reabsorbs environment CO₂ [36]. Thermodynamic analysis shows that magnesia cement cannot absorb CO₂, whereas at the same time, Portland cement can absorb approximately 250 kg of CO₂ per ton of cement.

Therefore, Shen et al. [36] conclude that magnesia cement is not a promising low carbon cement. Decomposition of magnesite produced more CO₂ emissions than decomposition of calcium carbonate of Portland cement. In addition, fuel-derived CO₂ emissions are higher. The overall carbon footprint of magnesia cement is bigger than the one of Portland cement.

Shen et al. [36] claim that Portland cement blended with waste-derived supplementary cementitious materials (SCMs), for example fly ash or blast furnace slag, have greater environmental benefits and better performance than magnesia cement. The most promising low carbon cement is alkali activated cement (see section 2.3.2.3) because it is mainly made with industrial waste products and requires only a cement milling step

as preparation [3]. Reactive magnesia cement could contribute to improve alkali activated cement by prolonging setting time and reducing shrinkage when added [36].

Different companies have developed and merchandised types of magnesia cement, for example Grancrete (US Gypsum), TecEco cements (TecEco) and Novacem (Novacem Ltd.) [1]. Novacem is a blend of magnesium oxide and hydrated magnesium carbonates. It is composed of magnesium silicates mixed with water and special additives [36]. It claims to be a carbon negative product absorbing more CO₂ than it produces during its manufacturing process. Hydrated Novacem cement supposedly absorbs respectively emits -100 to +320 kg CO₂ per ton of produced cement. Furthermore, strength development is supposed to be similar to OPC.

Novacem is made of magnesium silicate burned at low temperatures (700°C), emitting less fuel-derived CO₂ emissions and almost no raw material CO₂ [36]. Therefore, it has a lower carbon footprint than Portland cement. Drawback of Novacem is that its hydration products cannot react rapidly with SCMs preventing development of a blended Portland cement with Novacem.

The 2010 MIT Technology Review ranked Novacem to be among the top ten emerging technologies [1] [40]. Despite the material's promise, the Novacem company could not attract investors and raise enough funds [30]. The company sold its intellectual property to Calix Limited, an Australian technology company, and was liquidated in September 2012.

2.3.2.6 Sequestered carbon cement

A Californian company called Calera Corporation has developed a cement that mimics natural marine cement found in coral reefs [1]. When making their shells and reefs, coral take the calcium and magnesium in seawater and use it to form carbonates

at normal temperatures and pressures [41]. Calera cement is produced by filtering captured CO₂ gas (e.g. from power or cement plants) through sea water. Calcium and magnesium from the sea water react with CO₂ and produce cement [1]. Calera calls the production process “Mineralization by Aqueous Precipitation” [42]. Calera cement is of snow white color, air permeable and has higher strength than regular OPC [1]. The company is running a pilot plant, fueled with natural gas that produces up to two tons of cement from CO₂ and industrial waste per day, sequestering about 400 kg of CO₂ in each ton of the material [30]. California Department of Transport is interested in using Calera cement for building sidewalks respectively streets [1]. However, Calera Corporation meanwhile finds it more profitable to use the material to make fiber cement boards used in bathroom tile backing or exterior siding [30].

Other companies using similar ideas are Carbon Sciences and Carbon Sense Solutions [41]. Carbon Sciences plans to use flue gas and leftover water from mining operations, so-called mine slime, often containing magnesium and calcium, to create cements similar to Calera cement. Carbon Sense Solutions wants to accelerate the natural process of cement absorbing CO₂ by exposing a fresh concrete batch to flue gas.

2.3.2.7 Carbonate binders

Carbonate binders, also calcium carbonate binders, could have a great impact on effectively reducing the carbon footprint of the cement and construction industry. Calcium carbonate binder can be produced through the reaction of a Ca(OH)₂ source, e.g. hydrated lime, and CO₂ [43]. At the same time, carbonate binders form over thousands of years in nature. Examples of naturally occurring calcium and/or magnesium carbonate binders are: limestone, beachrock, dolomite, magnesite, and

marble. These geological formations have a compacted, interlocked and well-developed crystalline calcium and/or magnesium carbonate microstructure. Thus, these formations often have superior chemical and physical properties. Secondary carbonate rocks, formed by mineral trapping, have a high compressive and tensile strength, indicating that mineral carbonation can be used to form sustainable binders [44]. To develop artificial carbonate binders with similar microstructures, knowledge about key characteristics can be drawn from the geological evolution of carbonate binders in nature [43].

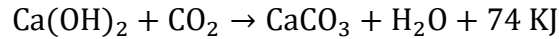
Carbonation of a cementitious material occurs naturally but the reaction is very slow due to a “low” concentration of CO₂ in the atmosphere [45]. Exposing the material to pressurized CO₂ leads to a faster CO₂ uptake, microstructure densification and rapid compressive strength gain.

By using industrial by-products, such as metallic iron powder waste (see section 2.3.2.7.2), subjecting it to a pressurized CO₂ curing regime, and replacing Portland cement, the carbon footprint of cementitious materials could be significantly lowered [45].

2.3.2.7.1 Lime carbonation

One way of obtaining artificial calcium carbonate is through the so-called lime carbonation process. Calcium carbonate is obtained through the reaction of calcium hydroxide, i.e. hydrated lime (Ca(OH)₂), and CO₂, as it occurs during carbonation of cement [43]. Cement hydrates (calcium hydroxide and calcium silicate hydrates) react with CO₂ and form calcium carbonate that improves durability of the concrete.

The exothermic carbonation reaction starts with a CO₂ diffusion process, followed by the formation of calcium carbonate (CaCO₃) [43]. The chemical reaction for carbonation of hydrated lime is as follows:



The presence of water is important to the carbonation process because it occurs through a dissolution-precipitation mechanism [43]. However, the diffusion of CO₂ in water is much slower than in air. Therefore, cement saturated with water slows down the carbonation reaction. Initial porosity and water content influence the rate of CO₂ diffusion because the newly formed CaCO₃ is accommodated in the internal pores, resulting in reduced permeability of the material. In addition, the formation of CaCO₃ depends on the amount and solubility of available Ca(OH)₂ and on the CO₂ concentration. Increasing CO₂ concentration and pressure increases the dissolution of CO₂ in water and therefore increases the amount of Ca(OH)₂ conversion and depth of carbonation. However, both the rate of carbonate formation and CO₂ diffusion decrease with increasing compaction pressure due to decreasing porosity of the hydrated lime. The solubility of Ca(OH)₂ and CO₂ in water decreases with increasing temperature. Other factors, such as relative humidity and thickness of the specimen, also influence the rate of carbonation of hydrated lime. Nonetheless, it should be pointed out that not the amount of Ca(OH)₂ controls the strength of the binder but rather the morphology (crystalline structure).

2.3.2.7.2 Iron carbonation

Das et al. [44] developed a sustainable novel binder that utilizes the chemistry of so-called iron carbonation that resorts to the essential idea of basic mineral carbonation. However, Das et al. [44] take this concept one step further by carbonating

metallic waste iron powder instead of the already mentioned hydrated lime (see section 2.3.2.7.1).

Subject of the present paper is to test the performance of this novel sustainable concrete under extreme dynamic loading conditions in a so-called split Hopkinson pressure bar system to indicate durability under extreme dynamic stresses.

Determination of the dynamic stress-strain curve of a material is one of the objectives of an SHPB test [46]. From the stress-strain curve, mechanical properties, such as dynamic failure strength and dynamic Young's modulus, can be derived.

For more detailed information about Iron Carbonate please refer to chapter 3. For more detailed information about the split Hopkinson pressure bar experiment please refer to chapter 4.

2.3.2.7.3 *Portland cement-fly ash-magnesia blend carbonation*

Mo et al. [45] produced a supposedly low-carbon cementitious binder by blending Portland cement with fly ash (see section 2.3.1.1) and reactive magnesia (see section 2.3.2.5), and exposing it to a pressurized CO₂ curing regime to accelerate carbonation [45]. Carbonating the MgO-containing cement blend not only decrease CO₂ emissions but also enhances the microstructure of the carbonate products (CaCO₃ and/or (Ca, MgCO₃) and improves mechanical properties.

Up to 60% of Portland cement was replaced by fly ash and reactive MgO [45]. According to the authors of the study, the combination of 20% MgO and 40% fly ash has the lowest carbon footprint (562.8 kg CO₂ per ton of cement blend). CO₂ emissions of the cement paste decrease with increasing content of fly ash but increase with increasing MgO content.

2.3.2.8 Other types of cementitious systems

Besides the more common and promising alternative cements presented in this report, numerous other alternative binders exist but are only produced in small quantities. These alternative cements will be briefly described in this section.

One new hydraulic binder is an improved version of supersulfated cement (see section 2.3.2.4) called “0 per cent Portland cement binder” [5]. This type of cement uses no Portland cement but instead anhydrite and some alkali rich cement kiln dust (CKD). The binding properties rely on the formation of massive and very stable ettringite crystals.

Another new type of hydraulic binder is a mixture of Portland cement and CalCiFrit (High Fluoride and aluminosilicates) that is obtained by processing spent pot liner (SPL) from the aluminum industry [5]. Pots are electrolytic cells in which aluminum is extracted from alumina. Those cells have to be replaced every 6 to 8 years. They are composed of refractory bricks, graphite, cryolite and usually contain SiO_2 , Al_2O_3 , CaO , Na_2O and F. However, SPLs are classified as hazardous waste because they also contain cyanids. The company NovaPb has developed a process to transform SPL into non-hazardous slag or binder that can be blended with Portland cement.

A ternary blended cement that contains two industrial by-products is also a new type of binder. It is composed of 70% Portland cement, 20% CalCiFrit, 5% silica fume and 5% gypsum [5].

Numerous cements have been developed but are only used in very small quantities. Those cementitious materials include – amongst others – cement based on: zinc oxychloride, aluminum oxychloride, silicophosphate, sodium metaphosphate,

calcium phosphate, zinc phosphate, magnesium phosphate, ammonium phosphate and magnesia, ammonium tripolyphosphate and magnesia, aluminosilicates and magnesia [5].

Alinite is also an alternative cement that can substitute up to 20% of Portland cement [5]. It is produced by introducing calcium chloride as a source of lime in the raw meal. Main advantage of alinite is its relatively low processing temperature (1150°C) compared to OPC.

Another alternative cement similar to alinite is so-called belinite [5]. It is produced by introducing magnesia in the raw meal.

2.4 Specifying alternative binders

There are two different types of specifications for building materials, namely prescriptive and performance-based specifications [18]. Other than performance-based regulations, prescriptive standards prevent the use of alternative, non-Portland cement binders. However, both types of regulations are included within the ASTM standards. ASTM C150 has prescriptive standards, whereas ASTM C1157 has performance-based standards but is not widely accepted among state regulatory authorities.

The RILEM Technical Committee 224-AAM develops international standards for non-Portland cements with a focus on alkali-activated binders [18]. The Committee suggests using performance instead of chemistry as primary criterion for acceptance of a binder type.

Composition-based (prescriptive) standard mix specifications should be replaced by performance-based specifications [2]. Challenge for introducing such standards is the development of testing regimes to test and validate a wide range of binders [5], often very different from common OPC binders. Aïtcin [5] calls for tests being “restrictive enough to ensure good performance of materials when they are mixed and placed under less-controlled real-world conditions”.

2.5 Preliminary Summary and Conclusion

The Portland cement production is responsible for roughly 3% of the global anthropogenic greenhouse gas emissions and 5-7% of all anthropogenic CO₂ emissions, making the cement industry a heavy polluter. Many different approaches try to make cement manufacture more sustainable and reduce the carbon footprint of OPC.

The International Energy Agency (IEA) [26] developed a technology roadmap for the cement industry and pointed out ways of CO₂ emission reduction. According to them, the following actions should be taken to reduce the carbon footprint of cement: improving thermal and electric efficiency of the cement plant, use of industrial process wastes (use of alternative, less carbon intensive fuels in the production process and substitution of carbon-intensive clinker with low-carbon materials having cementitious properties), and use of carbon capture and storage technologies.

The existing technologies (fuel efficiency, alternative fuels, clinker substitution) would enable reaching only half of the IEA's CO₂ reduction goal by 2050. To fulfil the other half of the reduction, new CCS-technologies, capturing and storing CO₂ emissions from the production process, are necessary. By now, the most powerful approach, according to the IEA, is the use of alternative fuels.

Other general approaches for CO₂ reduction are: use of chemical admixtures, recycling concrete, and nanoengineering. The latter focuses on increasing the strength of a cement-based concrete on the nanoscale level through increased packing-density. An increase in strength would result in a decrease of its environmental impact because less material would be needed.

The modification of the cement recipe itself is another major concept for improved sustainability. Main possibilities are blending OPC with so-called supplementary cementitious materials (SCMs), thus reducing the amount of OPC clinker, or developing new, alternative binders that can be manufactured at lower kiln temperatures.

SCMs are usually industrial by-products that would be landfilled otherwise. Common SCMs for OPC-based blended cement include fly ash, ground granulated blast furnace slag (GGBS), ground limestone, silica fume, metakaolin and others. Silica- or alumino-silicate-rich SCMs react with calcium hydroxide (CH) from OPC to form C-S-H phases. The carbon footprint of blended cement is much lower than of pure OPC due to lower processing temperatures of most SCMs and reduced OPC clinker content.

Alternative binders include calcium aluminate cement (CAC), calcium sulfoaluminate cement (CSA), alkali-activated cement (AAC), supersulfated cement, magnesia cement, sequestered carbon cement, and carbonate binders.

CAC contains primarily monocalcium aluminate (CA) and like Portland cement, it is made in a rotary kiln. But instead of the typical calcium silicates found in clay, bauxite is used for mixing with limestone. CAC has many advantages over Portland Cement (PC): rapid hardening respectively strength gain and enhanced durability through better resistance to sulfate attack, alkali-silica reaction and abrasion (denser microstructure). In addition, CAC production has a lower carbon footprint than PC production. Major drawback and challenge of CAC is the inevitable conversion process that occurs in hydrated CAC over time: metastable hydrates

convert to stable hydrates, increasing the porosity of the microstructure and consistently reduce strength of the material.

CSA contains ye'eliminte ($C_4A_3\bar{S}$) as major component and cementitious phase. They can be manufactured in conventional Portland cement plants. However, manufacturing CSA requires less heat and therefore 25% less energy because CSA calcination needs lower temperatures compared to OPC and reduces CO_2 emissions about 20%. Good strength development, durability and acceptable setting times are achieved by rapid formation of ettringite and variable quantities of amorphous gel phase. Major drawbacks of CSA cement are high costs of bauxite, higher tendency of shrinkage and increased SO_2 emissions.

AAC is not based on limestone or calcium silicate, instead their chemistry is based on an aluminum-silicon system. The two main components of AAC are a cementitious component and an alkaline activator. Different industrial by-products and waste materials, e.g. granulated blast furnace slag, fly ash, silica fume and metakaolin, can be used as the cementitious respectively aluminosilicate component. Alkali activation is the key element of this kind of cement. The alkaline solution decomposes the precursors into silicate and aluminum units which then re-combine to produce an alkaline aluminosilicate hydrate, N-A-S-H gel.

Advantages of AACs are: high strength, durability in aggressive environments, faster setting process, good heat and fire resistance, and a low environmental impact. Substituting Portland cement in concrete for alkali-activated binders could reduce CO_2 emissions by roughly 80%. Drawbacks are high permeability, sensitivity of activation conditions and possible degradation of common superplasticizers.

Supersulfated cement contains ground granulated blast furnace slag as main constituents, calcium sulfate and low quantities (<5%) of an alkaline activator, usually Portland cement clinker. By the alkaline pore solution dissolved aluminum, calcium and silicon ions react with the added calcium sulfate to form C-S-H phases, ettringite and minor hydration products.

Main advantages of supersulfated cements are their very low heat of hydration, good durability in chemically aggressive environments and good resistance against chlorides, seawater, high sulfate concentrations. In addition, supersulfated cements are made almost entirely from waste materials. Drawback is sensitivity of the mixture to chemical composition of the slag and to too high amounts of alkaline activator. Other disadvantages are longer setting times compared to OPC, and slow and poor early age strength development, as well as carbonation causing decomposition of ettringite.

Magnesia cement consists of normal hydraulic cement, such as Portland cement, reactive magnesium oxide, and a certain amount of pozzolans, for example fly ash. The key constituent is reactive magnesium oxide (MgO). Hydration of reactive magnesia leads to transformation into the main hydration product brucite ($\text{Mg}(\text{OH})_2$) which carbonates to magnesite (MgCO_3). Main advantage of magnesia cement is its permeability and a supposedly lower environmental impact due to burning reactive magnesia at lower temperatures and – more importantly – subsequent reabsorption of CO_2 by the main hydration product brucite. Drawback is the cost of magnesium oxide.

However, a life cycle carbon emission study shows that magnesia cement is not as environmentally friendly as it is widely believed and actually has a bigger life

cycle carbon footprint than Portland cement. Furthermore, the study claims that there is no proof that magnesia cement reabsorbs environment CO₂.

Calcium carbonate binder can be produced through the reaction of a Ca(OH)₂ source, e.g. hydrated lime, and CO₂, as it occurs during natural carbonation of cement. Exposing the material to an artificial pressurized CO₂ environment leads to a faster CO₂ uptake, microstructure densification and rapid compressive strength gain. Main reaction product is calcium carbonate that reduces permeability and thus improves durability of concrete.

The iron carbonated binder is produced through mixing metallic iron powder waste containing metallic iron together with fly ash, limestone powder, metakaolin and an organic reducing agent, to react with aqueous CO₂ in a pressurized curing regime. The iron carbonation reaction results in the formation of complex iron carbonates that have binding capabilities and mechanical properties comparable to OPC. The use of iron carbonated binders has strong environmental benefits because it consumes and sequesters CO₂ from GHG-emitting industries.

This *chapter 2* covers many interesting and promising approaches to reduce the carbon footprint of the cement production. So far, the most promising approaches seem to be increased use of SCMs like fly ash and the use of alkali-activated binders, as well as carbonate binders such as Iron Carbonate. In addition, understanding the nanostructure and increasing the packing density through nanoengineering and adjusted Ca/Si molar ratio, seems promising. Nonetheless, the author thinks that there is not just one way to go. In fact, a combination of improved cement plant efficiency, use of alternative fuels, use of carbon capture and storage technologies, together with

the use of SCMs and/or alkali-activated and carbonate binders, supported by findings of the nanoengineering concept, could be the solution for lowering the overall carbon footprint of cement production. In addition, primary criterion for specifying binders should change from a prescriptive towards a performance-based standard to facilitate the development and acceptance of new alternative binders such as Iron Carbonate.

For that, a rethinking by many protagonists is needed, such as customers, cement producers, cement lobbies, governments, and many more. Understandably, cement producers fear high investments and pushing off their main and best-selling product for unproven alternative binders. Therefore, the individual governments and the whole international community must react by introducing stricter CO₂ and GHG emittance rights, while at the same time offering incentives for production of sustainable binders. The author realizes that this will probably not happen in the near future due to egoistic interests of the individual governments, i.e. the U.S. government, that do not want restrict economic growth in their own countries. Also, many heavy polluters are developing countries such as China and India, for whom protecting the environment is not their priority. The author also wants to point out that protecting the environment is not so much about a potential climate change but about preserving the world we know for following generations and simply respecting our surrounding natural environment.

3 Iron Carbonate

3.1 Introduction

Das et al. [44] developed a novel carbon-negative sustainable binder that utilizes the chemistry of iron carbonation. Metallic iron powder waste is produced as a by-product during steel manufacturing in electric arc furnaces and shot-blasting operations of structural steel sections and generally landfilled at great economic and environmental costs. Several million tons of iron powder waste are landfilled all over the world nowadays, as it seems not economically feasible – yet – to retrieve iron from the disposed dust.

The use of iron carbonated binders has strong environmental benefits because it consumes and (chemically) sequesters CO₂ from GHG-emitting industries [44]. The sequestration is permanent as opposed to often leaking physical trapping methods. Iron Carbonate could replace cementitious binders and thus reduce the overall production of Portland cement, resulting in a significant reduction of the carbon footprint of the cement and building industry. At the same time, iron carbonated binders have good mechanical properties similar to OPC.

Drawback of the material is the slow rate of reaction product formation – which could potentially be solved by using organic dissolution agents that enhance the reaction rate [44]. Another disadvantage is the sensitivity of the reaction products to the starting material composition.

Objective of this thesis is the testing of Iron Carbonate (IC) specimens in a split Hopkinson pressure bar system to simulate extreme dynamic loading conditions. Determination of the dynamic stress-strain curve of a material is one of the goals of an

SHPB test [46]. From the stress-strain curve, mechanical properties, such as dynamic failure strength and dynamic Young's modulus, can be derived.

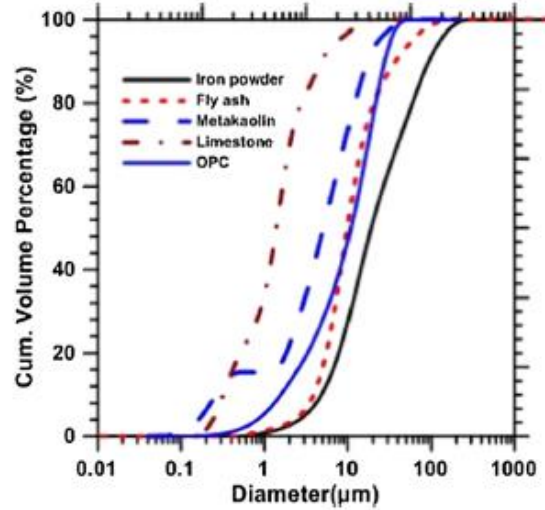
The IC samples were manufactured by Dr. David Stone, a former colleague of Dr. Das at Arizona State University, and his company Iron Shell LLC, Tucson, AZ.

3.2 Composition and carbonation reaction

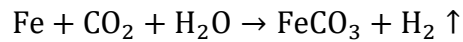
The iron powder consists of 88% Fe, around 10% of O and small quantities Cu, Mn and Ca [44]. Nonetheless, carbonation efficiency and mechanical properties are very sensitive to the starting material composition. Silica- and alumina-containing additives that are also common to Portland cement concrete, such as Class F fly ash (ASTM C618 conform), limestone powder (ASTM C568 conform) and metakaolin (ASTM C618 conform), facilitate iron dissolution and beneficially effect later-age properties. Thereby, fly ash is a source of silica, limestone powder provides nucleation sites, and metakaolin provides cohesiveness and keeps the consistency of the mixture. Metakaolin also minimizes the water demand. However, a too high content of metakaolin decreases compressive strength. It should be pointed out that iron powder is coarser than all the other components (see *Figure 9*).

To produce the binder, all constituents (iron powder, fly ash, limestone powder, metakaolin, sodium carbonate, sodium bicarbonate, powdered organic reducing agent, (weak organic acid)) are dry mixed together before water is added [44]. It is important to note that water is added to obtain a uniform cohesive mixture and to ensure workability. Water is reduced in the chemical reactions but does not form part of the carbonated binder because the carbonation process of iron does not incorporate water.

Figure 9 - Particle size distribution of metallic iron powder, OPC, fly ash, metakaolin, and limestone powder [47]



After Iron Carbonate is filled into molds, the specimens are demolded immediately and exposed to a pressurized CO₂ regime, e.g. a plastic bag filled with 100% CO₂ that leads to slow external diffusion [44]. Exposing the material to CO₂ results in a faster CO₂ uptake, microstructure densification and rapid compressive strength gain [45]. The carbonation of iron particles results in the formation of complex iron carbonates (FeCO₃) that have binding capabilities and mechanical properties comparable to OPC [44]. The chemical reaction of metallic iron is as follows:



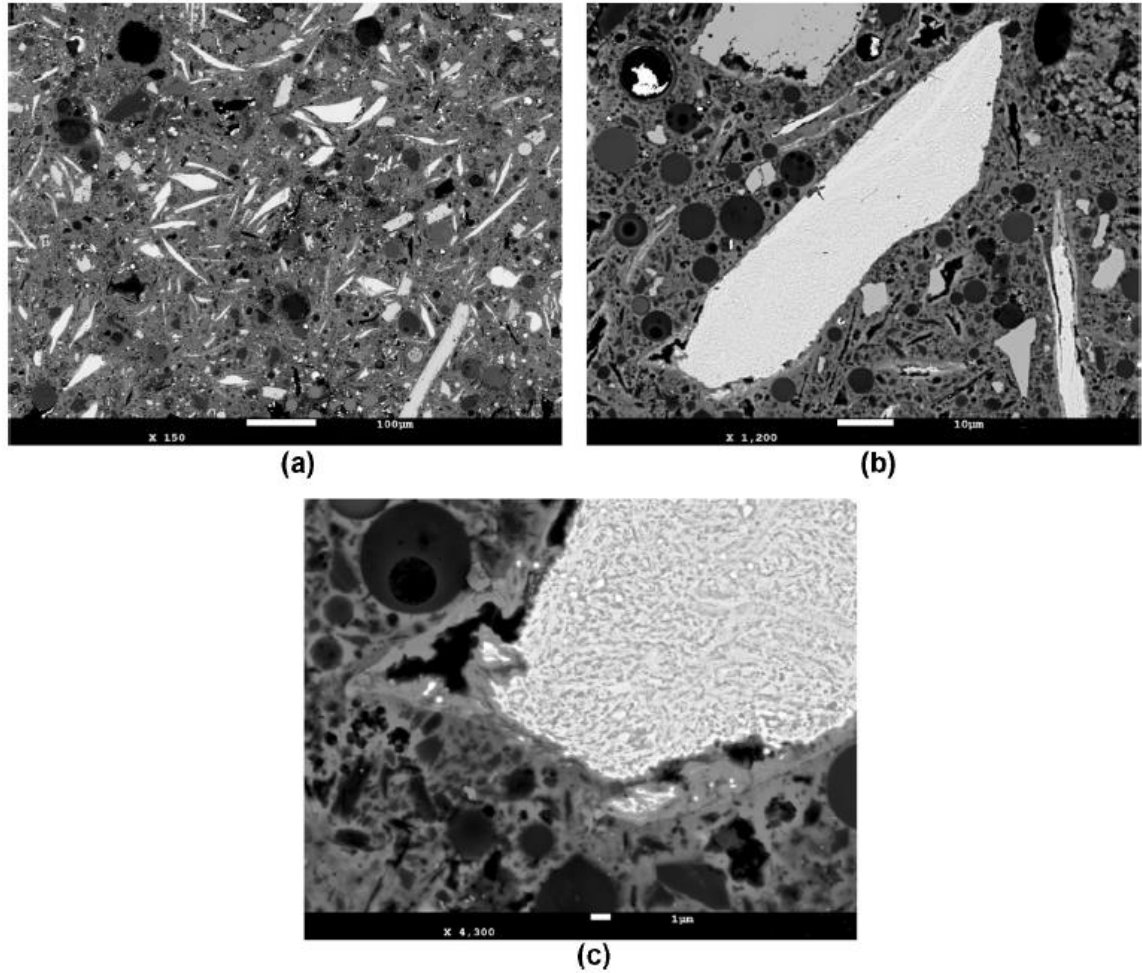
During the synthesis of Iron Carbonate, only a small fraction of the metallic iron powder is carbonated, which results in the presence of large amounts of residual metallic powder in the microstructure that increases the toughness of the binder compared to other OPC-based binders [48].

3.3 Microstructure

The microstructure is heterogenous and contains angular iron particles, spherical fly ash particles and other porous reaction products [49]. The dense reaction products (grey phases in the microstructure (see *Figure 10*)) are formed from the carbonation of smaller iron particles and their complexation with the other minor ingredients in the mixture [48].

Figure 10 - Microstructure of iron-based binder:

(a) lower magnification (150x) image (scale bar corresponds to 100 μm); **(b)** higher magnification (1200x) image showing an elongated iron particle and the surrounding regions (scale bar corresponds to 10 μm); and **(c)** showing dissolution of Fe^{+2} from iron particle into the surrounding matrix (4300x) (scale bar corresponds to 1 μm) [48]



The final carbonated binder reaction product is an iron-oxalate-carbonate complex incorporating silica. It contains iron, calcium, aluminum, and silicon. Higher carbonation duration results in more reaction product formation and increased density because the reaction products fill the pores of the paste. The reaction products are passive and stable when exposed to air and do not deteriorate.

This research study takes a step further to enhance the carbonation efficiency by the following two approaches: (i) supplementing the existing external carbonation with a suitable internal carbonation process at the binder scale (sodium carbonate (Na_2CO_3), sodium bicarbonate (NaHCO_3) and organic acid trigger a CO_2 releasing chemical reaction within the binder itself); (ii) tuning the porosity at concrete scale by using optimal aggregate gradation in order to provide easier access to CO_2 into the material structure. It is anticipated that such an effort will enable formation of a uniform material structure in large-scale structural components and develop opportunities where an efficient high-performance multifunctional material (akin to Portland cement concretes) emerges to satisfy the growing demand for ecologically friendly construction materials.

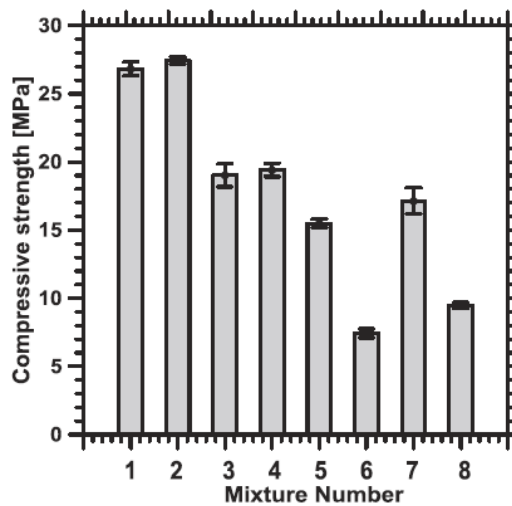
3.4 Material properties

Material properties of Iron Carbonate are equal or better in comparison to conventional, non-sustainable OPC-based binders. The metallic particulate phase incorporated in the binders' microstructure increases the toughness of Iron Carbonate because of the energy dissipation by plastic deformation of the unreacted and elongated iron particles which are strong and ductile [48]. In addition, the matrix contains other additives including harder fly ash particles, softer limestone particles,

and ductile clayey phases which significantly influence the overall fracture performance of the novel sustainable binder.

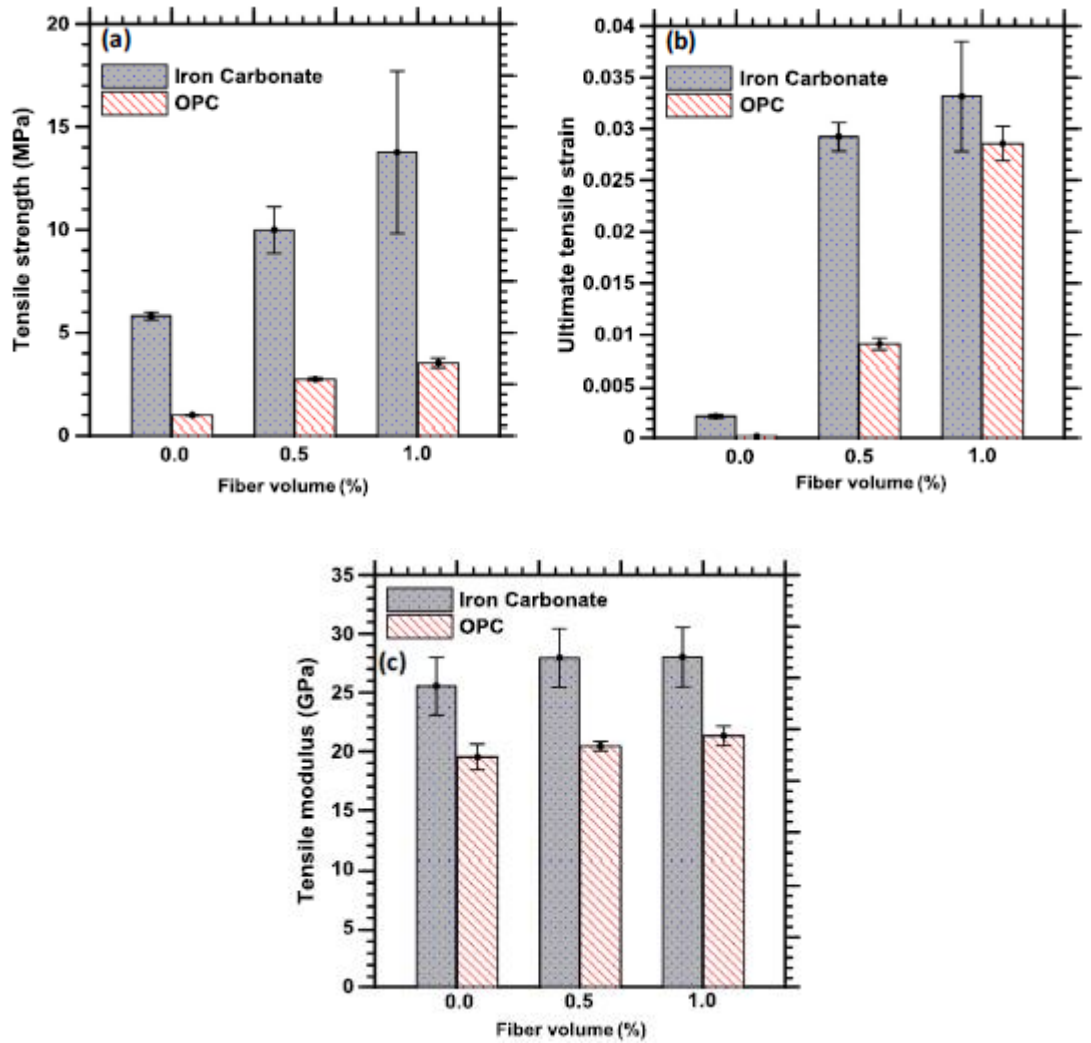
Iron Carbonate binders can attain compressive strengths between 35–40 MPa which is the upper limit for achievable compressive strength of OPC-based concretes [47]. However, the compressive strength could be partially restricted by the presence of higher amounts of larger pores (average size > 0.2 μm) even though the total pore volumes are comparable to OPC-based binders [48]. Earlier tests with less refined mixtures and curing methods already indicated an enhanced compressive strength behavior (see *Figure 11*).

Figure 11 - Compressive strengths of the iron carbonate mixtures (exposure condition: 3 days in CO_2 and 2 days in air) [49]



According to Dr. Das, tensile strength of Iron Carbonate is 4–6 MPa (see *Figure 12*). Unreacted iron particles of the Iron Carbonate are surrounded by carbonate reaction products and form a strong ductile matrix phase (see *Figure 10, section 3.2*) that could be responsible for the enhanced tensile strength [47].

Figure 12 - Comparison between OPC and iron carbonate binder (control and fiber reinf.): (a) tensile strength, (b) ultimate strain; (c) tensile modulus [47]

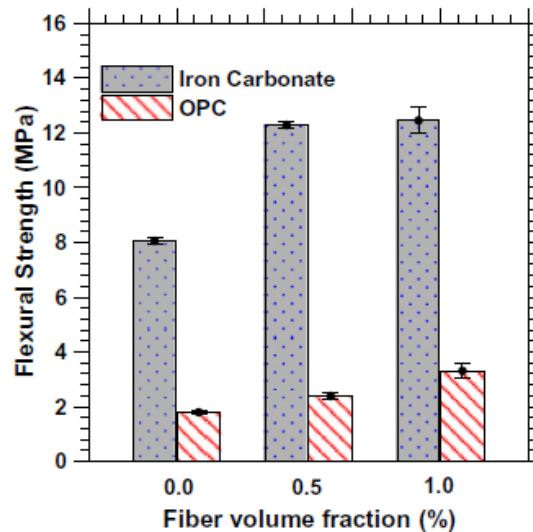


Iron Carbonate binders also have demonstrated to have four to six times higher flexural strengths than OPC-based binders (see *Figure 13*) [48]. This can be attributed to the combination of the strong carbonate matrix in combination with the presence of unreacted iron particles in the microstructure.

Unreacted iron particles also result in a significantly higher peak load and improved post peak response compared to OPC binders [48]. Both the peak load and the residual load are significantly higher for the iron carbonate binder, with and

without fiber reinforcement. Furthermore, Iron Carbonate binders show an enhanced fracture performance due to the beneficial effects of the elastic, partially reacted or unreacted metallic particles on crack bridging and deflection [47]. Iron Carbonate has significantly higher crack growth resistance than OPC binders has also been shown to provide significantly higher total fracture energy than OPC. The additional incorporation of fibers in the microstructure improves the resistance even more.

Figure 13 - Comparison of flexural strength of 6-day carbonated iron carbonate sample and OPC paste after 28 days for different fiber dosage (the error bars represent one standard deviation of flexural strength obtained from four replicate specimens) [48]



Further material properties, provided by Dr. Das, include a young's modulus of 34 GPa. The higher value of the elastic modulus in comparison to OPC-concrete could be due to the presence of metallic iron particulate inclusions [47].

Tensile strain at failure of Iron Carbonate is 0.00035, according to Dr. Das. Controlled compressive strain tests have not been performed yet. Compressive strain at failure of ordinary concrete is 0.005 which could serve as a guiding value for Iron Carbonate; Dr. Das and the author expect an enhanced performance under compression of the Iron Carbonate binder.

Objective of the present paper is to carry out a traditional analysis of a split Hopkinson pressure bar (SHPB) experiment on Iron Carbonate specimens. Analysis of Strain gage output signals using a MATLAB program [50] will eventually provide stress, strain-rate and strain in the tested specimen under dynamic compression [51].

3.5 Preliminary summary

Iron Carbonate is a novel carbon-negative sustainable binder that is made from metallic iron powder waste and utilizes the chemistry of iron carbonation. To produce the binder, usually landfilled iron powder and other constituents (fly ash, limestone powder, metakaolin, sodium carbonate, sodium bicarbonate, powdered organic reducing agent, and water) are mixed together and exposed to a pressurized CO₂ regime that leads to slow external diffusion. Exposing the material to CO₂ results in a faster CO₂ uptake, microstructure densification and rapid compressive strength gain. The carbonation of iron particles results in the formation of complex iron carbonates (FeCO₃) that have binding capabilities and mechanical properties comparable or better compared to OPC. The metallic particulate phase incorporated in the binders' microstructure increases the toughness of Iron Carbonate because of the energy dissipation by plastic deformation of the unreacted and elongated iron particles which are strong and ductile. In addition, the matrix contains other additives including harder fly ash particles, softer limestone particles, and ductile clayey phases which significantly influence the overall fracture performance of the novel sustainable binder.

4 Dynamic concrete tests using split Hopkinson bar systems

4.1 Importance of understanding dynamic strain-rate effects on concrete

Material properties such as yield stress or ultimate strength are generally obtained with standardized testing procedures under quasi-static loading conditions [52]. However, understanding the behavior of concrete at high strain rates is important for a wide range of both military and civilian applications [51]. Analyzing the response of concrete to dynamic loading, i.e. impact or explosive loading, is essential for destruction of military targets and for effective protection of defense structures, such as protective concrete shells of nuclear power plants or protecting public buildings from terrorist attacks. It is important for the design of airport runways that have to withstand repeated dynamic loads during aircraft takeoff and landing. Also, dynamic loading occurs from natural hazards such as tornadoes, earthquakes and ocean waves. Therefore, the characterization of concrete behavior under impact and impulse loading is a prerequisite for the design of concrete structures [53].

Dynamic loads or forces are the forces necessary to change respectively accelerate the motion of a body [54]. A suddenly applied load is referred to as impact load. A system under impact loading will vibrate until equilibrium is established if there is elastic action.

The material behavior under highly dynamic conditions is significantly different from material response under quasi-static conditions [51]. This is mainly due to strain-rate dependence of the material response and high levels of hydrostatic pressure. In order to understand and model concrete structure damage from high-velocity impact and blast loads, it is necessary to understand the strain rate effects on

cement-based materials [53]. The split Hopkinson (Kolsky) pressure bar (SHPB) system can be used to test dynamic compressive mechanical response and failure behavior of cement paste and concrete under high strain rates between 10^2 s^{-1} to 10^4 s^{-1} (ϵ/s) [51] [52].

It should be pointed out that experimental studies on the dynamic behavior of cement-based materials at high strain rates are quite limited [53]. The accurate characterization of the dynamic behavior under valid testing conditions still faces many difficulties.

Conventional concrete is commonly made with ordinary Portland cement and has two major issues that make it unsustainable: a high carbon footprint and restricted durability under extreme dynamic loading conditions that makes frequent repair and replacement necessary.

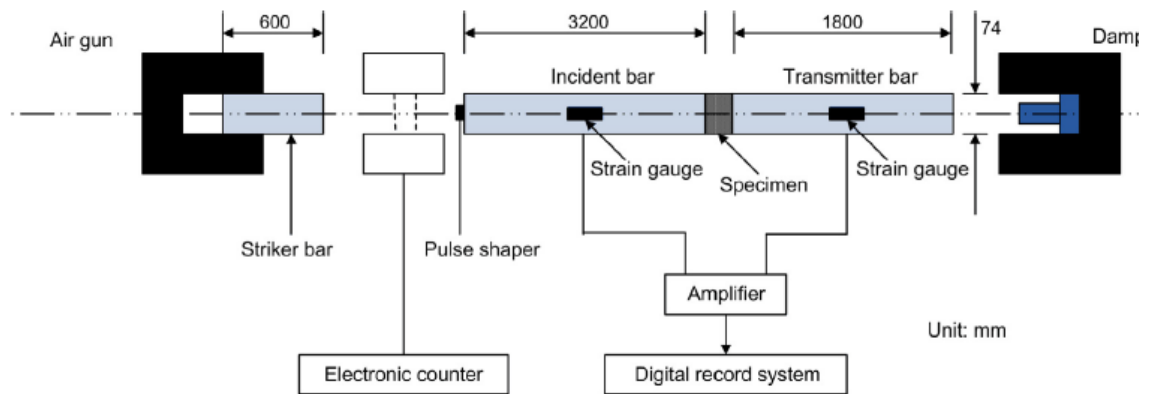
The performance of novel concrete, made from industrial iron powder waste, under extreme dynamic loading conditions, will potentially establish exceptional dynamic load mitigation characteristics for the carbon-negative sustainable binder under extreme combined environments. Enhanced durability of the novel sustainable concrete through better resistance against dynamic loading would prolong its lifetime and make it even more sustainable.

4.2 History of split Hopkinson pressure bar system

In 1872, John Hopkinson investigated the propagation of stress waves in iron wires [46]. Later (1914 [55]), his son Bertram Hopkinson invented a pressure bar system to obtain the pressure-time curve with the dynamic load produced by detonation [56]. However, this measurement technique was limited and its results were not accurate [46]. In 1949, Kolsky developed the so-called split bar system, consisting of a separated incident and transmitter bar with the specimen in between and condenser microphones [57]. Therefore, the split Hopkinson pressure bar (SHPB) is also referred to as Kolsky bar. In 1954, the system was modified by a striker bar to produce repeatable impact stress waves in the incident bar and by adopting strain gauges for measuring stress waves [58]. The SHPB system has been continually improved for increased accuracy for different materials under high strain loading [46]. Originally, the SHPB was designed for dynamic compression testing of metals but SHPB tests for tensions and torsion have been subsequently developed [59]. All versions are based on the same principle and differentiate only in loading and specimen gripping methods [52].

4.3 Basic principle for split Hopkinson (Kolsky) bar

Figure 14 - Split Hopkinson pressure bar test system [53]

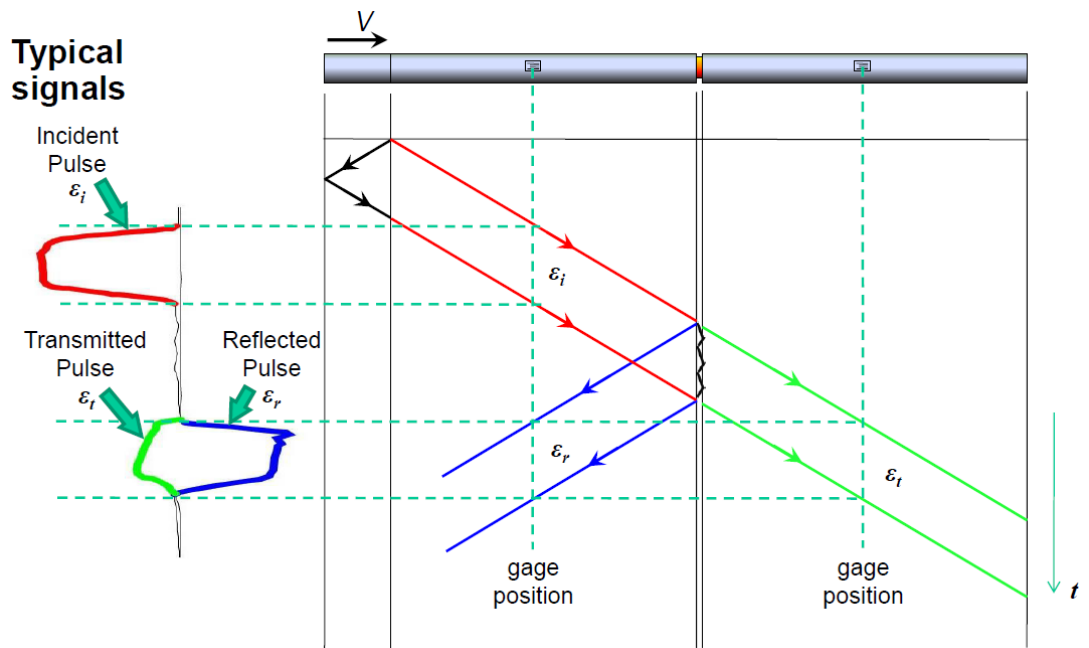


Dynamic tests are conducted using the split Hopkinson pressure bar (SHPB) respectively Kolsky bar systems [46]. The experimental arrangement involves mechanical and measurement systems [55]. A loading device (gas gun) and three aluminum or steel bars, aligned along a single axis [55], are included into the mechanical system: a striker bar, an incident bar, and a transmitted bar, as shown in *Figure 14* [46]. The design of the bars leads to stresses imposed during impact of the striker bar remaining within the elastic limit throughout the test [55]. Steel bars should be used for harder materials [60] like concrete. Ideally the bar material should be linearly elastic with a high yield strength because the stress waves inside the bars are measured by surface strains [52]. The striker has the same cross-section and ideally the same material as the incident and transmission bars [52].

The thin and usually cylindrical specimen is placed between the incident and transmitter bars aligned with the common axis of the bar system. It should be noted that the diameter of the specimen after the test should be smaller than the diameter of the pressure bars [60]. To test the specimen under high strain rates, the axially aligned gas gun launches the striker bar inside a long gun barrel toward the incident bar at a

known velocity; the striker is launched by a sudden release of compressed air or light gas in a pressure storage vessel [52]. The impact of the striker bar on the free end of the incident bar induces a stress pulse [53] respectively a longitudinal compressive wave propagating in both directions [46], the amplitude depending on the velocity of the bullet [53]. The speed of the striker can be controlled and varied by changing the pressure of the compressed gas in the tank or changing the depth of the striker inside the gun barrel [52]. The impact velocity relates to the pulse's stress level; the length of the pulse depends on the length of the striker bar [55]. The velocity of the striker can be measured optically or magnetically just before impact [52].

Figure 15 - SHPB system; x-t diagram of stress wave propagation in SHPB and typical strain gage signals [61]

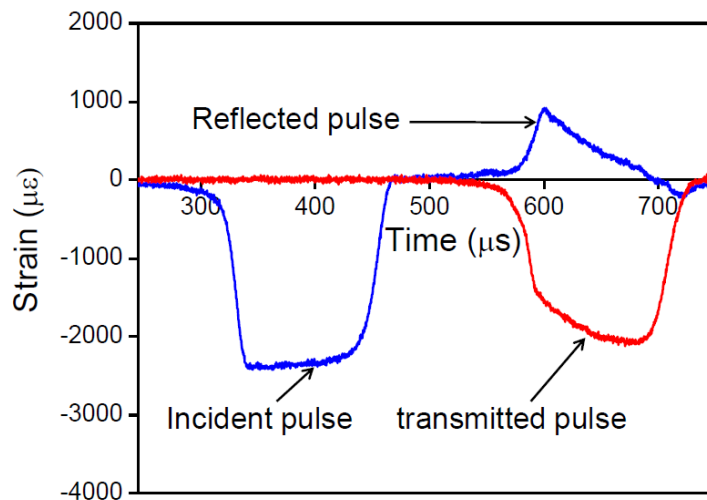


Due to the impact of the striker bar an incident pulse, a reflected pulse and a transmitted pulse are generated. At the free end of the striker bar, the left-propagating wave is fully released and forms an incident negative strain (compression) pulse ϵ_i (see *Figure 15*) [46]. The length and longitudinal wave velocity in the striker influence the

duration of ϵ_i . When reaching the bar-specimen interface, part of the incident wave is reflected as the reflected wave ϵ_r [46], creating a tensile pulse [53]. In order to avoid overlapping between the incident and reflected pulses, the incident bar should be at least twice as long as the striker [52]. Back and forth reflection (inside the specimen) is due to the wave impedance mismatch between the specimen and the bars [52, 53]. The remaining transmitted wave ϵ_t passes through the specimen to the transmitted bar [46] as a compression pulse [53]. Gradually the reflections build up the stress level in the specimen and compress it [52]. However, stress wave propagation in the specimen is usually ignored by assuming equilibrated stress in the sample because the specimens used in the experiments are very thin [52].

The mechanical energy of a stress wave propagating in a long rod or bar takes the form of the strain energy through bar deformation and the kinetic energy through bar motion [52]. *Figure 16* shows the typical pulse profiles.

Figure 16 - Typical pulse profiles [61]



The measurement system consists of strain gages, a dynamic signal conditioning amplifier and a signal acquisition system [55]. To record the stress wave pulse, strain gauges are usually affixed symmetrically on the incident and transmitted bar surface [46]. It should be noted that the strain gages location should be far from the bar ends (at least 10 bar diameters from both ends) [52].

The strain gage signals are conditioned with a Wheatstone bridge [52] and/or half bridge and transferred to a dynamic signal conditioning amplifier and then to a PC system or oscilloscope [55]. The signal amplifier is necessary to accurately record the low-amplitude voltage output (usually in the order of millivolts) with an oscilloscope [52]. To record the short signal, both the amplifier and the oscilloscope should have a sufficient high frequency response with a minimum of 100 KHz [52].

Determination of the dynamic stress-strain curve of a material is one of the objectives of an SHPB test [46]. From the stress-strain curve, mechanical properties, such as dynamic failure strength and dynamic Young's modulus, can be derived.

However, SHPB tests do not simulate high hydrostatic pressures that occur during impact and penetration and therefore post-fracture behavior such as pulverization and granular flow cannot be determined [51]. Nonetheless, SHPB tests do simulate early stages of material failure and deformation, i.e. fracture and fragmentation [51].

Different from conventional material testing machines, the small-diameter Kolsky bars are not drastically stiffer than the specimen itself. Furthermore, the SHPB-system does not have a closed-loop feedback control system. Loading conditions cannot be monitored in real time and adjustment of the loading conditions

is not possible. The loading conditions must be determined without knowing the response of the specimen which makes Kolsky-bar experiments quite complex. [52]

Figure 17 shows the 0.5 in.-diameter SHPB system as it is currently installed at the Dynamic Photomechanics Laboratory at the University of Rhode Island.

It should be noted that in order to obtain statistically valid results from split Hopkinson (Kolsky) experiments, at least tests of 30 specimens are required [52].

Figure 17 - SHPB system (0.5 in. diameter) at the Dynamic Photomechanics Laboratory



4.3.1 Strain-rate definition

The mean strain-rate is defined as the total strain during loading divided by the total period [51]. However, this definition does not represent the actual strain-rate [53]. The instantaneous strain-rate can be higher than the mean strain-rate [62]; the strain-rate corresponding to the ultimate strength is more relevant to the compressive

failure of specimen [53]. Alternatively, the mean-strain rate can be defined as “average magnitude of the strain-rate histories over a period, in which the strain-rate is within 80% of the strain-rate at failure point” [63]. Chen et al. [53] used the strain-rate at failure point as representative strain-rate in their SHPB tests.

For material property characterization, a dynamic stress equilibrium and constant strain-rate need to be achieved within the specimen [52]. It should be noted that ideal testing conditions are not satisfied over the entire duration of the Hopkinson (Kolsky) experiment because the specimen is initially at rest. Over time the stress waves simultaneously bring the specimen into near equilibrium and the strain-rate to a desired constant level. However, the specimen can fail as the strain-rate is still rising if the desired strain-rate is too high. Therefore, the strain-rate needs to be limited to a maximum.

4.3.2 Pulse shaping technique

Standard SHPB tests cannot be used for compressive testing of brittle concrete materials because elastic response is predominant before failure under uniaxial compression [53]. Due to small failure strains ($< 1\%$) of brittle materials, the specimens could fail non-uniformly if loading is too fast as in conventional SHPB tests [46]. Thus, modification of the incident pulse is required to match the elastic response [53]. In order to experience a quasi-static load and uniform deformation (minimize wave dispersion [52]), dynamic loading of the specimen has to be slow enough [46].

Figure 18 - Clay as pulse shaper on an 0.5 in. incident bar at the Dynamic Photomechanics Laboratory



The so-called pulse shaping technique controls damage of brittle materials by placing a thin disk made of copper or any other soft material between the striker and the incident bar. The Dynamic Photomechanics Laboratory [60] of the University of Rhode Island (URI) generally advises the use of (Roma Plastilina) standard clay (see *Figure 18*) or lead pulse shapers that are lubricated with a thin layer of Dow Corning lubricant [60]. *Figure 19* shows different loading pulses produced by pulse shaper of different materials.

The pulse shaper disc can have a thickness between 0.1-2.0 mm [46]; Chen et al. [53] used a 2.0 mm diameter. The striker bar impacts on the pulse shaper before the incident bar and generates a non-dispersive ramp shaped pulse compared to the standard rectangular shape [46]; *Figure 20* shows the stress-strain curve of cement mortar with and without pulse shaping [53]. The incident pulse has a slow-rising front

and propagates into the incident bar. Thus, the pulse shaper facilitates the dynamic force balance [46] respectively dynamic stress equilibrium [53] in the specimen.

Figure 19 - Loading pulses produced by pulse shapers of different materials [64]

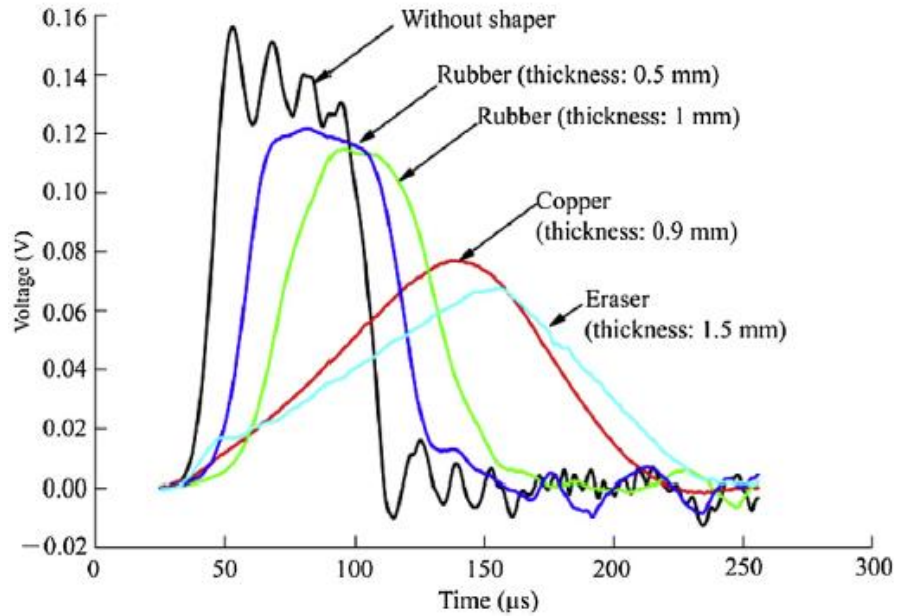
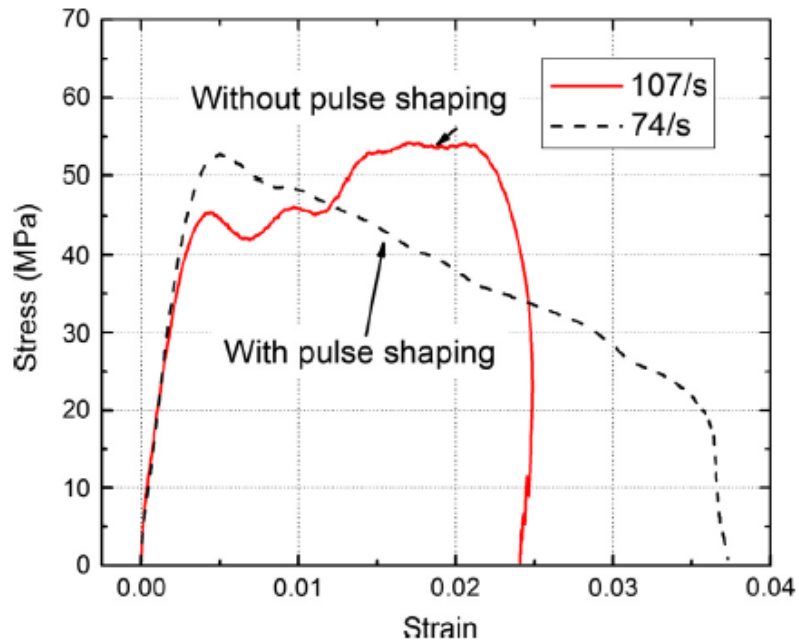


Figure 20 - Stress-strain curve of cement mortar with and without pulse shaping [53]



In conclusion, use of the pulse shaper has the following main functions: filter out high frequency noise generated during impact of the striker bar [53], ensure constant strain-rate during loading [46], and maintain force equilibrium across the sample [46] [53]. The time for rising of the incident wave is extended while the loading rate is reduced [53].

4.3.3 Dynamic compression tests

Dynamic compression tests of SHPB are based on the assumptions of 1D elastic wave propagation in the bars and homogenous (uniform) deformation of the sample [46].

In SHPB experiments, the incident and transmitted bars must remain linearly elastic. Thus, the elastic wave theory can be used for data reduction; surface strains are linearly related to the stress waves inside the bars. Therefore, a high-strength bar material, i.e. alloy steel, is preferred. The yield strength of the bar material directly determines the upper limit of the striker impact speed. [52]

One-dimensional elastic wave propagation can be achieved by using long bars [46] that also facilitate large deformation in the specimen [52]. The length of the stress pulse is supposed to be much larger than the bar diameter; the stress pulse is usually at least 10 times the size of the bar diameter [55]. The bars must be physically straight and able to move freely on their supports with minimized friction [52]. Furthermore, the whole bar system has to be aligned perfectly along the straight loading axis of the system [52].

Even a minor misalignment along the bar system can result in a bending wave [52]. Signals from the bending waves can also be detected by strain gages on the bar

surface and may cause distortion in the strain gage measurements. Also, a loading in bending subjects one face to tension and the other one to compression. Proper connections of the strain gages (on opposite legs or on the same leg) can automatically remove bending from the strain gage measurements. Ideally the bending wave should be eliminated by physically aligning the bar system.

To ensure elasticity of the bar deformation throughout the SHPB test, the impact velocity of the striker bar is limited [46]. However, the stress pulse must be long enough to create at least 3 to 10 reverberations within the length of the specimen to create uniform longitudinal deformation [55]. Furthermore, the boundary interfaces between the sample and the bars must be well lubricated to achieve uniform radial deformation [55].

The homogeneity of the specimen deformation is influenced by the inertial effect (see *section 4.3.3.1*) and the interfacial friction effect (see *section 4.3.3.2*) [46].

4.3.3.1 Inertia effects and slenderness ratio

The inertial effect becomes relevant for high strain-rates and has to be reduced in order to obtain valid dynamic tests [46]. The slenderness ratio, meaning the length to diameter ratio of the specimen (L/D), plays a major role in the inertial effects during SHPB tests. In order to limit the inertial effects associated with stress wave loading, the slenderness ratio should be limited. Davies et al. [65] proposed an optimal slenderness ratio of $L/D = \sqrt{3}/2$, where L is the length of the cylindrical specimen, and [65] ≈ 0.5 [51]. For the present SHPB experiment the optimal L/D ratio of the Iron Carbonate specimens was chosen to be 0.4 with a More information about the slenderness ratio can be found in the subsequent section 4.3.3.2.

4.3.3.2 Friction effect

Interfacial friction on both ends of the specimen affects the SHPB testing results [57]. The friction between the specimen ends and the bars holds the specimen in place in the SHPB test setup [66] but can also lead to an apparent increase in obtained strength [51].

The specimen expands radially when loaded by the compressive stress wave, due to the Poisson's effect [46]. The resulting interfacial friction force reduces accuracy of the testing results by applying a dynamic confinement to the compressive specimen and creates an inhomogeneous (three dimensional [52]) stress state [46].

To limit the interfacial friction force the boundary interfaces between the bars and the sample should be sufficiently lubricated [46] with Molybdenum disulfide lubricant [60] or WD-40. In addition, the bars must move freely [60]. Furthermore, the slenderness ratio L/D of the compressive specimen should be large enough. The International Society of Rock Mechanics (ISRM) recommends a slenderness ratio of 2 or larger for testing rock-like materials [67]. However, the slenderness ratio still has to be short enough to limit the inertia effects [46]. According to Li et al. [68], the optimal slenderness ratio for metals lays between 0.5 and 0.61 to limit inertia effects on the accuracy of the experiment. For concrete-like specimen in SHPB experiments the acceptable slenderness-ratio ranges from 0.3 to 1.0 [68]. In this case, the optimal L/D ratio was chosen to be 0.4 for Iron Carbonate specimens. Thus, the cylindrical Iron Carbonate samples with a set diameter of 1.5 in. had to be cut to 0.6 in. length to fulfill the chosen ratio. As already mentioned, an optimal L/D ratio is needed to minimize both the inertial and friction effect.

Because the surface of concrete specimens is much coarser than the surface of metallic samples, the friction effect has to be considered even though the boundary interfaces are lubricated [68]. Not properly lubricated interfaces between a specimen and the pressure bars could result in stress and strain non-uniformity which could eventually lead to a significant over-prediction of the strain-rate effect (see *section 4.3.3.4*).

4.3.3.3 Compressive strength and dynamic increase factor (DIF)

The dynamic compressive strength increases with increasing strain-rate [51, 53]. This increase in compressive strength with increasing strain-rate could be attributed to “the generation and dynamic growth of interacting, compressive induced tensile micro-cracks” [69]. The moisture content in concrete also strongly influences the strain-rate sensitivity [70]. Inertial effects of the added water and increased fracture toughness of wet concrete could also be responsible for increased dynamic strength [70]. Other reasons for strength increase include the viscoelastic nature of hardened cement paste and time-dependence of crack growth [71].

However, contradictory findings exist regarding the strain-rate dependence of the compressive strength in SHPB experiments. Li et al. [68], Watstein [72], Takeda and Tachikawa [73], and Kvirikadze [74] agree with Grote et al. [51] and claim that dynamic compressive strength increases with increasing strain-rate. Hatano and Tsutsumi [75], and Cowell [76] report a constant compressive strength with increasing strain-rate. Others, e.g. Hughes and Watson [77], even claim that strength decreases with increasing strain-rate. Grote et al. [51] attribute those contradictory findings to inconsistency among the testing methods.

The ratio between the dynamic and static strength, known as *dynamic increase factor (DIF)*, represents the strain-rate effect on the compressive strength [53]. It is an important parameter for the measurement of the strain-rate effect on the strength of cement-based materials such as concrete and other concrete-like materials [68].

Studies have shown that the DIF increases about 50% in average when the strain-rate varies from 10^{-5} to 10^1 s^{-1} [78]. However, another study by Li et al. [68] claims that lateral inertia confinement in SHPB tests causes the strain-rate dependence of the DIF (see *section 4.3.3.4*). They conclude that the SHPB-obtained DIF has to be modified to eliminate lateral inertia confinement effects [68].

4.3.3.4 Lateral confinement

According to Li et al. [68], lateral confinement in SHPB tests can cause the already mentioned, apparent dynamic strength enhancement (of concrete samples) with increasing strain-rate. Lateral confinement in SHPB experiments is caused by contact surface restriction and lateral inertia effects during rapid compression. Lateral confinement effects on SHPB measurements are usually ignored for metallic samples. The use of lubricant, such as Molybdenum disulfide or WD-40, successfully reduces contact friction between metallic specimens and the steel bars. Also, the metal's plasticity is hydrostatic-stress-independent. Therefore, lateral inertia induced lateral confinement does not affect the flow stress and dynamic strength.

However, concrete and concrete-like samples respond completely different to lateral confinement because the material's plasticity is hydrostatic-stress-dependent [68]. The measured uniaxial dynamic compressive stress of concrete-like materials can be greatly enhanced by lateral confinement due to lateral inertia. Li et al. [68] claim that this strength enhancement is often misinterpreted as strain-rate enhancement in

other publications, i.e. by Grote et al. [51]. Nonetheless, according to findings of Li et al. [68], the lateral inertia confinement effect can be neglected for strain-rates up to 10^2 s^{-1} which represents the transition point from weak strain-rate sensitivity to strong strain-rate sensitivity.

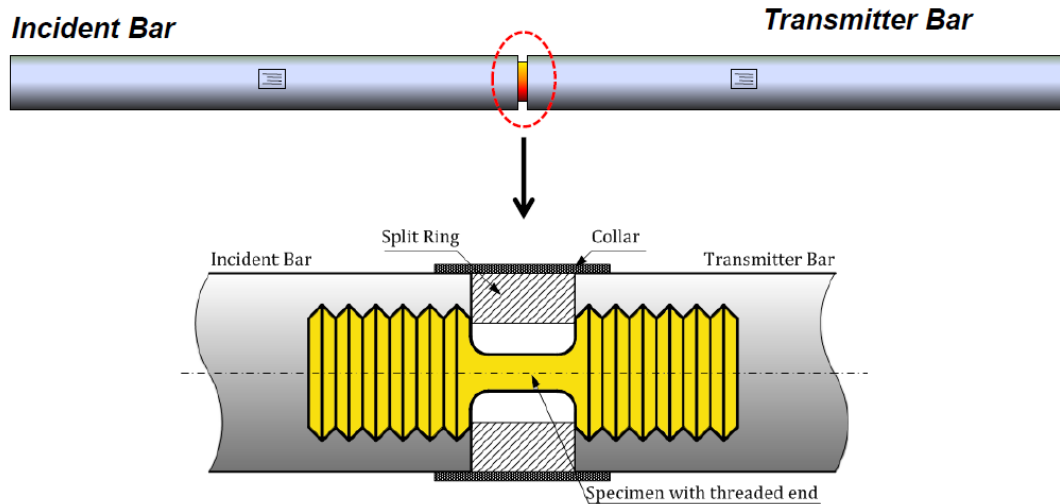
4.3.3.5 Elastic modulus

According to Chen et al. [53] the elastic modulus increases slightly when increasing the strain rate. Yan et al. [79] suggest that delay of crack development is responsible for an increase of the elastic modulus. The delay of both the creation of micro-cracks and the propagation of initial micro-cracks is due to the viscous resistance of free water and resistance of the coarse aggregates in the concrete [79]. Further addition of sand and coarse aggregates further increases the elastic modulus [53]. Rigid inclusions within the concrete matrix create greater stiffness to the matrix and also reduce dimensional instability of the matrix [53]. However, addition of stiff aggregates leads to internal stress gradients and strain concentrations.

4.3.4 Dynamic tension tests

Three common experimental arrangements (direct tension methods [46]) of split Hopkinson tension bars exist to generate tension stress waves to subject a specimen to dynamic tensile loads. As for dynamic compression testing, a striker bar initially produces a compression wave [55]. The split Hopkinson tension bar uses the same data analysis procedure as it is used for the split Hopkinson pressure bar [61].

Figure 21 - Split Hopkinson tension bar: first arrangement [61]

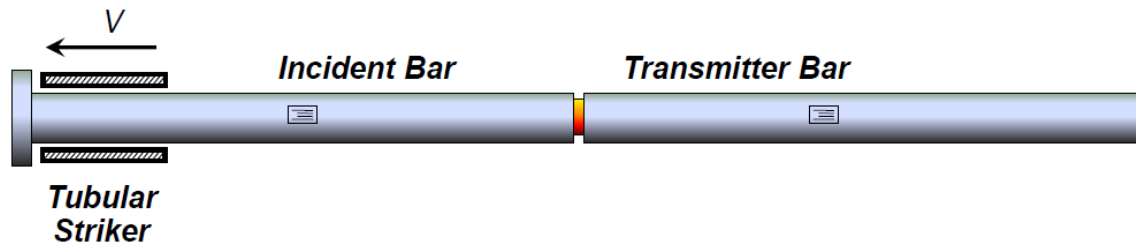


In the first arrangement (see *Figure 21*), the reflection of a compression stress wave at the free end of a bar generates the tension stress wave [55]. For experiencing tensile stresses the specimen has to be mounted (i.e. adhesive or threaded ends of the specimen that allow it to be screwed into the bars). An important feature of the arrangement is a so-called split ring that allows the initial compression wave to propagate through it without reflection. Thus, maintaining the specimen within the elastic region and letting the striker-induced compression wave propagate into the transmitter bar. At the free end of the transmitter bar, the compression wave is reflected as a tension stress wave which is then used as an incident pulse. Because the split ring cannot transmit any load (tension), it separates from the bar; the total tension pulse is applied on the sample. Reflected and transmitted pulses are generated within the bars which are used to analyze high strain rate behavior of the specimen.

In the second arrangement (see *Figure 22*), a flange plate is attached to the end of the specimen to directly apply the incident tension stress pulse on the specimen to be tested [55]. By launching a striker bar at the flange plate, a compression wave is

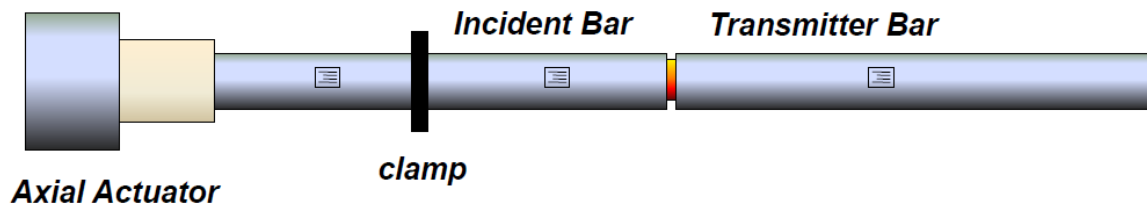
generated. The compression wave is then reflected as tension stress wave from the free surface of the plate.

Figure 22 - Split Hopkinson tension bar: second arrangement [61]



In the third arrangement (see *Figure 23*), the incident bar is first fixed (clamped) at one position [55]. Tensile strain is stored within the left side of the bar by an axial actuator that pulls on the left side of the incident bar. Then, the clamp is suddenly released and the stored tensile strain energy generates a tensile stress pulse which is applied on the specimen. As in the second arrangement, the incident tension stress pulse is generated directly in the specimen.

Figure 23 - Split Hopkinson tension bar: third arrangement [61]



4.3.5 Split Hopkinson (Kolsky) bar experiments on brittle materials

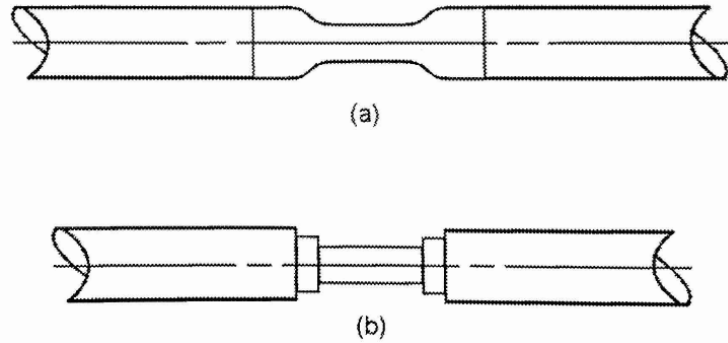
Brittle materials, such as glass or concrete, usually deform in a linear elastic manner under compression until they fail at small strains (typically <1%) [52]. Measurement of the deformation with bar signals is difficult. Therefore, a loading

pulse with constant stress rate is required to achieve deformation of a linear elastic specimen at a constant strain rate.

Specimens made of brittle materials, which are used in SHPB-experiments, are very sensitive to stress concentrations because the material cannot yield locally [52]. Stress concentrations around the edges of brittle materials lead to premature failure and normally arise as a result of three main sources: non-parallel loading surfaces and poor flatness, bar misalignment, and indentation of a stiffer specimen into compliant bar end faces. Locally concentrated stresses cause uneven and premature failure of a specimen. With increasing stiffness of the material susceptibility to local stress concentrations increases, too.

To reduce stress concentrations at the specimen's edges two types of specimen configuration have been proposed [52]: Dumbbell shaped ceramic specimen (see *Figure 24(a)*) and specimen sandwiched between hard material-platens (see *Figure 24(b)*). Platens between the specimen and the bars not only minimize indentation and stress concentration but also protect the bar end faces from sharp fragments. A commonly used platen material is Tungsten carbide (WC). The diameter of WC platens is about 12.7 mm to match the impedance with 19 mm- bars. A commonly used platen thickness is 6.35 mm; a thin platen can bend significantly when pressed by a hard, small diameter specimen. Therefore, the platens are often confined by press-fit metal rings to ensure integrity. Deformation of the plate along radial direction should match that of the specimen.

Figure 24 - Brittle specimen configurations [52]



Besides having an adequate surface quality, the geometry of a brittle sample should be carefully designed, too [52]. The specimen diameter should be calculated in a way that stress in the transmitted bar is less than 30% of the bar yield strength. The incident pulse stress will be higher than the transmission pulse stress and should terminate shortly after specimen failure. For low strength specimen made of limestone or concrete, the diameter of the specimen should be the same as that of the steel bars to minimize stress concentrations on the specimen.

Furthermore, the length-to-diameter specimen ratio in quasi-static compression experiments should be 2:1 to minimize end effects (see ASTM standard C39) [52]. To achieve high strain rates a short specimen should be used; the strain rate in a Hopkinson (Kolsky) bar experiment is inversely proportional to the specimen thickness. However, the achievable strain rate is limited by the small failure strain of the (brittle) specimen material. Brittle materials will fail before a constant strain rate is reached – during strain acceleration – if the expected strain-rate is too high. A too thick of a specimen in turn will prematurely fail from impact end, before even loading across its thickness, due to small failure strains.

However, Li et al. [68] claim that accuracy and more importantly validity of SHPB results for non-metallic materials such as concrete have not been thoroughly studied yet and are therefore questionable.

4.3.5.1 Stress-strain behavior and toughness

The stress-strain behavior of cement-based materials such as concrete is very sensitive to the strain rate [53]. Strain softening after peak stress is reflected by the descending of the stress-strain curves and reflects fragmentation of the specimens [80]. With increasing strain rate the stress-strain curves become less non-linear and characteristics become more linear [53].

The toughness of cement-based materials increases with the strain rate [53]. Higher strength and strains at high strain rates are responsible for the increase in toughness.

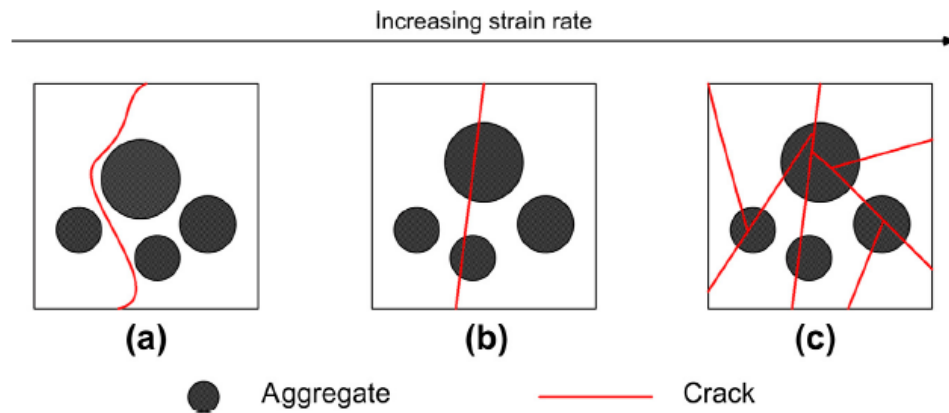
4.3.6 Failure mode

Fracture, fragmentation and pulverization occur when concrete experiences dynamic loading of sufficient amplitude [51]. According to Chen et al. [53] the dynamic failure pattern of cement paste, mortar and concrete specimen under high strain-rate loading resulted in the disintegration of the middle portion of the test cylinders into small pieces. The size and number of fragments are directly related to the strain-rate: the higher the strain-rate, the larger are the number and the smaller are the sizes of the fragments.

Failure cracks in cement paste are generally straighter, longer and cleaner compared to the cracks in concrete specimens [53]. Schematic failure patterns of concrete at different strain-rates are displayed in *Figure 25*. Under static loading, cracks pass through the mortar and propagate along the interfaces (see *Figure 25(a)*),

whereas for high strain rates, the cracks are propagating in a more direct way fracturing particles (see *Figure 25(b)*). Reason for that is the rapid increase in stress before the cracks had time to extend along the path of least resistance. At higher strain rates the concrete is fractured into small pieces to dissipate energy (see *Figure 25(c)*).

Figure 25 - Schematic failure patterns of concrete at different strain rates [53]



4.3.7 Calibration of SHPB systems

To check the alignment of the bar system, the striker bar should be launched directly on the incident bar [52]. Thereby the incident bar should be in direct contact with the transmitted bar without any specimen in between. An analytically predictable trapezoidal profile of the incident pulse with a clean baseline indicates a good alignment of the bars (see *Figure 26*). The complete incident pulse in the incident bar should be transmitted into the transmitted bar without any reflection, since both are in direct contact.

If the incident bar is not in good alignment with the striker, the incident pulse is distorted while the baseline is fluctuating (see *Figure 27*) [52]. Misalignment between the incident and the transmitted bar generates a reflected pulse; the

transmitted pulse profile differs from that of the incident pulse (see *Figure 27*). A SHPB system that is misaligned should not be used for material characterization

Figure 26 - Stress wave in the bars in good alignment [52]

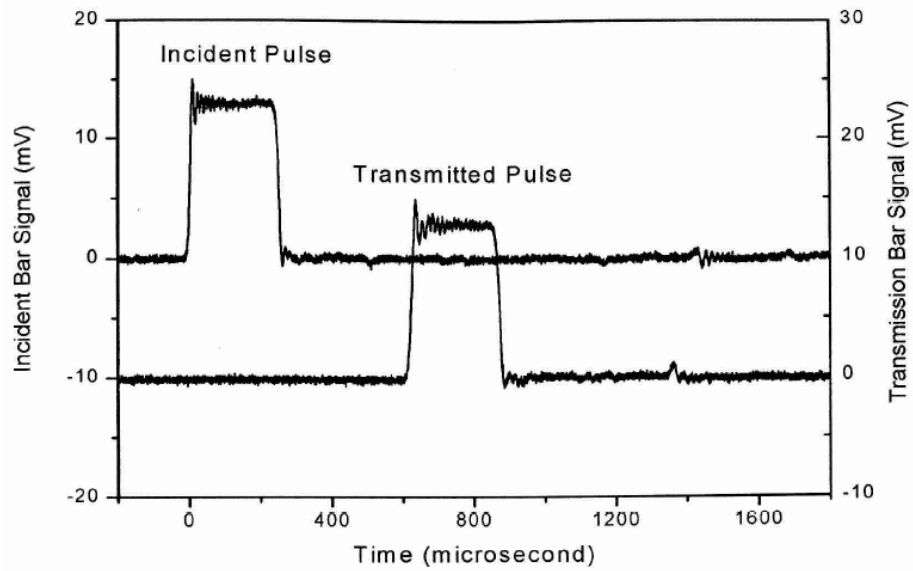
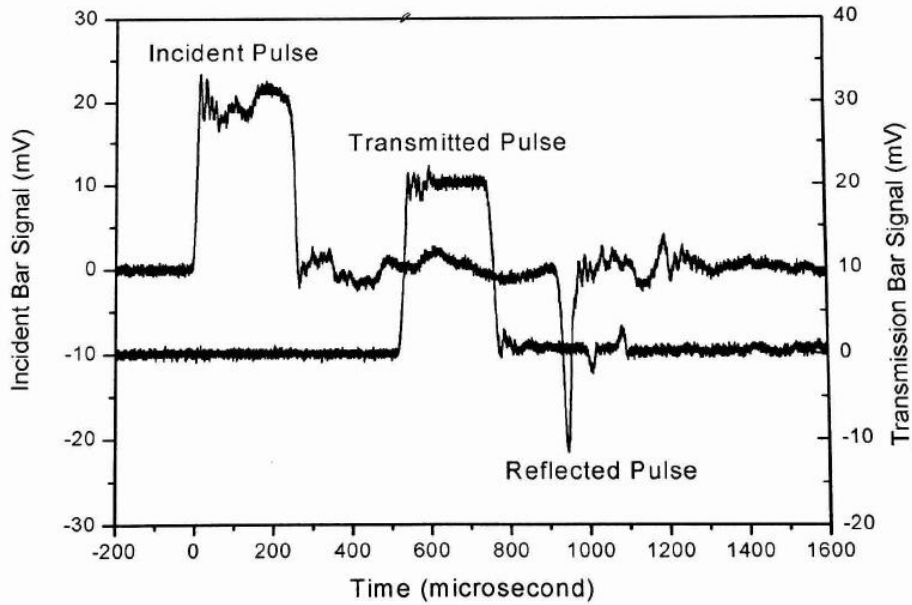


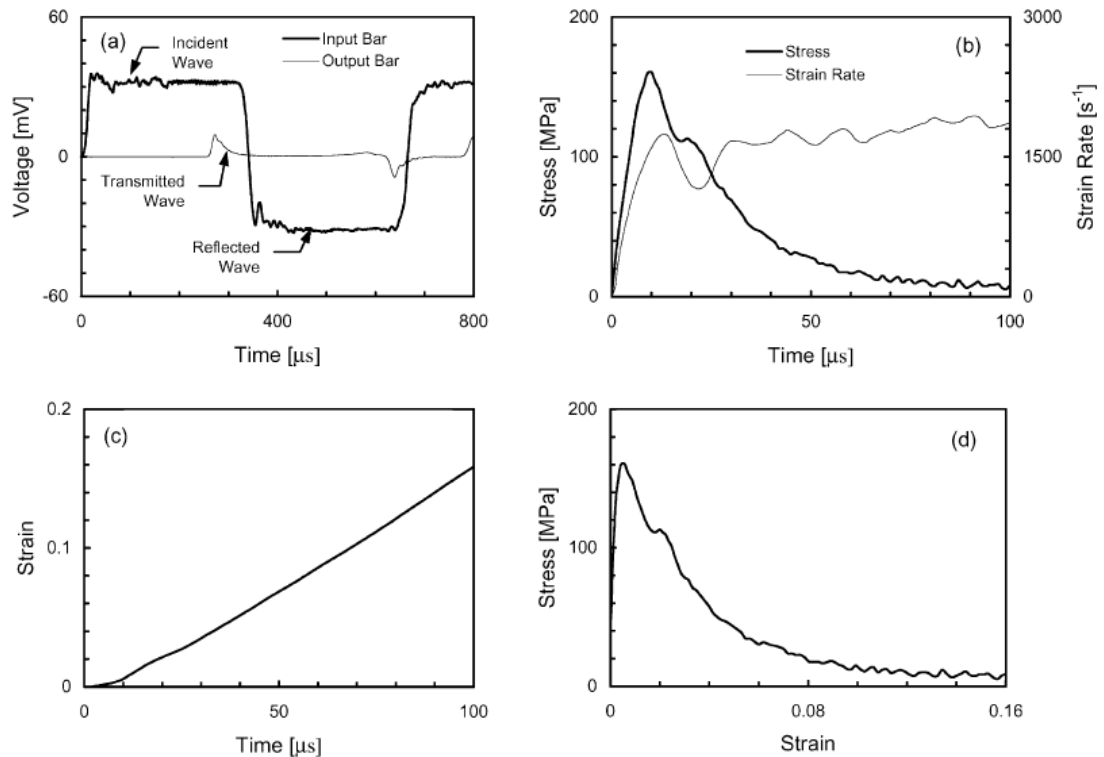
Figure 27 - Stress wave in the bars in misalignment [52]



4.3.8 Analysis of SHPB test

A traditional analysis of a Split Hopkinson pressure bar (SHPB) experiment provides stress, strain rate and strain in the tested specimen [51]. Strain gage output signals are recorded on a digital oscilloscope; at the Dynamic Photomechanics Laboratory a Tektronix TDS 3014C Digital Phosphor Oscilloscope is used for recording. Strain measurements from the incident and transmitted bar are used to determine the time histories of the stress, strain and strain-rate in the tested sample during deformation. From the reflected and transmitted strain histories (see *Figure 28(a)*), the stress and strain rate histories (see *Figure 28(b)*) can be obtained.

Figure 28 - Data analysis for an SHPB experiment; (a) measured strain gage signals, (b) computed stress and strain rate histories, (c) computed strain history, and (d) stress-strain relationship [51]



The strain rate is not constant throughout the period due to the dynamic nature of the experiment [51]. Therefore, an average strain rate has to be calculated and used for the duration of loading. The stress-strain relation (see *Figure 28(d)*) can be obtained by combining the history of strain (see *Figure 28(c)*) with the history of stress (see *Figure 28(b)*).

The DPML uses a MATLAB program to read and analyze the data from the pulses [60]. The program uses one-dimensional wave theory stress and strain equations along with the pulses to determine the equilibrium and true stress-strain plots of the specimen.

A guideline about how the analyzes the results obtained by the oscilloscope along with the MATLAB code was prepared by the Dynamic Photomechanics Laboratory.

4.4 Preliminary Summary

Understanding the behavior of concrete at high strain rates is important for a wide range of both military and civilian applications [52]. Therefore, the characterization of concrete behavior under impact and impulse loading is a prerequisite for the design of concrete structures. The material behavior under highly dynamic conditions is significantly different from material response under quasi-static conditions.

Dynamic tests of concrete are conducted using the split Hopkinson respectively Kolsky bar systems [46]. The Hopkinson bar (SHPB) consists of three bars: a striker bar, an incident bar, and a transmitted bar. The specimen is placed between the incident and transmitter bars. To test the specimen under high strain rates, the striker bar is launched toward the incident bar at a known velocity. The impact of the striker bar on the free end of the incident bar induces a stress pulse [53] respectively a longitudinal compressive wave propagating in both directions.

Standard SHPB tests cannot be used for compressive testing of brittle concrete materials because elastic response is predominant before failure under uniaxial compression [53]. The so-called pulse shaping technique controls damage of brittle materials by placing a thin disk made of copper or any other soft material such as clay between the striker and the incident bar.

A Hopkinson (Kolsky) bar can also be used for dynamic tension and torsion testing but standard experimental set-up has to be modified. There are three common experimental arrangements (direct tension methods [46]) of split Hopkinson tension bars to generate tension stress waves to subject a specimen to dynamic tensile loads [55]. As for dynamic compression testing, a striker bar initially produces a

compression wave. The split Hopkinson tension bar uses the same data analysis procedure as it is used for the split Hopkinson pressure bar [61].

The stress-strain behavior of cement-based materials such as concrete is very sensitive to the strain-rate [53]. The strain rate also influences the compressive strength and elastic modulus of the concrete: with increasing strain rate both the compressive strength and the elastic modulus increase.

The ratio between the dynamic and static strength, known as dynamic increase factor (DIF), represents the strain rate effect on the compressive strength [53].

A traditional analysis of a Split Hopkinson pressure bar (SHPB) experiment provides stress, strain rate and strain in the tested specimen [51]. Strain gage output signals are recorded on a digital oscilloscope and can be read and analyzed by using a MATLAB program [50] by the Dynamic Photomechanics Laboratory of the University of Rhode Island.

5 Testing of Iron Carbonate with SHPB system

5.1 Iron Carbonate sample preparation

Objective of the thesis is to test the performance of this novel sustainable concrete under extreme dynamic loading conditions in a 2 in.-diameter split Hopkinson pressure bar (SHPB) system to indicate durability under extreme stresses.

The Iron Carbonate samples for testing were kindly provided by Dr. David Stone and his company Iron Shell LLC, Tucson, AZ. Dr. Stone sent 6 cylindrical Iron Carbonate samples (1.5 in. diameter, 2.6 in. long), 2 cubic samples, and 2 tiles that arrived on May 22, 2017.

Figure 29 - Samples provided by Iron Shells LLC. P-series contains polypropylene fibers; S-series contains steel fibers



The cylindrical samples were composed of steel dust, fly ash, limestone powder, metakaolin, and oxalic acid in powdered form, following the standard mixture recipe mentioned in the *section 3.2*. In addition, polypropylene fibers respectively steel fibers at 1% fiber volume fraction were added to both mixtures; the fracture energy is approximately 4 times higher at 1% fiber volume fraction [47]. The “P”-labelled samples (see *Figure 29*) are made from one batch of standard Iron Carbonate mixture and contain polypropylene fibers. The three “S”-labelled cylinders (see *Figure*

29) are made from another batch of standard Iron Carbonate mixture and contain 1 in.-thin steel fibers, according to Dr. Stone.

Table 3 shows the exact dry mixture composition of the samples by weight percentage and the individual component manufacturer respectively the brand name.

Table 3 - Iron Carbonate standard dry mixture composition

Components material	Manufacturer	% by mass of the total powder
steel dust	Schuff Steel	62
fly ash (Type F)	Boral	21
limestone powder	Imerys	9
metakaolin	Burgess Pigments (Optipozz)	4
oxalic acid	Univar	4

All mentioned components (steel dust, fly ash, limestone powder, metakaolin, oxalic acid, polypropylene or steel fibers) are initially dry mixed together. Water is added to obtain a uniform cohesive mixture and satisfying workability. Depending on the constituent proportions, the mass-based water-to-solids (w/s) ratio was chosen to be 0.3. As already mentioned water is not incorporated during the carbonation process of iron but serves as agent of mass-transfer and ensures desired workability and uniformity.

The mixture is then tamped into cylindrical molds in five layers using a Harvard miniature compaction apparatus (ASTM D 4609, Annex A1) until the molds are filled completely [49]. Using a specimen ejector the specimens were demolded immediately after and placed inside clear plastic bags. Then, the samples were exposed to pure CO₂ under positive pressure for 7 days while being kept damp during the entire curing period.

To limit inertial effects associated with stress wave loading in a SHPB system, the slenderness ratio, meaning the length to diameter ratio of the specimen (L/D), was chosen to be ≈ 0.4 . This results in a specimen length of 0.6 in., given the set 1.5 in. diameter of the cylindrical Iron Carbonate samples. Please refer to *chapter 4*, i.e. *section 4.3.3.1*, for more detailed information about the split Hopkinson pressure bar and inertial effects.

University of Rhode Island (URI) technical staff assistant Kevin Broccolo cut the cylindrical samples into 0.6 in.-thick specimen with a RYOBI circular saw using a DIABLO 10 in. saw blade. It was possible to cut the polypropylene fiber containing samples with a satisfying surface condition, although material and sample fabrication constraints limited accuracy and smoothness. The specimens' surfaces were then smoothed by hand using first coarse grit (3M Pro Grade Precision Advanced Abrasives P80) and then fine grit (3M Pro Grade Precision Advanced Abrasives P320) sanding paper in order to limit interfacial friction (see *section 4.3.3.1*) on both ends of the specimen that can affect the SHPB testing results. *Figure 30* shows four samples cut from a "P"-series cylinder and smoothed by hand with sanding paper.

Cutting of the steel fiber containing samples with the DIABLO 10 in. steel blade, however, resulted in rough and uneven specimen surfaces (see *Figure 31*). Those samples were not usable for the SHPB-experiments. In a second try, URI technical staff assistant of the Dynamic Photomechanics Laboratory, David Ferreira, cut the "S"-specimen with a QEP 4 in. diamond blade on a JET vertical milling machine resulting in surfaces of the samples being significantly smoother and more level (see *Figure 31*). However, all but one of the steel fiber containing samples failed

in the attempt to accurately cut them with the diamond blade. Therefore, only polypropylene fiber containing specimens could be tested in the SHPB.

Figure 30 - Cut and smoothed samples from „P1“-cylinder



Figure 31 - Steel fiber containing samples („S1“-series) cut with a diamond saw blade (left) and with a steel saw blade (right)



5.2 Experimental set-up

The split Hopkinson pressure bar (SHPB) system was set up in the Dynamic Photomechanics Laboratory (DPML) of the University of Rhode Island. The experimental arrangement involves a mechanical, a measurement, and a video recording system. The set-up basically follows the common SHPB buildup that has been described in *chapter 4*, i.e. *section 4.3*. *Figure 32* shows the 2 in.-diameter SHPB set-up.

Figure 32 - 2 in.-diameter SHPB system at the Dynamic Photomechanics Laboratory



5.2.1 Mechanical system

The mechanical system includes a loading device (gas gun) and three bars, aligned along a single axis [55]: a striker bar, an incident bar, and a transmitted bar, as shown in *Figure 14, section 4.3* [46]. Both, the incident and transmitted bar, are made out of steel, have a 2 in.-diameter and a length of 8 ft. each, and are guided by four respectively 3 clamps. The striker bar also has a 2 in.-diameter but is made of aluminum, has a length of 6 in. and weighs 992.4 g. At an earlier stage, trial experiments were carried out using a striker bar made out of steel, weighing roughly 2,000 g. To facilitate firing, the author decided to use a projectile made out of a much lighter material than steel. Since the loading unit can hold striker bars with up to 3.28 in. - diameters, two PE (TIVAR®) and/or Acetal Resin (DELRIN®) O-rings are screwed on the aluminum projectile (see *Figure 33*). That is to keep the striker centered within the loading device (see *Figure 34*) and to ensure alignment with the incident bar along the same axis. However, the entire striker unit had to be lifted using specially manufactured 0.25 in.-thick aluminum plates to ensure proper alignment.

Figure 33 - Aluminum striker with mounted O-rings

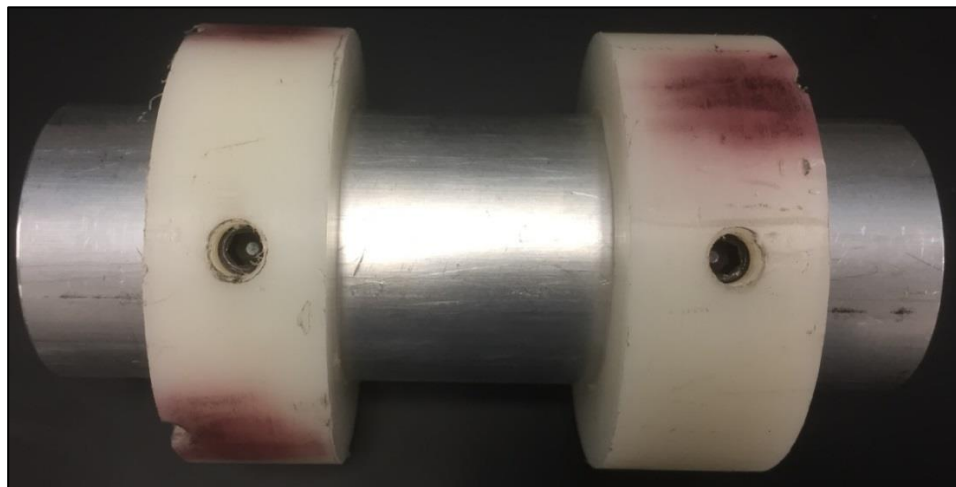


Figure 34 – Aluminum striker centered within gas gun by O-rings



The whole SHPB system is mounted on a 4.9 in.-wide steel I-beam with screw clamps and/or screws. The present SHPB set-up at the Dynamic Photomechanics Laboratory with an approximate overall length of 23.4 ft. turns out to be too long to entirely fit on the stand. Therefore, a KWIK-STAK portable elevating truck is used to support the overhanging part of the transmitted bar for the duration of the SHPB tests on Iron Carbonate specimens (see *Figure 35*). A clamped wooden board in combination with square lumps of clay are used to stop the transmitted bar respectively to absorb the axial thrust and to attenuate the impact on the forklift.

Figure 35 - KWIK-STAK portable elevating truck to support the overhanging part of the SHPB system



For firing the projectile, a compressed gas mechanism with automatic gas launcher and solenoid valve control box button is installed. The pressure regulator is clamped to the side of the stand whereas the gas tank is not mounted on the I-Beam (see *Figure 36*). However, for safety reasons the gas tank is strapped to the stand.

Figure 36 - compressed gas mechanism with gas tank, automatic gas launcher, and solenoid valve control box



Non-flammable nitrogen gas is used as fluid for the gas gun. By pressing the solenoid valve release button, the nitrogen gets released suddenly from the gas gun chamber and the striker bar is launched toward the incident bar creating an incident pulse.

For safety reasons, a Plexiglas box, manufactured by URI technical staff assistant David Ferreira, is placed over the interlocked specimen during the entire experimental procedure.

5.2.2 Measurement system

The measurement system consists of strain gages, a dynamic signal conditioning amplifier and a signal acquisition system [55]. To record the stress wave pulse, two strain gages are affixed symmetrically on each the incident and transmitted bar surface [46]. A 120 Ω strain gage in combination with a 350 Ω strain gage were mounted on each of the two bars using a Vishay M-Bond 200 adhesive kit and following the manufacturers' instructions for installing and soldering a CEA strain gage (refer to Vishay Instruction Bulletin B-127-14 [81]).

The strain gage output signals are conditioned with a half bridge, transferred to a dynamic signal conditioning amplifier (Vishay 2310A signal conditioning amplifier, model 2360) via BNC cables and then to a Tektronix TDS 3014C Digital Phosphor Oscilloscope. Thereby, the signal amplifier accurately records the low-amplitude voltage output (usually in the order of millivolts) with the oscilloscope [52]. To record the short signal, both the amplifier and the oscilloscope have a sufficient high frequency response with a minimum of 100 KHz [52].

It should be noted that loading conditions cannot be monitored in real time and adjustment of the loading conditions is not possible [52]. The loading conditions must be determined without knowing the response of the specimen.

5.2.2.1 Settings of the digital oscilloscope

The following *Figure 37* shows the settings of the oscilloscope (Tektronix TDS 3014C Digital Phosphor Oscilloscope) used for recording the strain gage output signals.

Figure 37 - Settings of the oscilloscope (red box)



5.2.2.2 Settings of the amplifier and half bridge

The following *Figure 38* shows the settings of the amplifier (Vishay 2310A signal conditioning amplifier, model 2360) used for conditioning the strain gage output signals. shows the settings of the half bridge. It is important to note that a set consisting of one 120 Ω strain and one 350 Ω strain gage is used on each the incident and transmitted bar. Settings of the half bridge have to be done accordingly for each corresponding channel.

Figure 38 - Settings of the amplifier

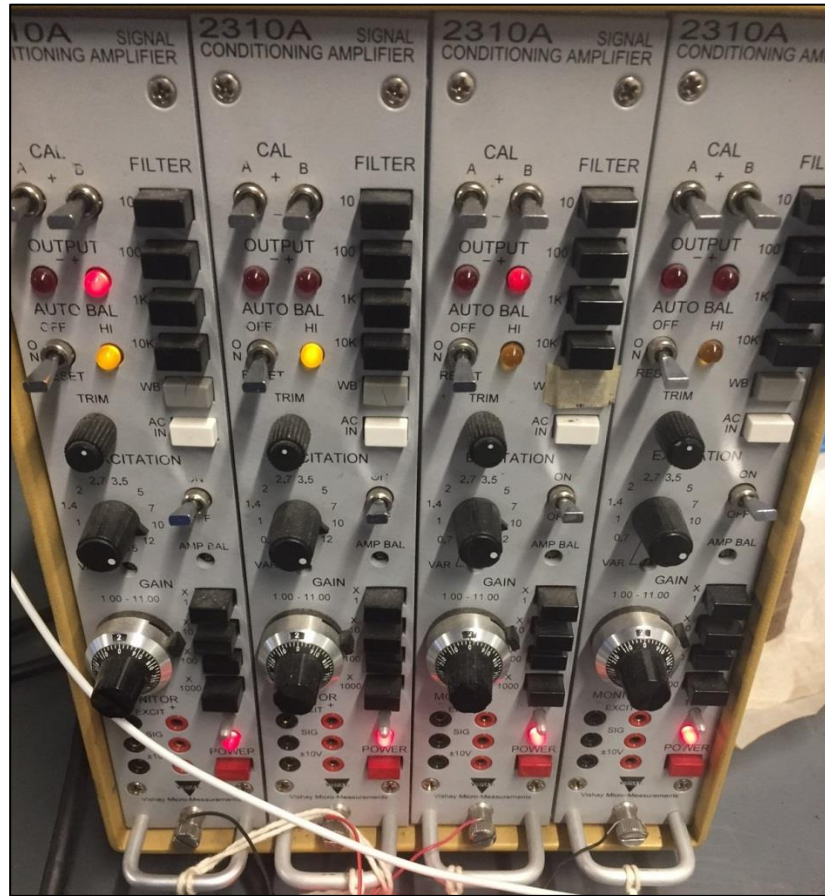
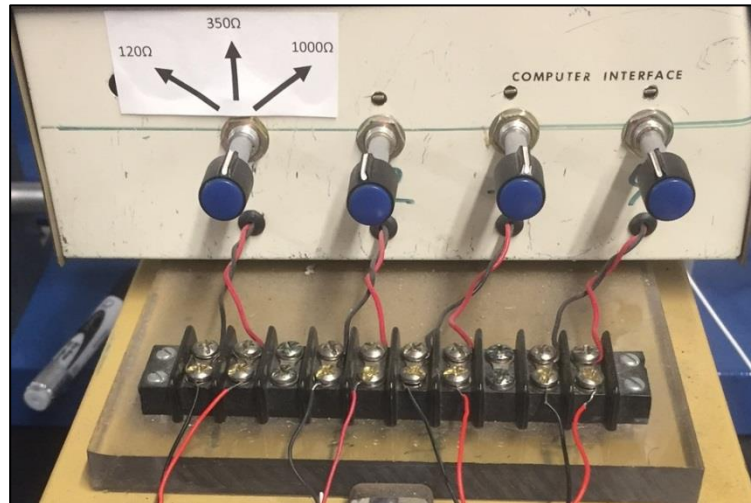


Figure 39 - Settings of the half bridge



5.2.3 Video recording system

To obtain slow-motion video footage of testing the Iron Carbonate specimens, a Photron Fastcam SA1.1 high-speed camera with a 180 mm lens and external trigger is used. The camera, mounted on a Quickset tripod, is connected to a Lenovo ideapad laptop with Photron FASTCAM viewer software to edit the video footage. The area of interest, i.e. a specimen placed between the incident and transmitter bars, is illuminated with two Frezzi HMI Super-Sun Gun 400 spotlights.

5.2.4 Challenges

The building up of the split Hopkinson pressure bar (SHPB) system in the Dynamic Photomechanics Laboratory (DPML) proved to be extremely difficult and challenging for a number of reasons listed below.

First of all, the setting-up was delayed because the Iron Carbonate samples, kindly provided by Iron Shell LLC, only arrived at the end of May instead of February 2017. Furthermore, the author prepared to carry out dynamic compression tests with the – already set up and calibrated – 0.5 in.-diameter SHPB in the DPML. After examination of the Iron Carbonate samples, the author was informed to use the not readily set up 2.0 in.-diameter SHPB in the DPML because the validity of testing small 0.5 in.-diameter samples would have been questionable.

Cutting of the polypropylene fiber containing cylindrical samples into 0.6 in.-thick specimen with a circular saw using a steel blade was possible, although material and sample fabrication constraints limited accuracy. Smoothing of the specimens' surfaces by hand in several grinding steps using sanding paper was time consuming. It was not possible to cut the steel fiber containing samples with the steel blade and to

obtain usable specimen. In a second try, a URI technical staff assistant of the DPML tried to cut the steel fiber containing specimen with a specially ordered diamond saw blade on a vertical milling machine. All but one of the steel fiber containing samples failed in the attempt to accurately cut them. Therefore, the steel fiber containing specimens were not usable for dynamic compression tests in the SHPB.

The set-up of the 2.0 in.-diameter SHPB was very difficult since the system was not been used for an unspecified amount of time. The overall length of 23.4 ft. turned out to be too long to entirely fit on the I-Beam stand. Therefore, a forklift is used to support the overhanging part of the transmitted bar for the duration of the SHPB tests on Iron Carbonate. Thus, good alignment and free movement of the steel bars for accurate results is very difficult and requires constant adjustment. For good alignment of the experiment the incident and transmitted bar should be in direct contact when pushed together. In the present set-up, however, there is a small gap between the two bars (see *Figure 40*) which the author was unable to close through adjustment of the bars and supporting clamps. Looking at *Figure 50*, it seems like the condition of the 2 bars could be the reason for them not being in direct contact; the transmitted bar seems to be larger than the incident bar. This misalignment may cause additional reflecting pulses.

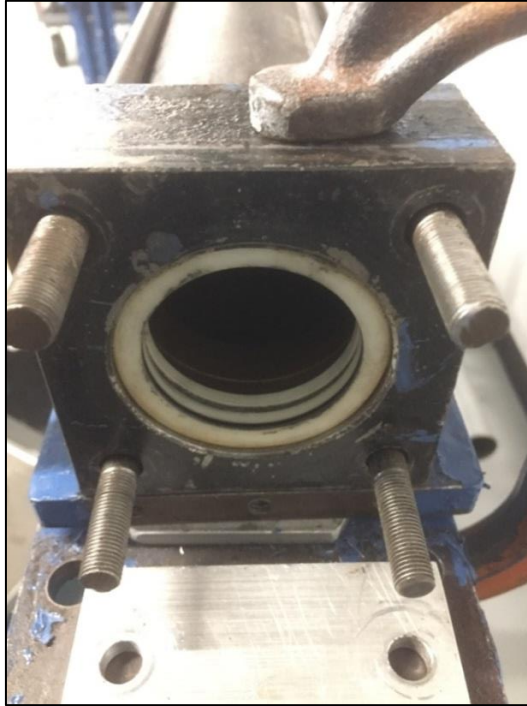
Figure 40 - Gap between incident bar (left) and transmitted bar (right) indicating misalignment



Also, the entire gas gun barrel had to be lifted using specially manufactured, 0.25 in.-thick, aluminum plates to ensure proper alignment of the projectile with the incident bar.

The existing drill holes in the I-Beam could only be used partially for mounting the SHPB system on the stand. Instead screw clamps had to be used to for fixing the experimental set-up.

Figure 41 – Opening of the SHPB gun barrel that had to be closed off



Also, the gun barrel had to be closed off on one side with a specially manufactured aluminum plate (see *Figure 41*). In order to use fasteners to attach the plate to the end of the barrel, the threads of the threaded rods had to be repaired by David Ferreira. However, the closure with the plate turned out not to be airtight so that nitrogen gas could escape during the firing procedure of the projectile. This potentially reduced the velocity of the striker bar and distorted the results, despite the use of high gas pressures (> 400 psi). Later a round sheet of tan pure gum rubber was used in addition to the aluminum plate to completely seal the opening.

Figure 42 – Repositioned pressure regulator with short connector mounted on the SHPB stand

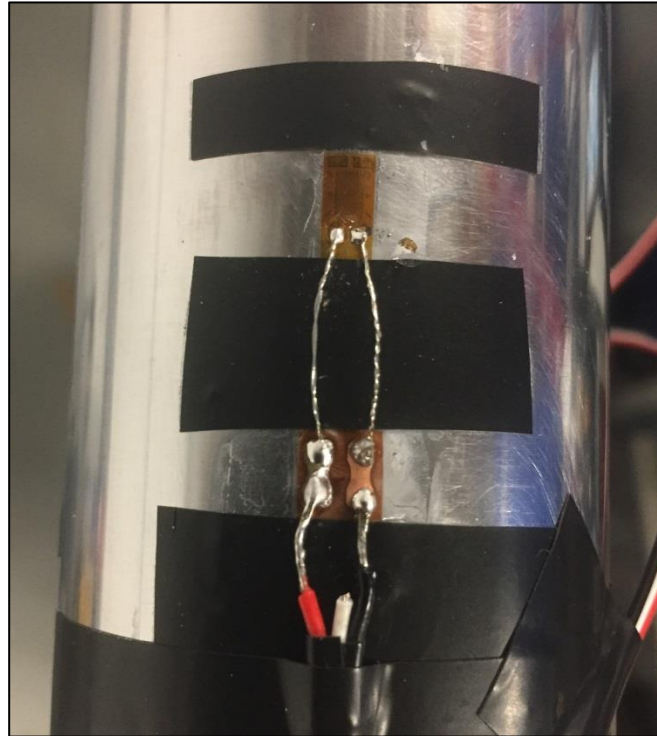


However, the leakage was not the only reason that compromised the impact velocity of the striker bar: the high-pressure hose connecting the pressure vessel to the gun barrel turned out to be too long so that an immediate and complete release of the pressurized gas from the pressure vessel into the gun barrel was not possible. In order to use a shorter connector piece, the compressed gas mechanism as well as the gun barrel had to be dismantled, moved and put back together. Because of the short connector the pressure regulator had to be clamped to the side of the I-beam stand (see *Figure 42*).

Furthermore, special couplings for connecting the gas tank to the pressure vessel had to be ordered and picked up from Grainger Industrial Supply in Warwick, RI.

A steel striker bar and later an aluminum striker bar with PE (TIVAR) and/or Acetal Resin (DELRIN) O-rings had to be specially manufactured in the machine shop of the DPML for the 2.0 in.-diameter SHPB (see *Figure 33, section 5.2.1*).

Figure 43 - 120 Ω - strain gage (top) with terminal installed by the author



Lastly, three out of four strain gages that were mounted on the incident and transmitted bar had to be replaced. Replacement was difficult and time consuming. Initially proper bonding of the strain gages on the steel bars was prohibited possibly by a thin layer of WD-40 on the bars' surface. After thoroughly cleaning the bars using denatured alcohol and roughening the surface using 220-, 320- and 400- grit sandpaper, it was possible to apply the strain gages following the manufacturers' instructions. For mounting the strain gages the Vishay M-Bond 200 adhesive kit was used. Since two out of four strain gages did not come with connected leadwires, the

wires had to be carefully soldered to the strain gage tabs. *Figure 43* shows a 120 Ω strain gage with terminal that was installed by the author.

In summary, it can be seen that setting up and calibration of the 2.0 in.-diameter SHPB, that had not been used for a long time, was very challenging and time consuming and could have still be improved. Many parts had to be ordered or manufactured individually by the DPML machine shop and the author for the SHPB.

5.3 Experimental procedure

As a first step, diameter and thickness of the to-be tested Iron Carbonate specimen have to be measured with a caliper gauge and noted down. Then, a cylindrical Iron Carbonate specimen is placed between the incident and transmitter bars aligned with the common axis of the bar system. The friction between the specimen ends and the bars holds the specimen in place [66]. However, to limit interfacial friction, the boundary interfaces between the bars and the sample are lubricated [46] with Molybdenum disulfide lubricant [60] or WD-40. For safety reasons a Plexiglas box is placed over the specimen. The bars and the guiding clamps, as well as the aluminum striker bar and gun barrel are lubricated with WD-40, so that the bars are able to move freely.

The projectile is placed into the striker unit and pushed to the end of the gas gun barrel with a flexible poly rod. As pulse shaper, a thin layer of clay is placed at the end of the incident bar facing the projectile (see *Figure 18, section 4.3.2*).

Afterwards, the amplifier and the digital oscilloscope are turned on. The excitation voltage and gain are set to 10V and 100V respectively [60]. The reset switch is turned on for all four channels. To check if the strain gages are working the

resistance on the gauges should read around 350 Ω (120 Ω if a different type of gage is used for monitoring). Then, the voltage levels, trigger position, and data duration time (2 ms – 4 ms) are set for all four channels in the digital oscilloscope, depending on the experiment. The half bridge has to be balanced for all four channels by turning the reset button. Then, the digital oscillation is armed to capture the strain gage voltage signals. If necessary trigger levels have to be adjusted. Also, high noise of more than 20mv should be avoided in the signals.

To test the specimen under high strain-rates, nitrogen gas is released from the gas tank into the gas gun chamber until the required pressure level, e.g. 100 psi, is achieved. Then the solenoid valve control box button is turned on. Before firing the projectile, it has to be ensured that the specimen is well aligned between the bars. Also, the status of the trigger hold has to be verified. The projectile can be fired by pressing and holding the solenoid valve release button that suddenly releases the compressed nitrogen gas from the pressure storage vessel into the gun barrel. The speed of the striker can be controlled and varied by changing the pressure of the compressed gas in the tank or changing the depth of the striker inside the gun barrel [52]. As soon as the projectile hits the incident bar, the already set up Photron Fastcam can be manually started to record by pressing the external trigger.

After the test, the captured voltage pulses are saved from the oscilloscope onto an USB flash drive for further analysis with a MATLAB program to determine the equilibrium and true stress-strain plots for the tested Iron Carbonate specimen. After the data is transferred from the oscilloscope to the USB flash drive, the data should be verified on a computer before turning off the amplifier and oscilloscope.

To complete the experiment, the solenoid valve release button has to be turned off. Also, it has to be made sure that all the left over nitrogen gas in the gas chamber is released.

5.4 Data analysis

The captured voltage pulses from the oscilloscope are analyzed using two MATLAB codes (Verify_Equilibrium and Steel_SHPB) provided by the Dynamic Photomechanics Laboratory of the University of Rhode Island. Objective is to determine the equilibrium and true stress-strain plots for the tested Iron Carbonate specimens.

Before running the codes, it has to be made sure that the code has the right properties and dimensions of the pressure bars [60]. These include diameter, wave speed and material properties like the young's modulus of the steel bars.

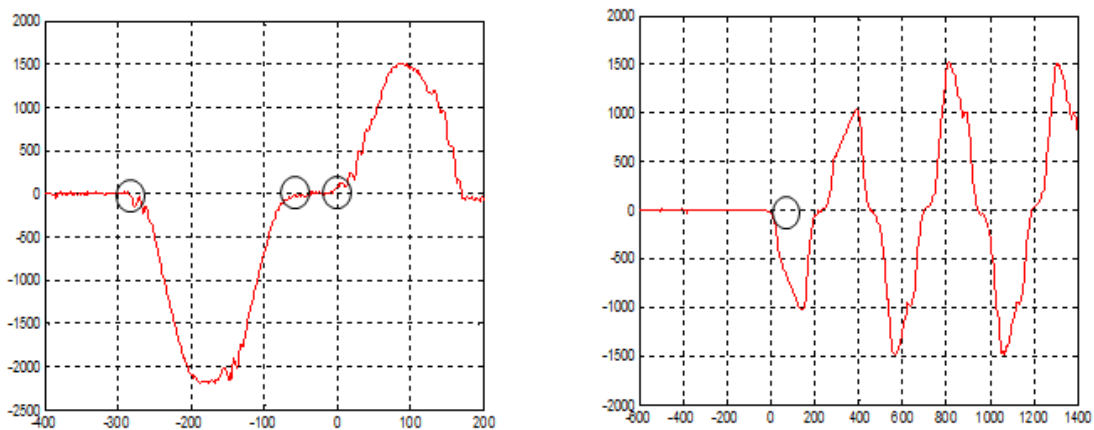
As a first step the "Verify_Equilibrium"-code should be run [60]. In order to do so, the data from the oscilloscope has to have the following names for the four channels: "TEK00000", "TEK00001", "TEK00002", and "TEK00003". "TEK00000" and "TEK00001" represent incident and reflected pulses (channel 1 and channel 2). "TEK00002" and "TEK00003" represent the transmitted pulses (channel 3 and channel 4). The code and the data have to be saved in the same folder on the computer because the code accesses the data, converts the voltage output to microstrains, and averages channel 1 and channel 2 respectively channel 3 and channel 4.

Default values for filtering are given in the code [60]. For incident and reflected pulse, a default value of 0.2 ($f_n = 0.2$) is used. For the transmitted pulse, a default value of 0.05 ($f_n = 0.05$) is used. Depending on the noise, the values of f_n can

be changed. The value of “fn” can range from 0.001 to 0.99, higher values of “fn” meaning that the pulses were not filtered.

When running the code, two figures are automatically created [60]: “Figure 1” gives the incident and reflected pulses; “Figure 2” gives the transmitted pulse (see *Figure 44*).

Figure 44 – Incident and reflected pulse (left) and transmitted pulse (right) created by the MATLAB code [60]



The incident starting time, incident end time, reflected starting time and transmitted starting time as shown in *Figure 44* (grey circles) have to be noted and entered into the MATLAB code [60]. The code then generates three more figures that show the incident, reflected and transmitted pulses. Thereby “Front face” represents the forces calculated on the incident and reflected pulses and “Back face” represents the force calculated on the transmitted pulse. Ideally, front and back face should match perfectly (see *Figure 45*) and force equilibrium is achieved.

Figure 45 - Force applied on the specimen over time; matching incident and reflected pulses [60]

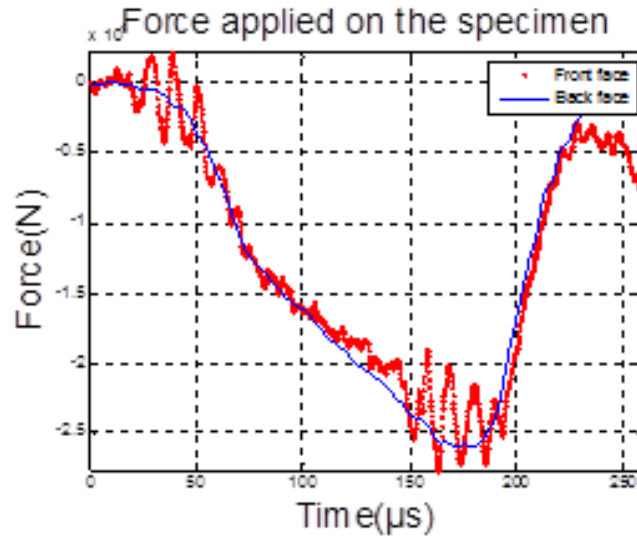
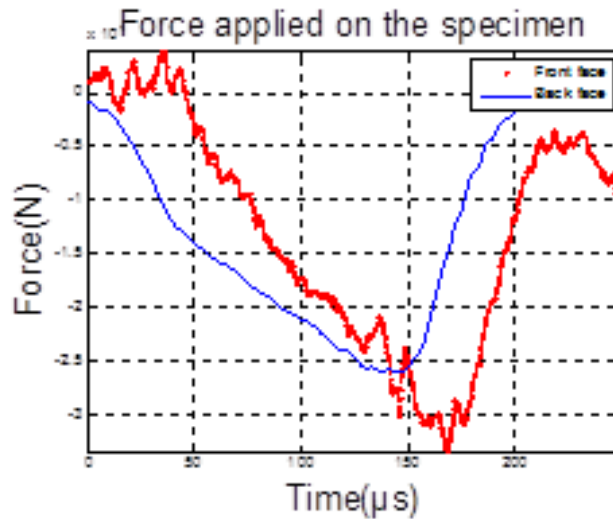


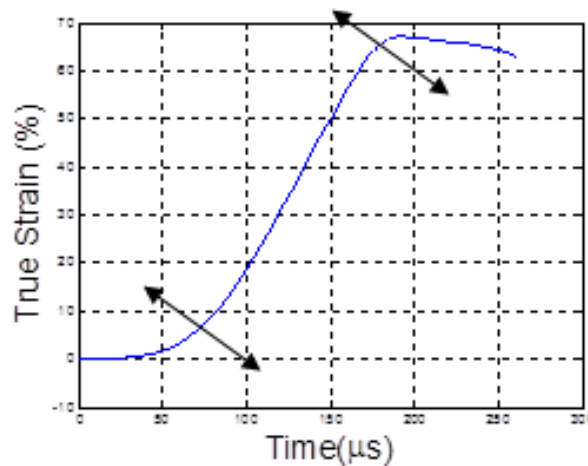
Figure 46 - Force applied on the specimen over time; incident and reflected pulses do not match [60]



However, most of the times the incident and reflected pulses do not match (see *Figure 46*) so that different values for the time of the incident pulse have to be tried [60]. Only the time of the incident pulse should be varied. The times of the reflected and transmitted pulses should not be changed.

After saving the obtained figures to the respective folder and noting down the used incident starting time, incident end time, reflected starting time and transmitted starting time, the “Steel_SHPB”-code should be opened [60]. The same values for filter as in the “Verify_Equilibrium”-code should be used. After entering the specimen thickness and diameter in inches, the code generates two figures: “Figure 1” shows the incident and reflected pulses; “Figure 2” shows the transmitted pulse. After entering the starting respectively end times of the pulses, the code creates an eng. stress-strain curve and true stress-time curve. By picking two points at the initial elastic region of the true stress-strain curve, the slope can be calculated. Following, two points at the linear region of the newly created diagram have to be picked (see *Figure 47*).

Figure 47 - True strain over time diagram [60]



In the MATLAB main window one can then see the strain rate value. Next, the final figure (eng. strain-rate vs. time) is created [60] and the analysis with the MATLAB codes is completed.

5.4.1 Digital Image Correlation

Digital Image Correlation (DIC) is a non-contact optical technique for measuring strain and displacement by comparing digital photographs of a component at different stages of deformation [82]. By tracking random blocks of pixels, a DIC system can measure surface displacement and build up full field 2D or 3D deformation vector fields and strain maps.

The edges of two tested Iron Carbonate specimens (P1-3 and P1-4) were painted white and provided with a random pattern of black dots to enable digital image correlation (DIC) while conducting split Hopkinson pressure bar experiments. In order to do so, deformation of each specimen in the SHPB was recorded using a Photron Fastcam camera (see *section 5.2.3*).

6 Results

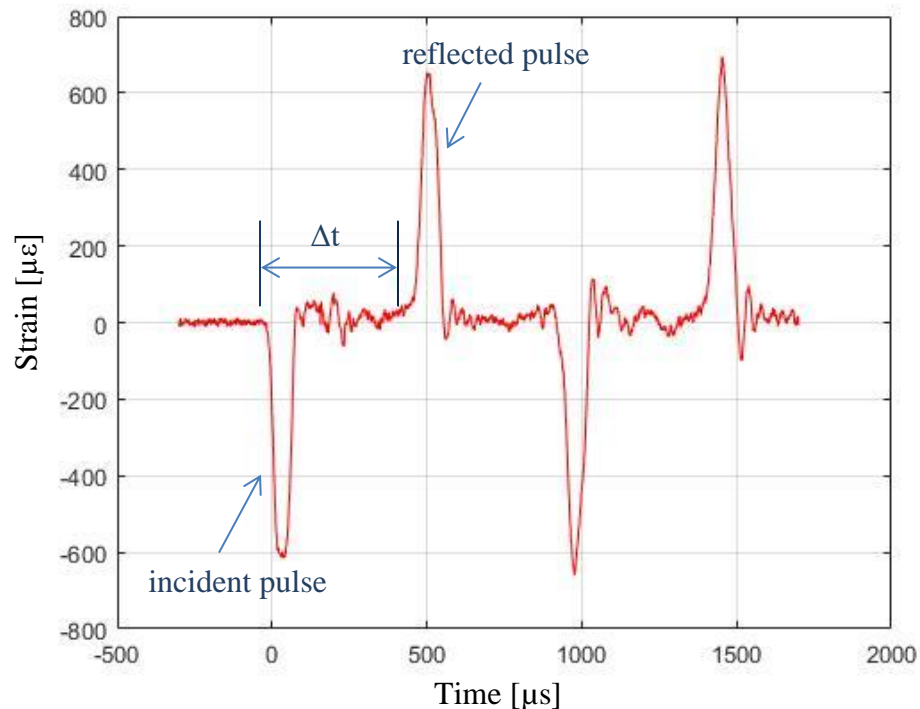
6.1 Verification of results

6.1.1 Single-bar experiment

By performing a single-bar experiment firing the striker solely at the incident bar, one can measure the true speed of sound in the bars and the time Δt between the start of the incident pulse and the occurrence of the reflected pulse. This time Δt can be used for indicating the beginning of the reflected pulse in a bar-to-bar experiment. Furthermore, bending of the incident bar can be determined on the basis of the pulses in the incident bar.

The single-bar experiment was carried out using a gas pressure of 150 psi. *Figure 48* shows the pulses obtained in the experiment. The time between the start of the incident pulse to the start of the reflected pulse was indicated to be $\Delta t = 480 \mu\text{s}$.

Figure 48 - Incident and reflected pulse obtained in a SHPB single-bar test

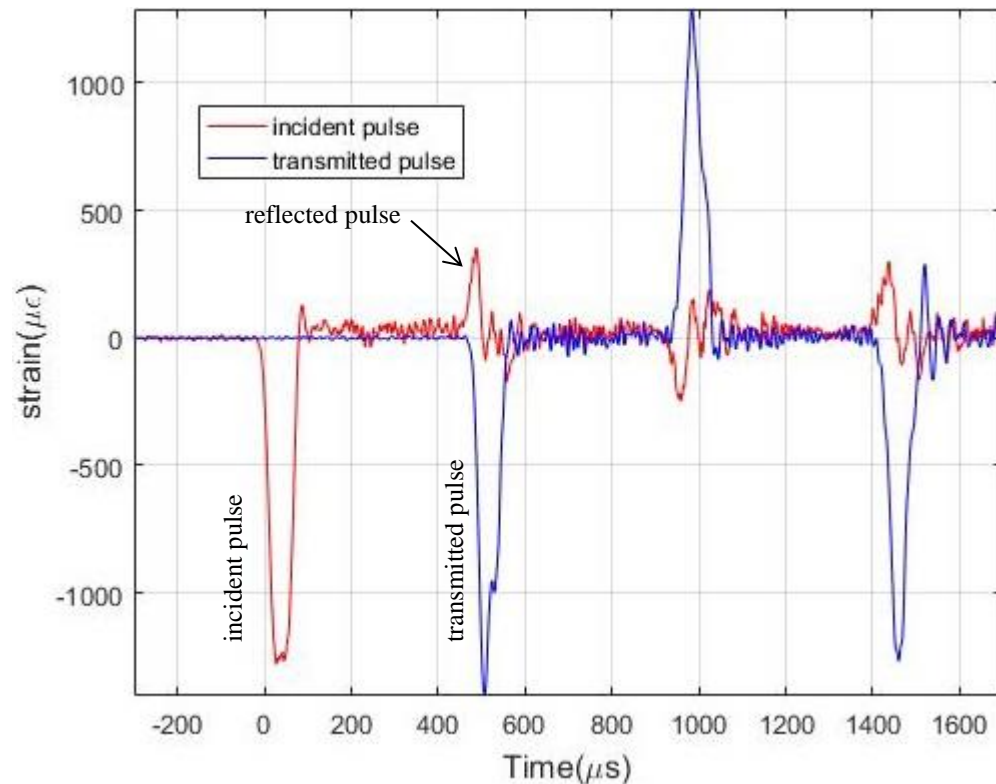


The smaller pulses in between incident and reflected pulse indicate a minor misalignment, i.e. bending, of the incident bar and could potentially influence the SHPB results.

6.1.2 Bar-to-bar experiment

To check the alignment of the bar system, the aluminum striker bar is launched directly on the incident bar using a pressure of 300 psi. The incident bar itself is in direct contact with the transmitted bar without any specimen in between.

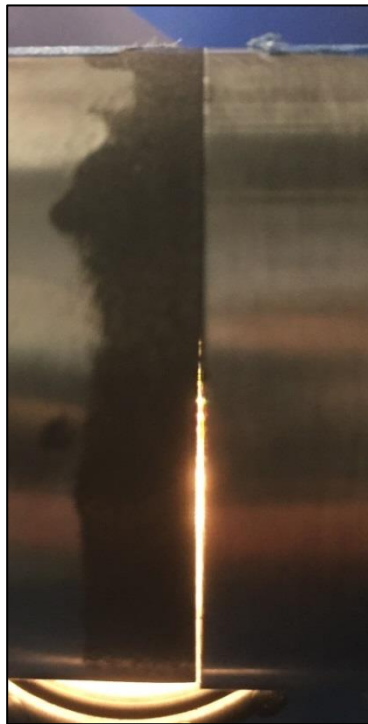
Figure 49 - Original pulses of SHPB bar-to-bar experiment (300 psi gas pressure)



The generated incident pulse in the incident bar should be transmitted into the transmitted bar without any reflection, since both are in direct contact. However, misalignments between the incident and the transmitted bar or bending of the bars generate a reflected pulse. Please refer to *chapter 4, section 4.3.7* for images of stress

waves in good respectively bad alignment. *Figure 49* shows the original pulses obtained from the bar-to-bar experiment. It can be seen that a – small – reflected pulse is generated indicating misalignment of the two bars. As can be seen from *Figure 50* the incident and reflected bar are clearly misaligned because they are not in direct contact. The author tried to adjust the alignment but did not succeed (see *section 5.2.4*). However, manufacturing constraints of the Iron Carbonate specimen comprise evenness of the specimens' surfaces, as well causing a potential misalignment and affecting results.

Figure 50 - Misalignment between incident (left) and transmitted (right) bar



For material property characterization, a dynamic stress equilibrium and constant strain-rate need to be achieved within the specimen [52]. The forces calculated on the incident and reflected pulses (front face) should match the force calculated on the transmitted pulse (back face) to achieve force equilibrium.

Figure 51 – Force equilibrium

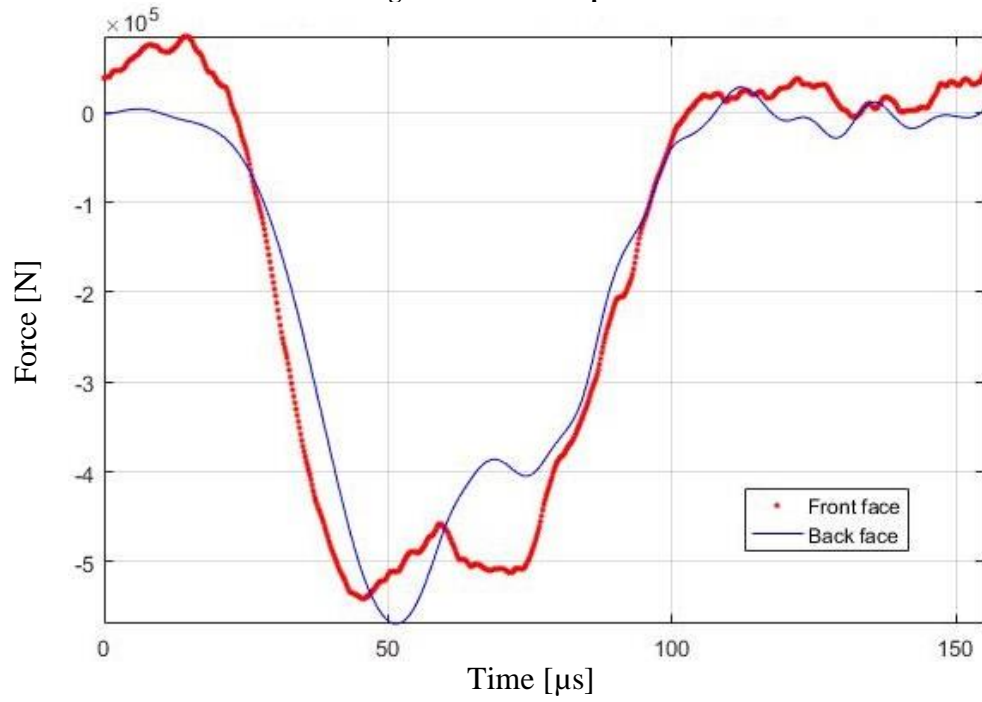


Figure 52 – Strain vs. time of incident-, reflected-, and transmitted pulses

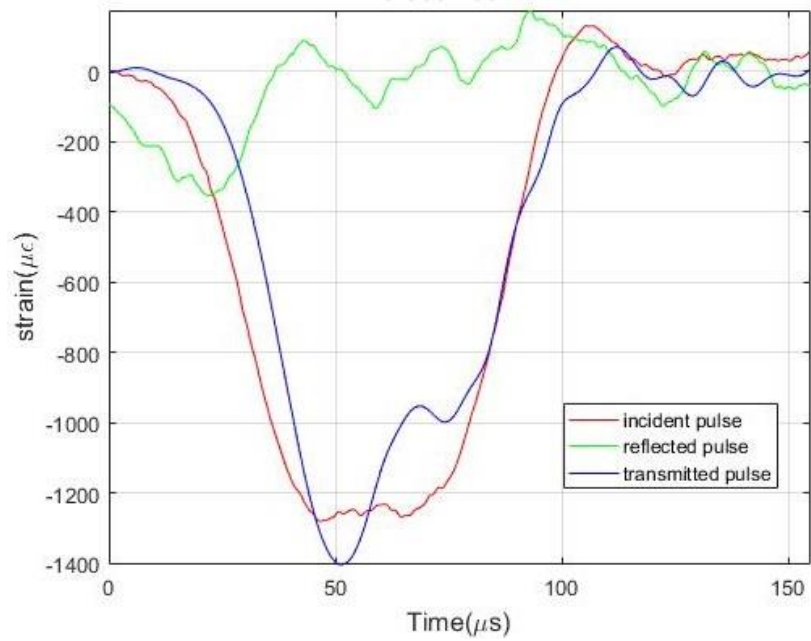
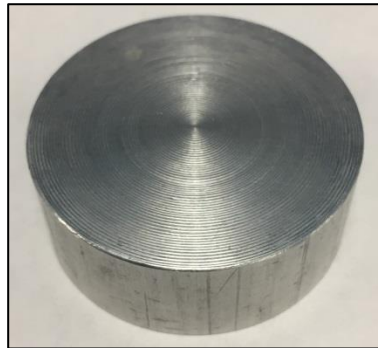


Figure 51 shows the forces that would be applied on a specimen between the incident and transmitted bar. Front face and back face nearly match, meaning that force equilibrium is achieved. *Figure 52* shows the transmitted pulse in relation to the incident and reflected pulses.

6.1.3 Testing of aluminum specimen

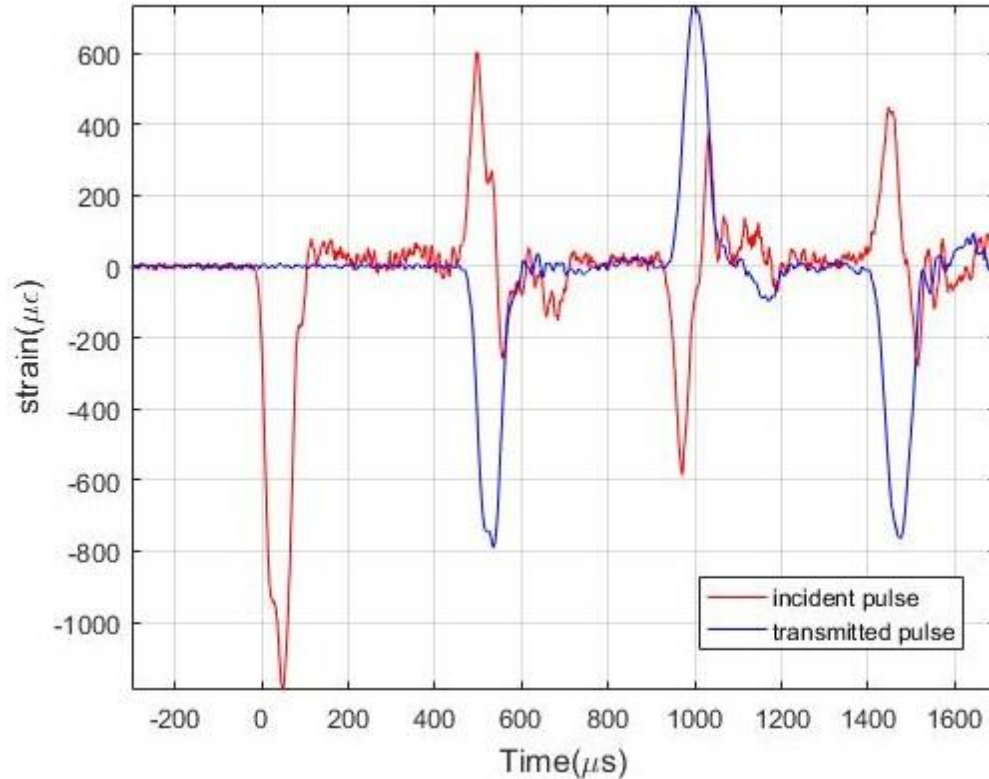
Before testing the prepared Iron Carbonate specimens, the results were verified by testing an aluminum 6061 specimen with the same dimensions (1.5 in. diameter, 0.6 in. length) as the novel binder samples (see *Figure 53*). The aluminum sample was lubricated with Molybdenum disulfide lubricant and placed between the incident and transmitted bar. The projectile was fired at the incident bar using a pressure of 350 psi following the experimental procedure described in *chapter 5, section 5.3*. As a pulse shaper a thin layer of clay was applied on one face of the incident bar.

Figure 53 - Aluminum 6061 specimen(1.5 in. diameter, 0.6 in. thickness) tested to verify future results

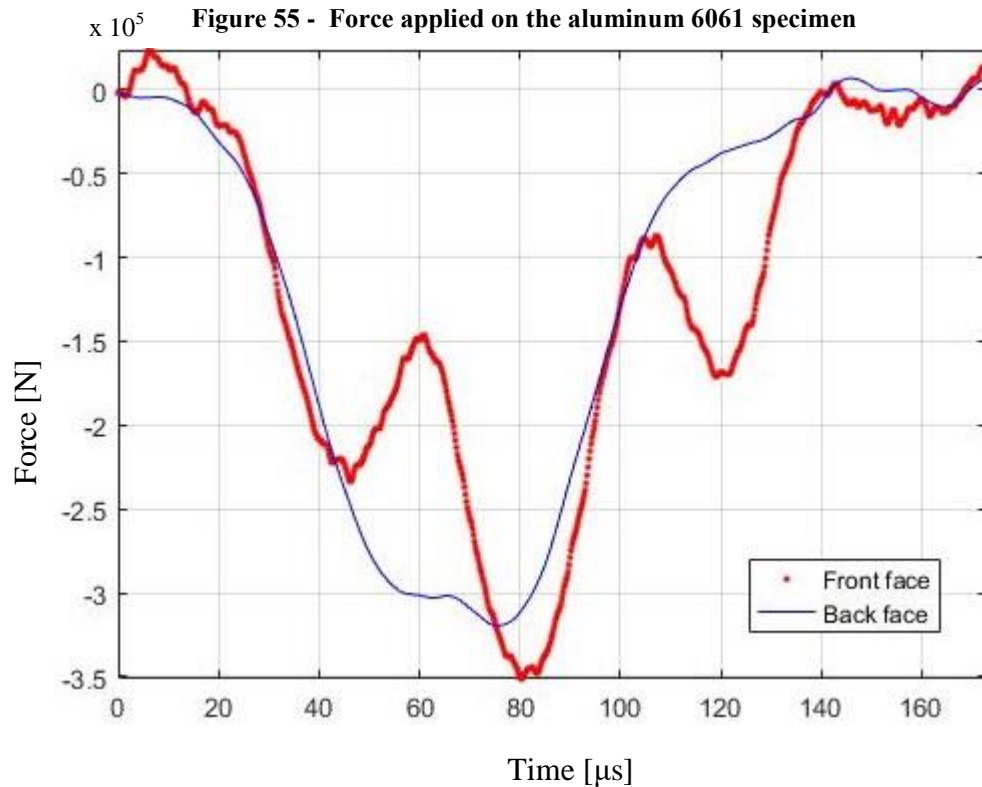


The data analysis was carried out following *section 5.4*. The following figures were obtained using the DPML-MATLAB codes “Verify_Equilibrium” and “Steel_SHPB”:

Figure 54 - Original pulses obtained by testing a cylindrical aluminum 6061 specimen



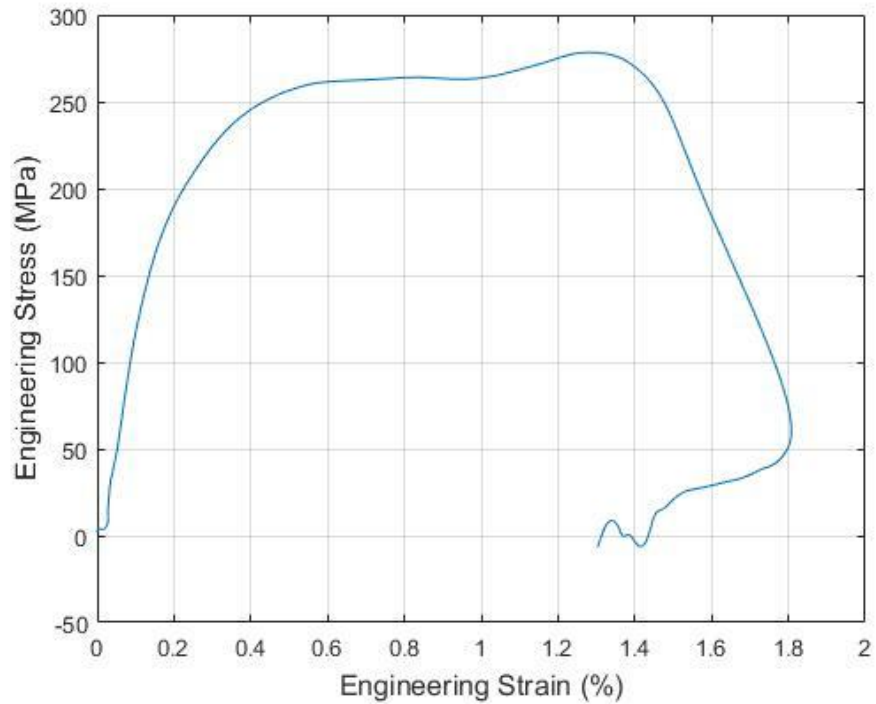
For material property characterization, a dynamic stress equilibrium and constant strain-rate need to be achieved within the specimen [52]. By adjusting the starting and ending times of the incident ($-28 \mu\text{s}$; $145 \mu\text{s}$), reflected ($435 \mu\text{s}$) and transmitted ($459 \mu\text{s}$) pulses, one can achieve near force equilibrium (see *Figure 55*). “Front face” represents the forces calculated on the incident and reflected pulses and “Back face” represents the force calculated on the transmitted pulse. Ideally, front and back face should match perfectly (see *Figure 45, section 5.4*) to achieve force equilibrium. Minor inaccuracies could possibly be due to a misalignment between the incident and transmitted bar and prevent a perfect match of the front and back face.



Using the same starting and ending times of the incident, reflected and transmitted pulses in the “Steel_SHPB”-MATLAB code, one can obtain an engineering stress-strain graph (see *Figure 56*). Engineering stress, also known as nominal stress, is the applied load divided by the original cross-sectional area of a material [83]. Engineering strain, also known as nominal strain, is the amount a material deforms per unit length.

By selecting the slope of the engineering stress-strain curve within the MATLAB-program, one can obtain the true strain-time graph (see *Figure 59*), the true strain conforming the natural logarithm of the quotient of current length over original length [83].

Figure 56 – Initial engineering stress vs. engineering strain of aluminium 6061



Comparison of *Figure 56* to *Figure 58* and *Figure 57* shows a similar initial stress-strain behavior of the tested aluminum specimen to results obtained by other researchers even though the tested aluminum 6061 specimen was barely deformed. However, comparison indicates that the present set-up of the split Hopkinson pressure bar is sufficient enough to give acceptable results.

Figure 57 - Dynamic stress-strain curves of Al-6061-T6 alloys showing (inset) material constants (m) and hardening coefficients (n) under the impacts at various strain rates [84]

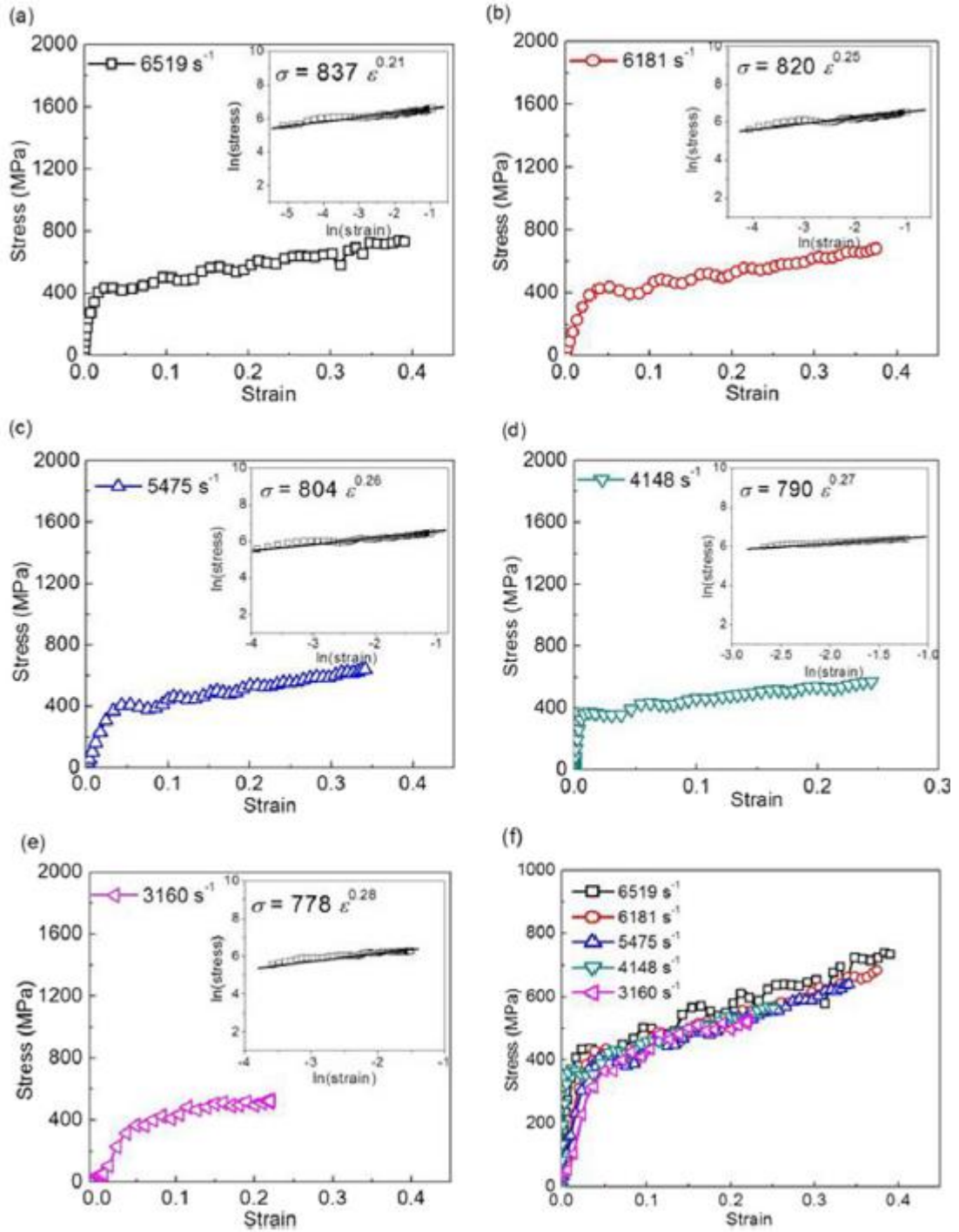
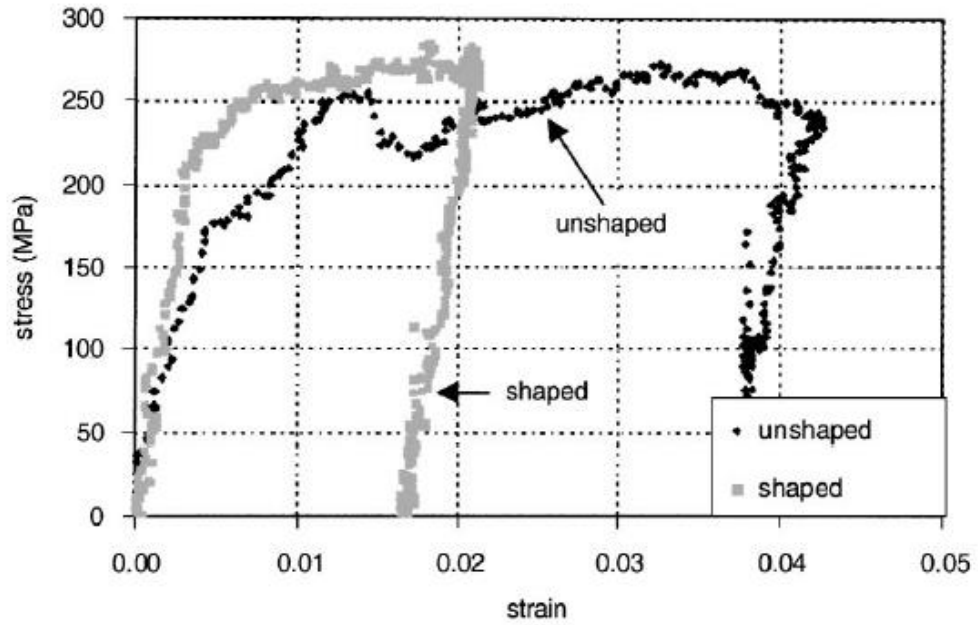


Figure 58 – Initial part of the dynamic stress-strain curve of aluminum [85]



Completing the data analysis of the aluminum specimen one can obtain *Figure 59* and *Figure 60*. The final strain-rate for aluminum provided by the MATLAB-code is 350 s^{-1} .

Figure 59 - True strain vs. time of aluminum 6061

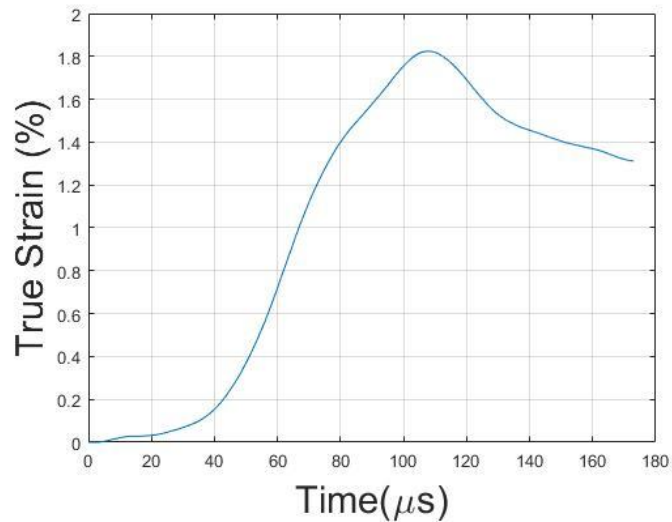
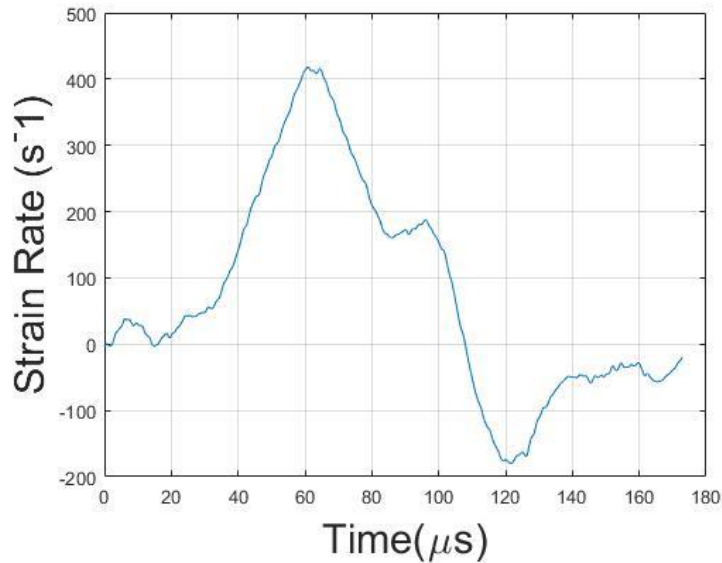


Figure 60 - Strain-rate vs. time of aluminum 6061



6.2 Expected results

As already outlined in *chapter 3, section 3.4*, the author expects an enhanced performance under dynamic compression testing for the Iron Carbonate binder. Compressive strain at failure of ordinary concrete is 0.005 and can serve as a minor guiding value for Iron Carbonate. Tensile strain at failure of Iron Carbonate is 0.00035, according to Dr. Das.

Other material properties of Iron Carbonate have shown to be equal or better in comparison to conventional OPC-based binders. Main reason is the metallic particulate phase incorporated in the novel binders' microstructure that increases the toughness of Iron Carbonate because of energy dissipation by plastic deformation of the unreacted and elongated, strong and ductile iron particles [48]. In addition, the matrix of Iron Carbonate contains other additives including harder fly ash particles, softer limestone particles, and ductile clayey phases which significantly influence the overall fracture performance of the novel sustainable binder.

Both Iron Carbonate mixtures contains polypropylene fibers respectively steel fibers at 1% fiber volume fraction; the fracture energy is approximately 4 times higher at 1% fiber volume fraction [47] and would also suggest an enhanced performance under dynamic compression in SHPB tests.

Figure 61 - Dynamic compressive strength of paste, mortar and concrete [53]

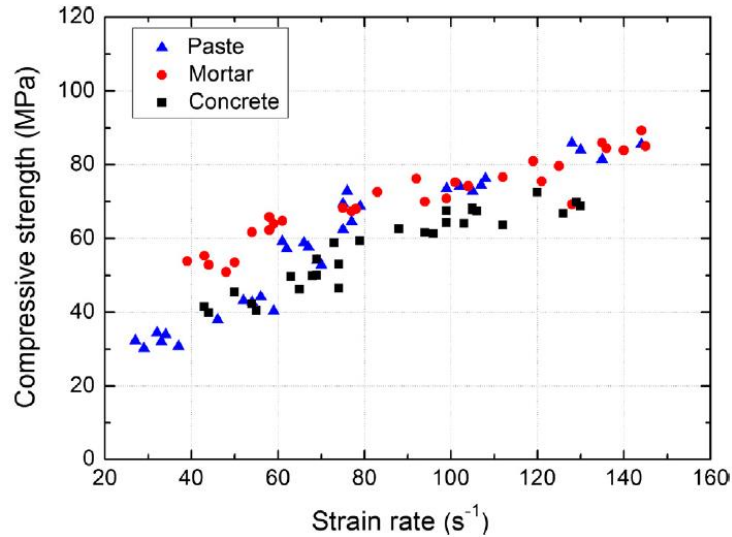
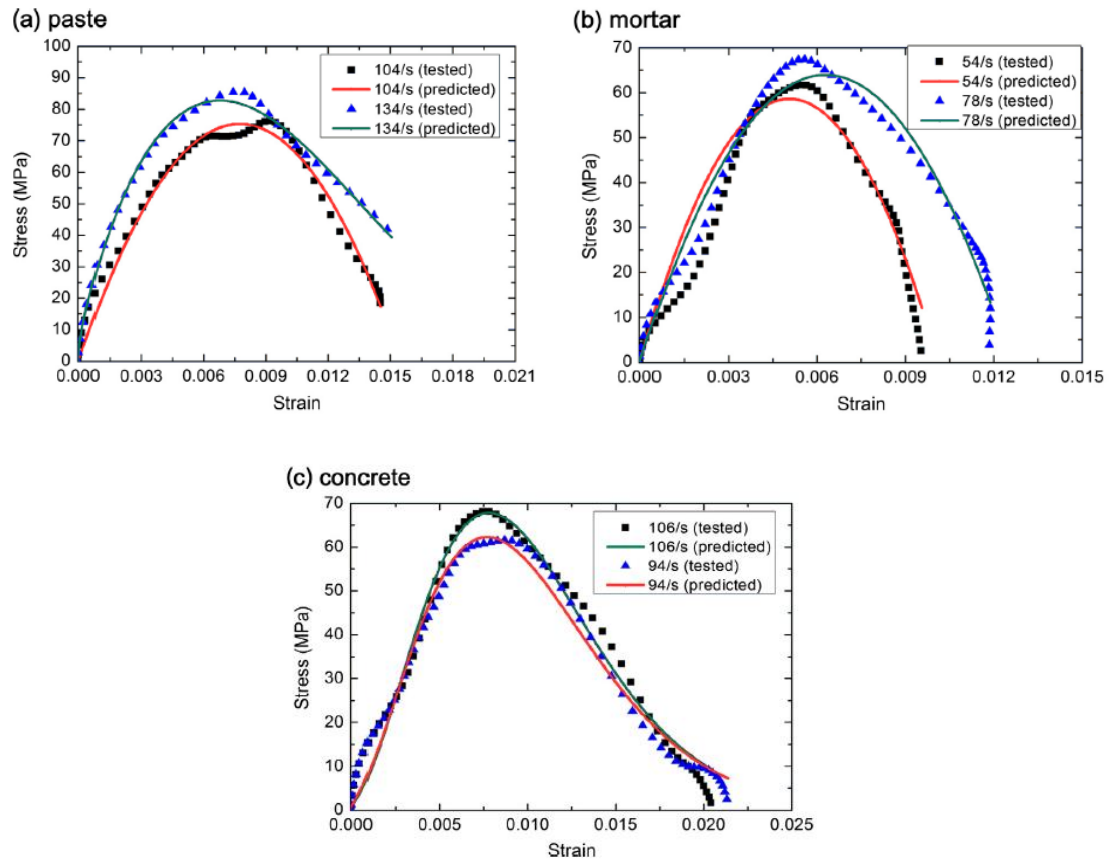


Figure 61 shows the dynamic compressive strength vs. strain-rate for cement paste, mortar, and concrete, according to Chen et al. [53]. It shows that dynamic strength increases approximately linearly with increasing strain-rate. A similar material behavior, i.e. strength enhancement at high strain-rates, has been shown for other materials like rocks, ceramics, composites and steel. The author believes that dynamic compressive strength of Iron Carbonate will also increase with increasing strain-rate.

Figure 62 shows the dynamic stress-strain curves of paste, mortar and concrete at various strain-rates as described by a model developed by Chen et al. [53] and corresponding experimental results [53].

Figure 62 - Comparison of stress-strain curves of specimens determined by experiments and model [53]



Mortar is found to have higher quasi-static compressive strength (~46 MPa) as compared to concrete (~30 MPa) due to different deformation and failure mechanisms [51]. Concrete fails premature due to development and growth of micro-cracks along aggregate-matrix interfaces as a result of high stress concentrations. Since mortar has a somewhat comparable material density (2100 kg/m^3) and quasi-static compressive strength (~46 MPa) to Iron Carbonate (2500 kg/m^3 ; 35–40 MPa), dynamic material behavior of mortar could serve as orientation for dynamic behavior of Iron Carbonate. Although, as already mentioned, incorporation of the metallic particulate phase in the novel binders' microstructure and the addition of polypropylene fibers suggest an enhanced performance under dynamic compression in SHPB tests compared to analog

binder materials. *Table 4* lists results of SHPB experiments on mortar carried out by Grote et al. [51].

Table 4 - SHPB experiments on mortar carried out by Grote et al. [51]

Test ID	Strain rate (s ⁻¹)	Compressive strength (MPa)	Specimen diameter, <i>D</i> (mm)	Specimen length, <i>L</i> (mm)	<i>L/D</i>	Diameter of pressure bar used (mm)
1	450	60	15.2	11.7	0.76	19.05
2	450	70	15.2	11.2	0.73	19.05
3	1000	110	10.1	5.5	0.54	19.05
4	700	65	10.1	10.5	1.04	12.70
5	480	60	10.8	16.0	1.48	12.70
6	500	60	10.8	15.2	1.41	12.70
7	650	65	11.3	14.2	1.27	12.70
8	1350	125	11.3	14.2	1.26	12.70
9	700	85	11.4	6.0	0.52	19.05
10	800	85	11.9	6.3	0.53	19.05
11	940	95	11.7	6.0	0.51	19.05
12	850	95	11.9	5.5	0.46	19.05
13	600	80	12.0	5.8	0.49	19.05
14	620	78	11.6	5.9	0.51	19.05
15	900	90	11.5	5.9	0.51	19.05
16	1350	110	11.4	4.8	0.42	19.05
17	400	55	11.8	11.4	0.97	19.05
18	290	50	11.9	11.7	0.99	19.05
19	700	65	11.9	11.9	1.00	19.05
20	300	45	12.1	17.7	1.47	19.05
21	350	60	11.5	17.8	1.55	19.05
22	280	40	12.3	17.3	1.4	19.05
23	400	70	12.0	12.3	1.03	19.05
24	1050	110	12.0	5.6	0.47	19.05
25	1500	160	11.2	5.5	0.49	19.05
26	1700	180	11.4	5.1	0.45	19.05
27	680	110	11.4	11.4	1.00	19.05
28	660	100	11.4	12.8	1.12	19.05
29	830	142	18.7	6.2	0.33	19.05
30	880	147	18.7	5.8	0.31	19.05
31	250	75	18.8	14.2	0.75	19.05

The stress in a specimen tested in a SHPB can be estimated based on one-dimensional wave propagation analysis using the following equation [86]:

$$\sigma(t) = \frac{2A_s \rho_s c_s}{A_0 \rho_0 c_0 + A_s \rho_s c_s} \frac{A_0}{A_s} \sigma_1(t) \quad (1)$$

In *Eq.(1)* ρ is the mass density, c is the elastic wave velocity of the bar material respectively the specimen, A is the cross-sectional area, and σ_I is the stress of the incident pulse [86] which can only be determined by carrying out a SHPB experiment (see *section 6.3*). Thereby, subscripts 0 and s represent the bar respectively the

specimen. Since the elastic wave velocity c_s for Iron Carbonate is unknown to date, the author assumed a wave velocity similar to conventional concrete, according to Mohr [87]. The following *Table 5* shows the values used to estimate the stress in an Iron Carbonate specimen during a conventional SHPB experiment according to *Eq.(1)*:

Table 5 - Values used in Eq.(1) to estimate stress in specimen during SHPB tests

bar	Iron Carbonate specimen
$A_0=3.14 \text{ in}^2$	$A_s=1.77 \text{ in}^2$
$\rho_0=8000 \text{ kg/m}^3$	$\rho_s=2500 \text{ kg/m}^3$
$c_0=5010 \text{ m/s}$	$c_s= 3162 \text{ m/s}$
$A_0\rho_0c_0 = 40,080,000$	$A_s\rho_sc_s = 4,446,563$
$\sigma_1=60 \text{ MPa}^*$ $* 12 \times 10^4 \text{ N acting upon } A_s$	

The estimated stress in the specimen during SHPB tests following *Eq.(1)* calculates to $\sigma(t) = 38 \text{ MPa}$. Lu and Xu [88] claim that the dynamic compressive strength of concrete materials (at a strain rate of order 100 s^{-1}) is about 1.5 times of the static compressive strength. Assuming a static compressive strength of 35 MPa for Iron Carbonate (see *section 3.4*) the dynamic compressive strength would come to 52.5 MPa. The dynamic tensile strength increases 7 times compared to the static tensile strength at the same strain-rate [88].

6.3 Results and Discussion

Following the experimental procedure described in detail in *section 5.3*, the author tested four polypropylene fiber containing Iron Carbonate specimens in the SHPB, hereafter referred to as specimens P1-1, P1-2, P1-3 and P1-4.

All specimens were tested using a gas pressure of 350 psi to fire the striker bar toward the incident bar. As pulse shaper a thin layer of standard clay was applied between the striker and the incident bar (see *Figure 63*). The surfaces of each specimen were lubricated with Molybdenum disulfide lubricant to reduce friction (see *section 4.3.3.2*). Although each experiment was carefully set up and monitored, testing of P1-3 failed to produce usable data for an analysis; the author suspects premature triggering of the digital oscilloscope as the reason for unsuccessful monitoring.

Manufacturing constraints of the Iron Carbonate specimens comprised evenness of the specimens' surfaces, causing misalignment between the steel bars and the specimens' surfaces, potentially affecting the results by creating additional reflecting pulses. As can be seen from *Figure 64* the specimen is clearly misaligned with the incident bar (left) because it is not in direct contact.

Figure 63 - Clay as pulse shaper on one face of the incident bar



Figure 64 - Misalignment of Iron Carbonate specimen P1-2

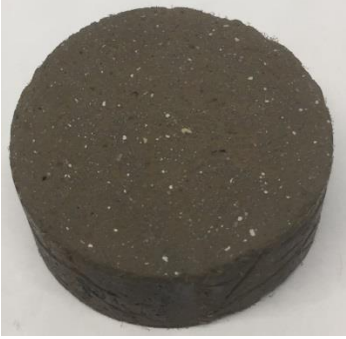
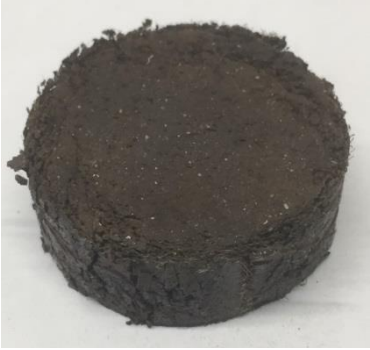







Non-parallel loading surfaces and poor flatness of brittle specimens (see *Figure 64*) as well as bar misalignment (see *Figure 50*) can lead to stress concentrations around the edges of the samples. Eventually those locally concentrated stresses cause uneven and premature failure of a specimen. Please refer to *section 4.3.5* for more detailed information.

Figure 65 shows pictures of the tested Iron Carbonate specimens before and after exposure to dynamic compression during the SHPB experiments. All specimens failed and exhibited cracking. However, plastic deformation near the impact end facing the incident bar seems to be greater than near the end facing the transmitted bar. This nonhomogeneous deformation could potentially indicate a non-equilibrium stress state. Slow motion side view video footage supports the authors' argument of nonhomogeneous deformation.

Nonetheless, the high strain-rate loading did not result in disintegration of the cylindrical samples into small pieces. This could be attributed to implementation of polypropylene fibers (at 1% fiber volume fraction) within the microstructure of the tested material; the fracture energy is approximately 4 times higher at 1% fiber volume fraction [47]. Also, as outlined in *section 3.4*, Iron Carbonate binders have demonstrated to have four to six times higher flexural strengths than OPC-based binders [48]. This can be attributed to the combination of the strong carbonate matrix in combination with the presence of unreacted iron particles in the microstructure. Unreacted iron particles result in a significantly higher peak load and improved post peak response compared to OPC binders [48]. Furthermore, Iron Carbonate binders show an enhanced fracture performance due to the beneficial effects of the elastic, partially reacted or unreacted metallic particles on crack bridging and deflection [47]. IC has significantly higher crack growth resistance than OPC binders and has also been shown to provide significantly higher total fracture energy than OPC.

Figure 65 - Undeformed and deformed Iron Carbonate specimens

	<i>undeformed</i>	<i>deformed</i>
<i>PI-1</i>	 A dark brown, cylindrical specimen with a relatively smooth, uniform surface and a slightly textured top.	 The same specimen after deformation, showing significant surface cracking and a rough, irregular top edge.
<i>PI-2</i>	 A dark brown, cylindrical specimen with a smooth surface and a small, light-colored circular mark on the top.	 The specimen after deformation, showing surface cracking and a slightly irregular top edge.
<i>PI-3</i>	 A dark brown, cylindrical specimen with a smooth surface and a slightly textured top.	 The specimen after deformation, showing significant surface cracking and a rough, irregular top edge.
<i>PI-4</i>	 A dark brown, cylindrical specimen with a smooth surface and a slightly textured top.	 The specimen after deformation, showing significant surface cracking and a rough, irregular top edge.

Before and after each SHPB experiment, diameter and thickness of the Iron Carbonate specimen were measured with a caliper gauge and noted down. *Table 6* shows the undeformed respectively deformed diameter and thickness of the tested Iron Carbonate samples.

Table 6 – Diameter \varnothing and thickness t of cylindrical Iron Carbonate specimens before (undeformed) and after (deformed) dynamic compression test in SHPB

sample	firing pressure	$\varnothing_{\text{undef.}}$	$\varnothing_{\text{def.}}$	Δ	$t_{\text{undef.}}$	$t_{\text{def.}}$	Δ
	[psi]	[in]	[in]	[in]	[in]	[in]	[in]
P1-1	350	1.564	1.635	+0.071 (+4.54%)	0.617	0.591	-0.023 (-3.73%)
P1-2	350	1.564	1.625	+0.061 (+3.90%)	0.635	0.619	-0.016 (-2.52%)
P1-4	350	1.555	1.621	+0.066 (+4.24%)	0.606	0.586	-0.02 (-3.30%)

The captured voltage pulses from the digital oscilloscope of each SHPB test are analyzed using two MATLAB codes (Verify_Equilibrium and Steel_SHPB), according to *section 5.4*. Objective was to determine the equilibrium, true stress-strain plots and strain-rate for the tested Iron Carbonate specimens. The MATLAB-plots on the following pages were obtained using the incident pulse starting time, incident pulse end time, reflected pulse starting time and transmitted pulse starting time, chosen from the initial voltage pulses plots. The chosen times are listed in *Table 7*. The single-bar experiment (see *section 6.1.1*) helped to choose accurate starting times of the reflected pulses by providing the approximate time $\Delta t = 480 \mu\text{s}$ between the start of the incident pulse to the start of the reflected pulse. For better filtering and noise reduction of the obtained transmitted pulses, the default value of 0.05 ($f_n = 0.05$) was changed to 0.015 ($f_n = 0.015$) in the MATLAB-code.

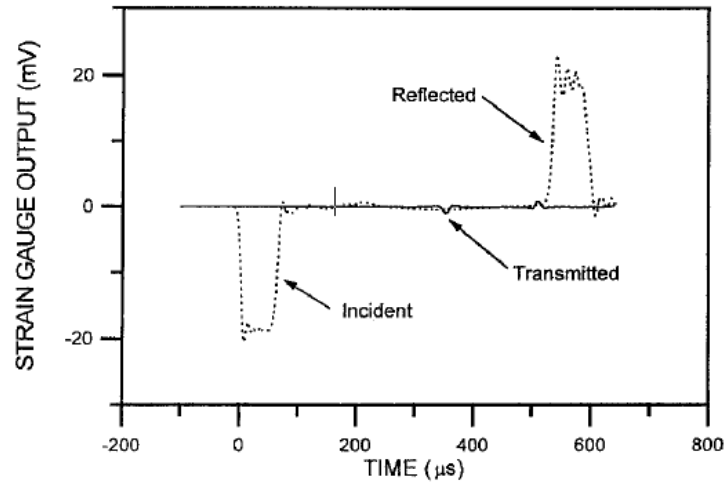
Table 7 - Incident pulse starting and end time, reflected pulse starting time and transmitted pulse starting time used in the MATLAB-codes

instant of time		P1-1	P1-2	P1-4
start incident pulse	[μ s]	-20	-20	-20
end incident pulse	[μ s]	180	180	160
start reflected pulse	[μ s]	465	465	465
start transmitted pulse	[μ s]	460	460	480

Figure 67 and *Figure 68* show the original pulses for each of the Iron Carbonate specimen. Noticeable are small transmitted pulses in comparison to the incident and reflected pulses. The transmitted pulses are hardly distinguishable from the pulses' noise preventing proper interpretation of the signals and making it difficult to obtain a reliable dynamic stress-strain response. It indicates inaccurate results of the SHPB experiments on Iron Carbonate.

Figure 66 shows typical pulses from a conventional SHPB experiment – akin to the set-up used for the present SHPB experiments – testing silicone rubber specimens having low mechanical impedance. The small amplitude of the transmitted pulse is similar to the transmitted signals in *Figure 67* respectively *Figure 68*.

Figure 66 - Strain time records for (low impedance) RTV630 silicone rubber specimen using a conventional SHPB [89]

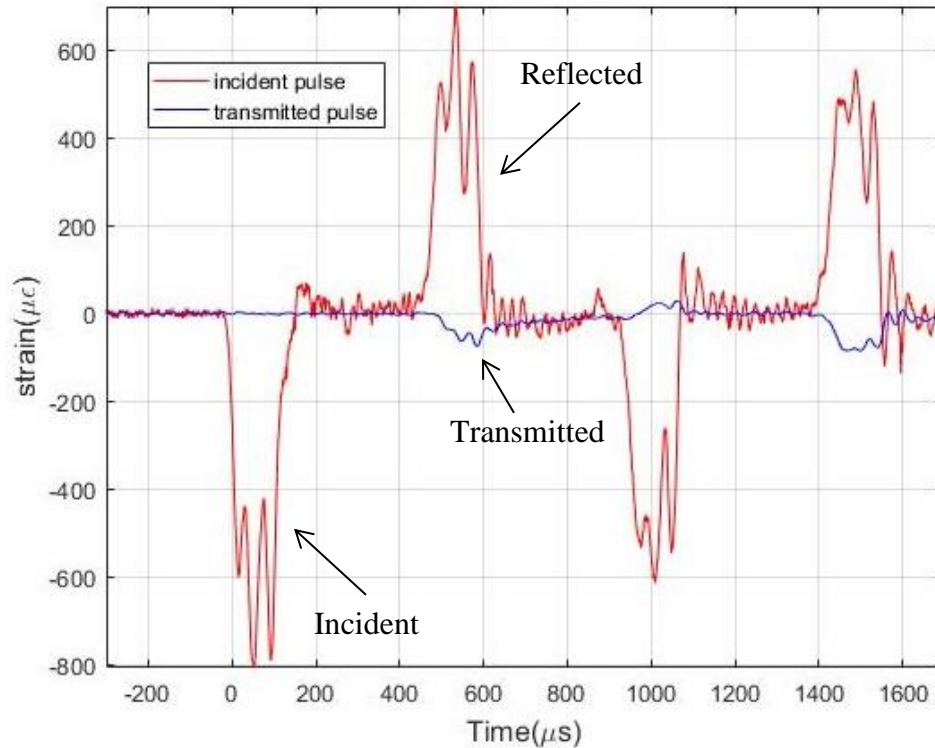


Testing specimens made of material with low mechanical impedance allows the incident bar-specimen interface to nearly move freely under stress wave loading [89]. Most of the incident pulse is reflected backward into the incident bar and only a small portion of the loading pulse is transmitted through the specimen into the transmission bar. The fact that the magnitude of the reflected pulse ($\sim 700 \mu\epsilon$) is insignificantly smaller than the initial magnitude of the incident pulse ($\sim 800 \mu\epsilon$) supports the argument (*Figure 67* and *Figure 68*). As a result the transmitted strain signal shows very small amplitude, as can be seen in *Figure 66* and, more importantly, in the strain signals of the tested Iron Carbonate samples (see *Figure 67* and *Figure 68*). The small amplitude makes it hard to accurately interpret the measured results.

$A_0\rho_0c_0$ respectively $A_s\rho_sc_s$ represent the mechanical impedance according to *Eq.(1)* in *section 6.2* [86]. If the mechanical impedance of the specimen is very low compared to that of the steel bar, the magnitude of the stress $\sigma(t)$ in *Eq.(1)* is very low. Since $\sigma(t)$ is proportional to the transmitted stress (see *Eq.(3)*), it too is very low.

Using values according to *Table 5, section 6.2*, the mechanical impedance of Iron Carbonate is roughly 11% of the impedance of the SHPB steel bars.

Figure 67 - Original pulses of specimen P1-1



If the dynamic yield strength of the specimen – within the rise time of the incident pulse (usually less than 10 μ s) – is smaller than the amplitude of the stress pulse, homogeneous deformation in the sample cannot be reached prior to occurrence of failure [89]. This is due to the low elastic wave velocity in low-impedance materials. As stated previously, the nonhomogeneous deformation of the Iron Carbonate specimens results in a non-equilibrium stress state. Loading pulses should travel back and forth more than three times inside the specimen in order to achieve equilibrium.

Also, both the incident and reflected pulse show some noise indicating an insufficient pulse shaping by the applied clay. Pulse shaping (see *section 4.3.2*)

increases the rise time of the incident pulse and thereby ensures homogenous deformation and stress equilibrium in low-impedance specimen [89].

Figure 69 shows incident-, reflected-, and transmitted pulses of specimen. Once again it becomes apparent that the transmitted pulse is of much smaller magnitude than the incident and reflected pulses preventing stress equilibrium.

Figure 68 - Original pulses of specimen (a) P1-1, (b) P1-2, and (c) P1-4

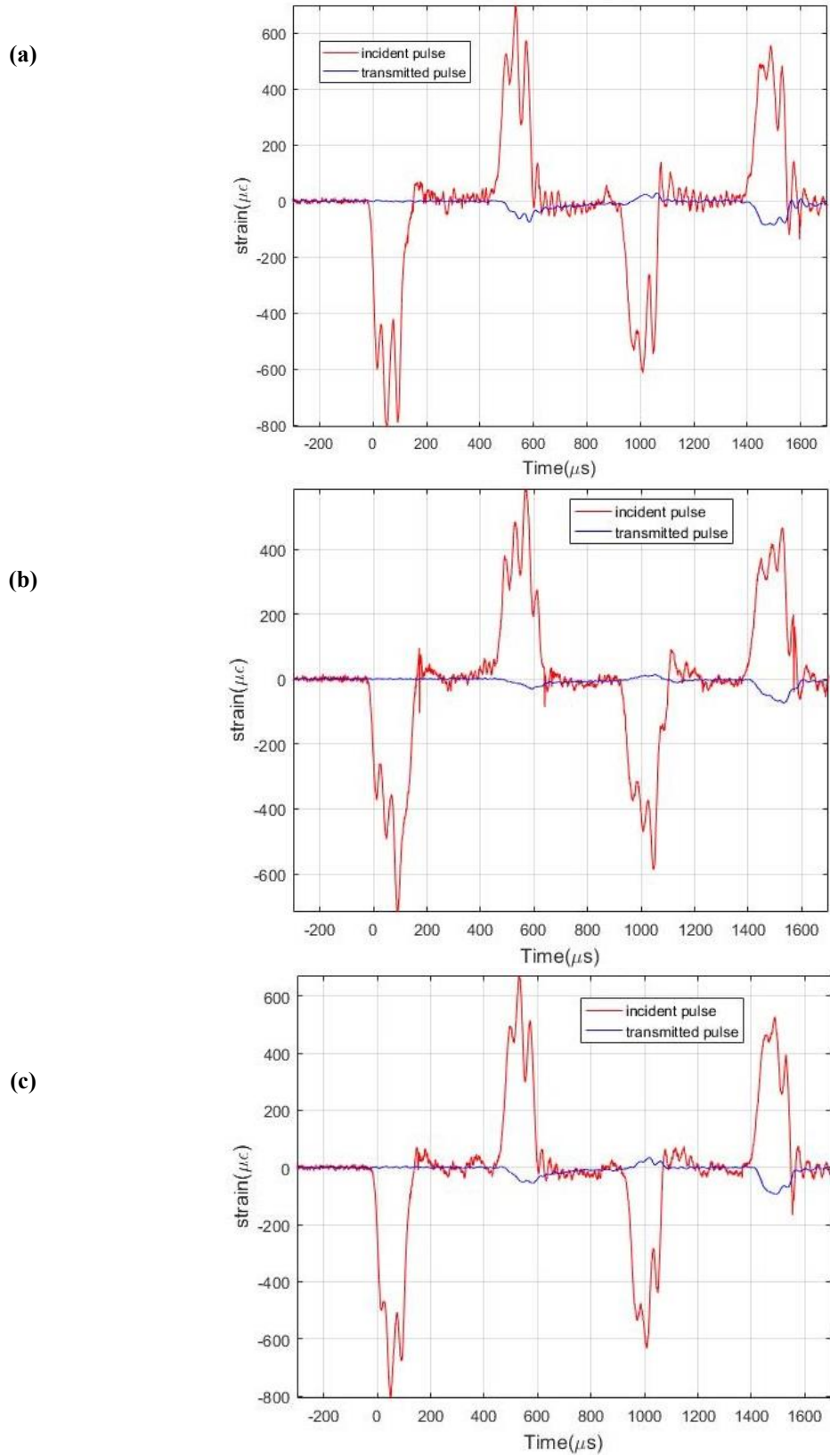
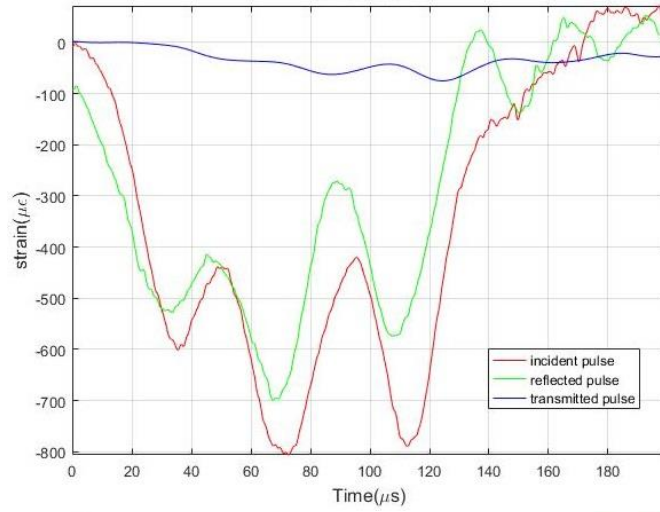
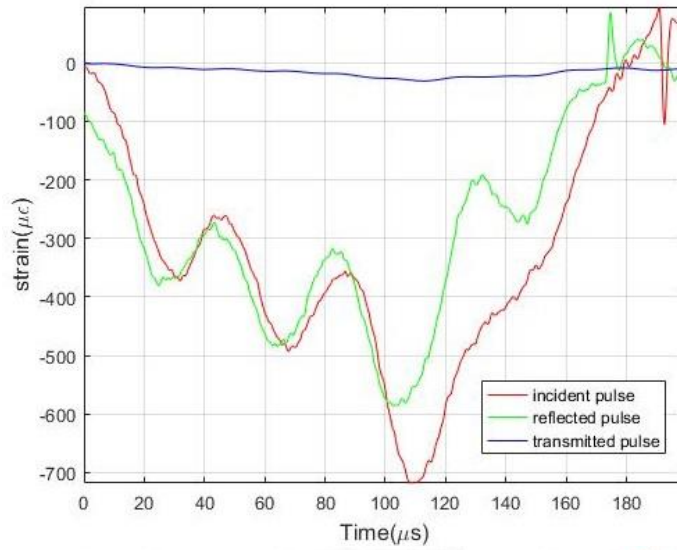


Figure 69 - Incident-, reflected-, and transmitted pulses of specimen (a) P1-1, (b) P1-2, and (c) P1-4

(a)



(b)



(c)

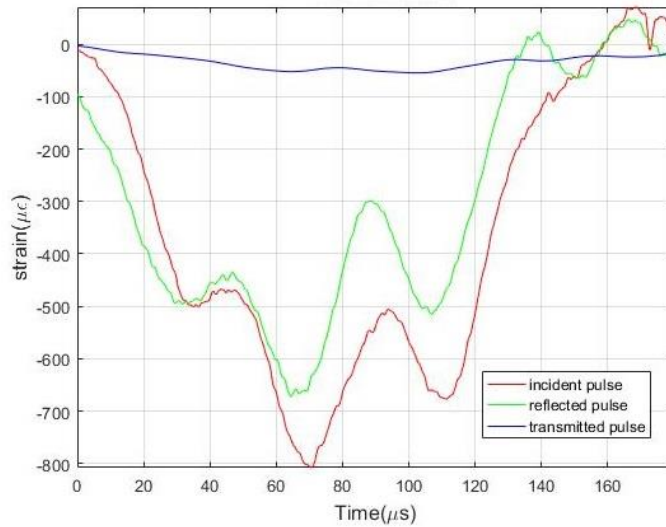


Figure 70 shows the forces applied on the Iron Carbonate specimens. “Front face” represents the forces calculated on the incident and reflected pulses and “Back face” represents the force calculated on the transmitted pulse. Ideally, front and back face should match perfectly to achieve (force) equilibrium. However, in the present SHPB results “Front face” and “Back face” do not match. As outlined before, the small amplitude of the transmitted pulse possibly prevents achievement of an equilibrium stress state.

For the sake of completeness, the obtained but possibly inaccurate MATLAB-plots of the stress-strain response of the Iron Carbonate specimens are included on the following pages. Although no stress equilibrium was achieved, the graphs of each specimen look somewhat similar in each *Figure 71*, *Figure 72*, and *Figure 73* indicating consistency of the experimental and analytical methods. The obtained but questionable strain-rates are listed in the following *Table 8*.

Table 8 - Strain-rates of specimen P1-1, P1-2, and P1-4 obtained with the MATLAB-code

specimen	strain-rate [s ⁻¹]
P1-1	318.99
P1-2	269.49
P1-4	320.77

Figure 70 - Forces applied on specimen (a) P1-1, (b) P1-2, and (c) P1-4

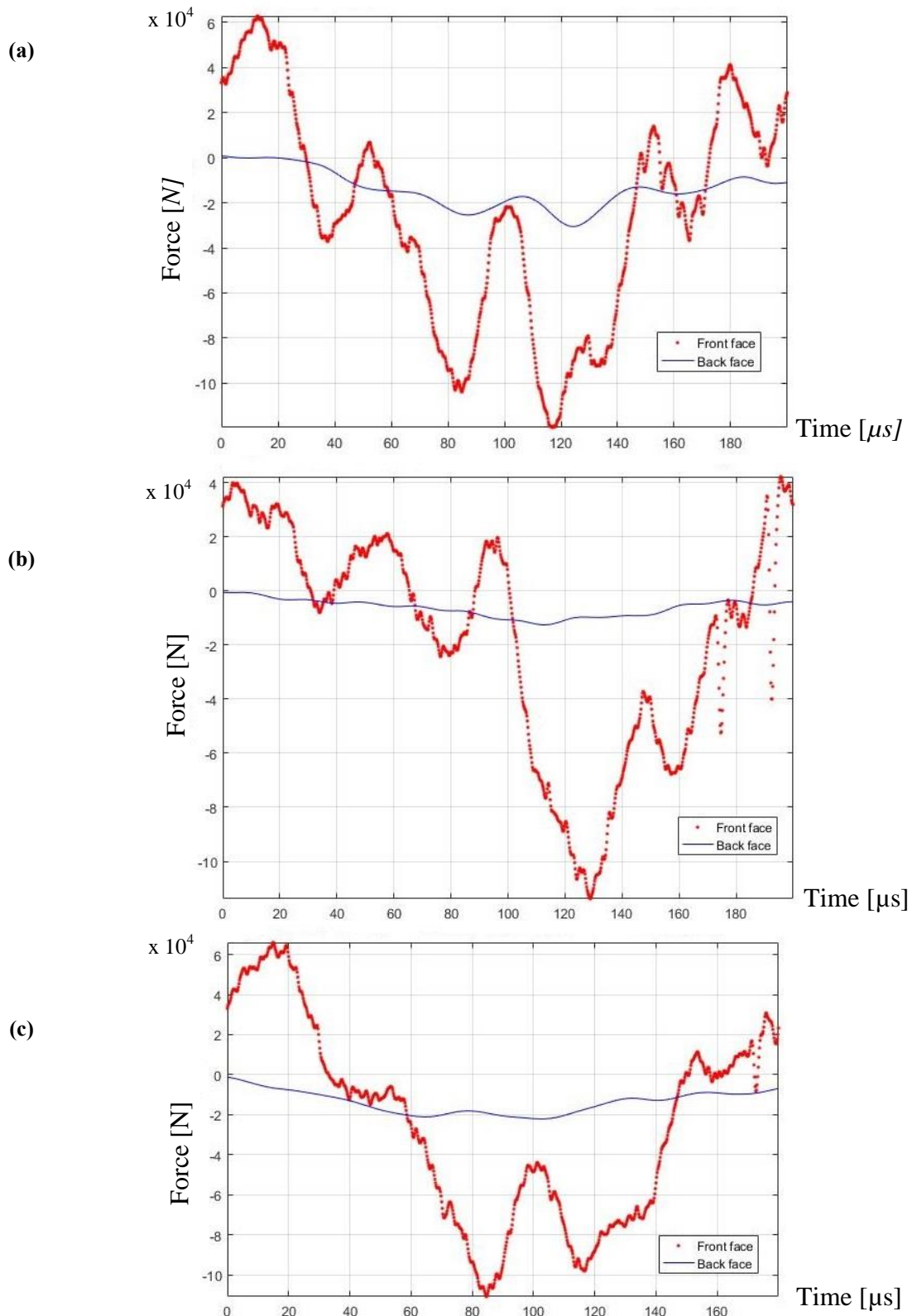
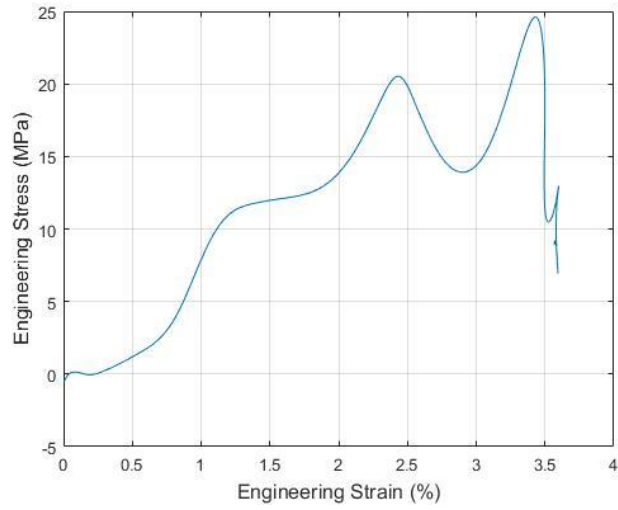
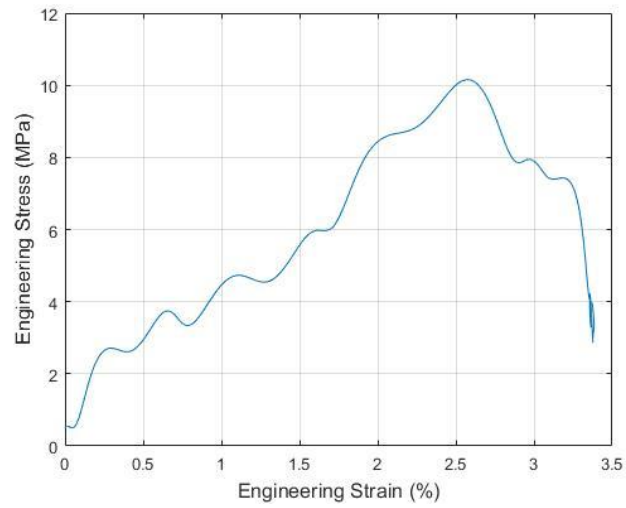


Figure 71 - Eng. stress vs. eng. strain of specimen (a) P1-1, (b) P1-2, and (c) P1-4

(a)



(b)



(c)

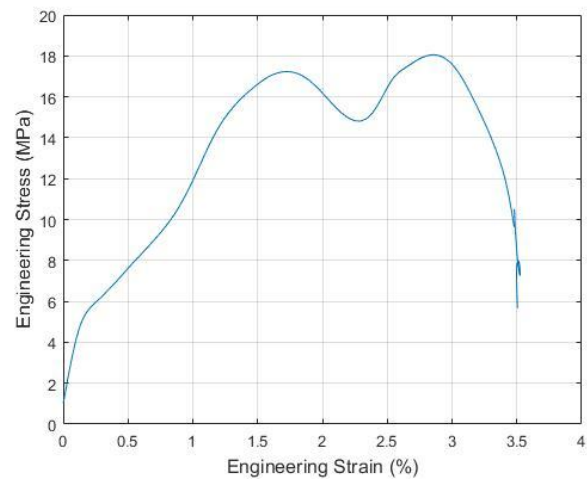


Figure 72 - True strain vs. time of specimen (a) P1-1, (b) P1-2, and (c) P1-4

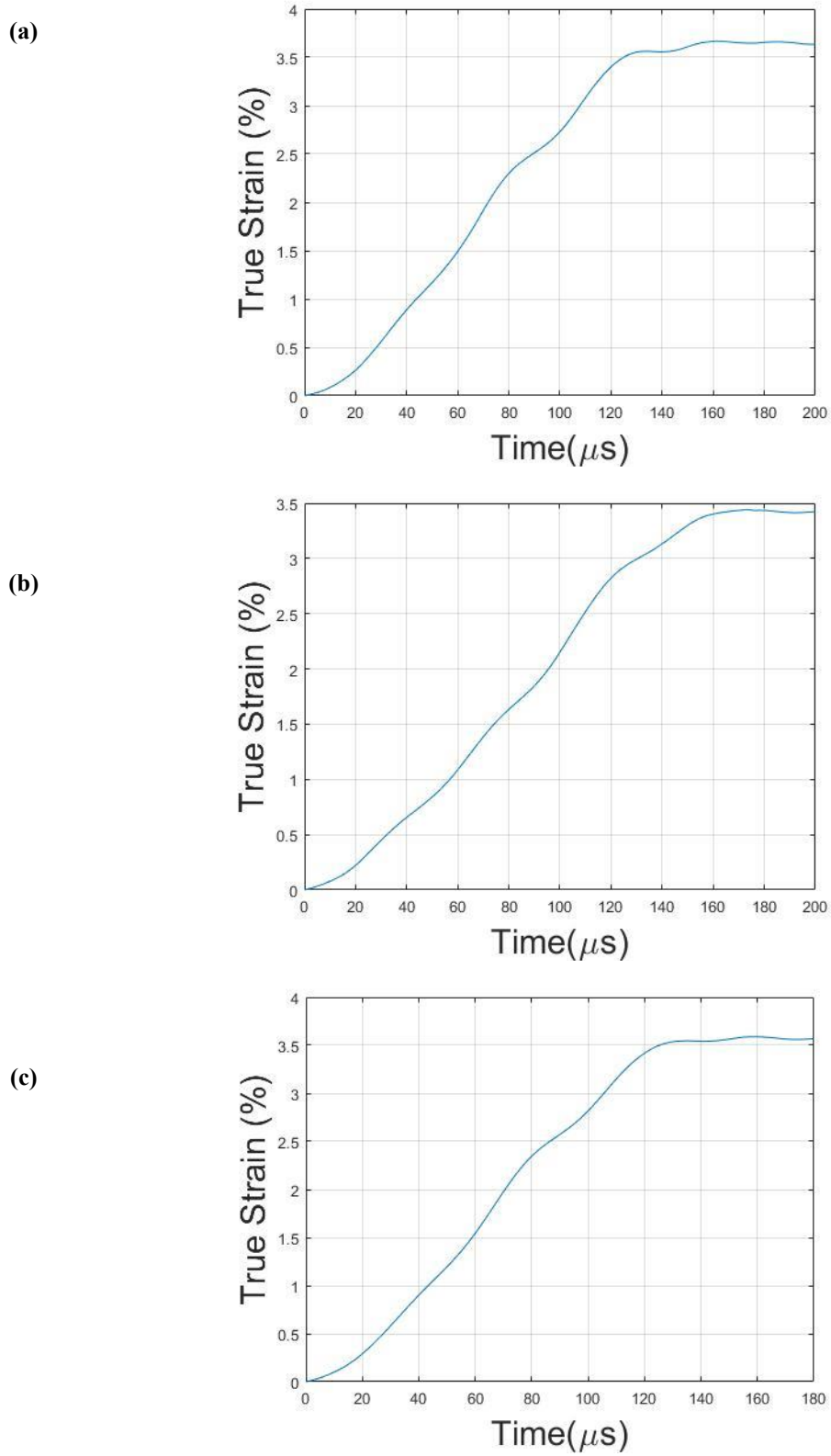
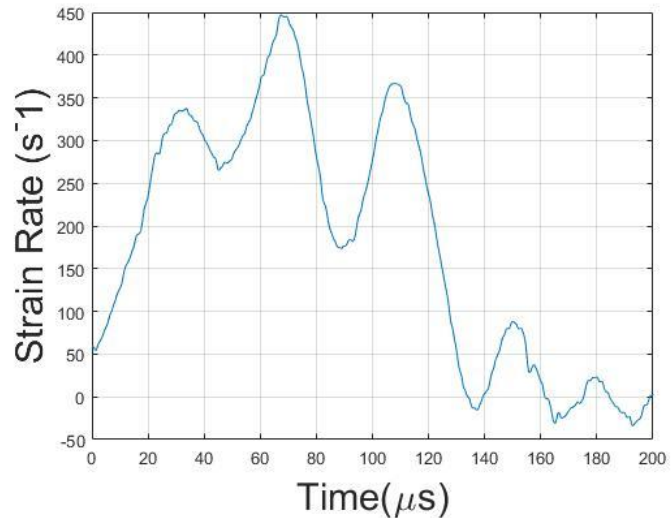
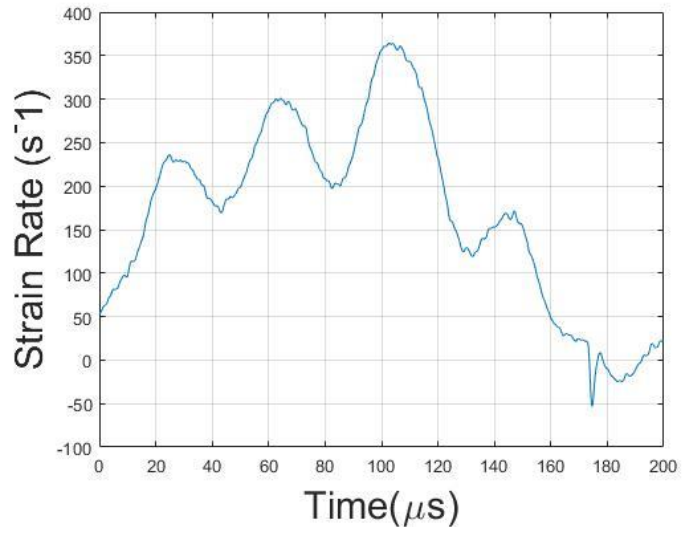


Figure 73 - Strain-rate vs. time of specimen (a) P1-1, (b) P1-2, and (c) P1-4

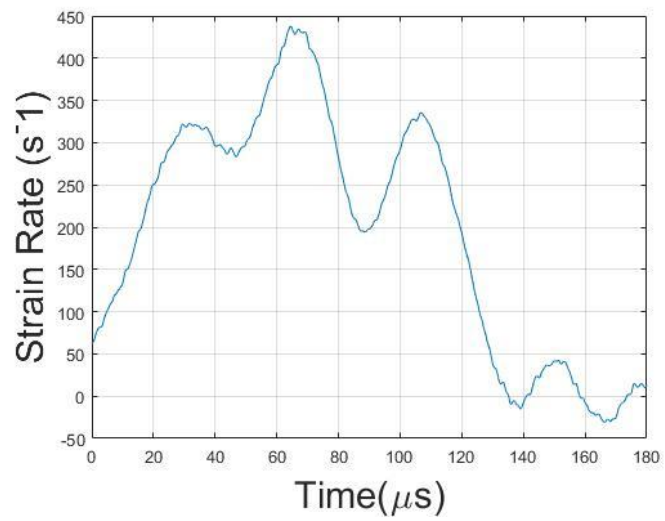
(a)



(b)



(c)



The engineering respectively nominal strain-rate $\dot{\epsilon}(t)$ in the specimen can be calculated based on the assumption of homogenous deformation of the specimens using the following equation [89]:

$$\dot{\epsilon}(t) = -\frac{2c_0}{L} \epsilon_r(t) \quad (2)$$

In *Eq.(2)* L is the original length of the specimen, $\epsilon_r(t)$ is the time-resolved strain of the reflected pulse in the incident bar, and c_0 is the elastic wave velocity of the bar material. The DPML MATLAB-code uses an elastic wave velocity of $c_0 = 5010 \frac{m}{s}$ for the SHPB steel bars.

The engineering respectively nominal axial stress σ in the specimen can be calculated using the following equation [89]:

$$\sigma(t) = \frac{A_0}{A_S} E \epsilon_t(t) \quad (3)$$

In *Eq.(3)* A_S is the cross-sectional area of the specimen, $\epsilon_t(t)$ is the time-resolved axial strain in the transmitted bar, A_0 is the cross-sectional area of the transmitted bar, and E is the Young's modulus of the bar material.

In order to achieve stress equilibrium within the specimen, the amplitude of the transmitted pulse has to be increased. Following *Eq.(3)* it becomes clear that for increasing the transmitted strain $\epsilon_t(t)$ under the same stress level $\sigma(t)$ in the specimen, one need to reduce the Young's modulus E of the bar material and/or the cross-sectional area ratio $\frac{A_0}{A_S}$ [89].

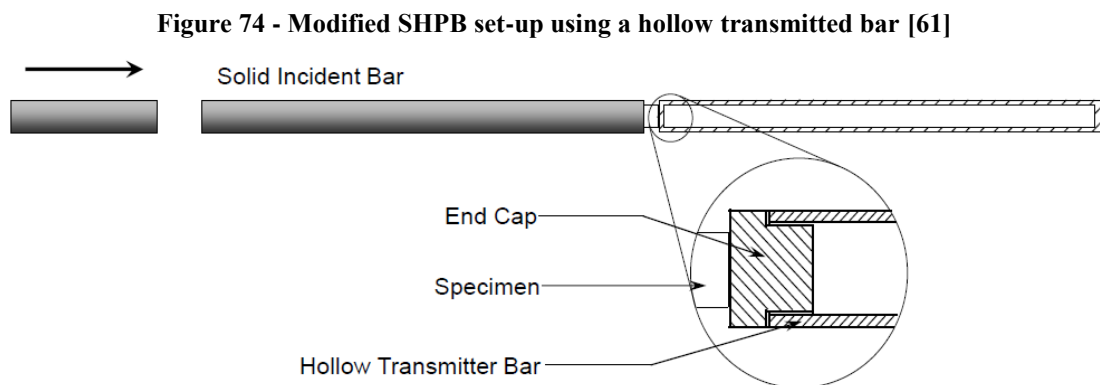
As a summary, it can be stated that the obtained transmitted pulses of the tested Iron Carbonate specimens are of much smaller magnitude than the incident and reflected pulses. As a result, achievement of stress equilibrium and homogeneous

deformation of the Iron Carbonate samples is prevented. The strain gage signals cannot be properly interpreted and obtainment of reliable dynamic stress-strain curves is averted because of the possibly low-impedance of Iron Carbonate. The conventionally used experimental set-up of the split Hopkinson pressure bar has to be modified in order to determine accurate dynamic stress-strain responses. Please refer to the following *section 6.4* for detailed information about future modifications of the experimental set-up.

6.4 Implications for future research

In general, alignment of the experimental set-up needs to be improved by adjusting the I-beam stand and clamps of the incident and reflected bars. Certainly, the portable elevating truck supporting the overhanging part of the transmitted bar should be replaced by a more stable and permanent stand. In addition, a more advanced system to stop the transmitted bar respectively to absorb the axial thrust and to attenuate the impact on the stand needs to be implemented.

As already outlined in the previous *section 6.3*, the amplitude of the transmitted pulse has to be increased to achieve stress equilibrium in the specimens, to enable proper interpretation of the strain gage output signals, and to eventually obtain reliable dynamic stress-strain responses. To increase the transmitted pulse amplitude the Young's modulus E of the bar material and/or the cross-sectional area ratio A_0/A_S have to be reduced. The conventional split Hopkinson pressure bar system should be modified by using a softer material, such as aluminum or magnesium, as transmitted bar material instead of steel. Also, the author suggests using a hollow bar instead of a solid bar. A possible experimental set-up is shown in the following *Figure 74*.



The lower Young's modulus of an aluminum alloy and the smaller cross-section of the hollow bar would increase the amplitude of the transmitted strain signals by at least an order of magnitude as compared to a conventional steel bar (see *Table 9*).

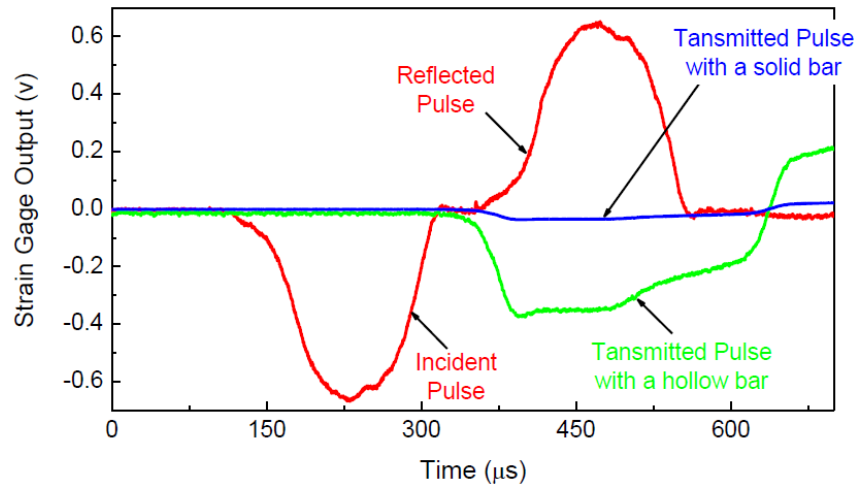
Table 9 - Magnifications in the transmitted signal for different incident and transmitted bar materials and area ratios [61]

Incident Bar	Transmitted Bar	Magnification
MS	MS	1
MS	Al ¹	3
MS	Al ²	12
MS	Lexan ¹	55
MS	Lexan ²	160
Al ¹	Al ¹	1
Al ¹	Al ²	3
Al ¹	Lexan ¹	55
Al ¹	Lexan ²	140

MS:	3/4 in maraging steel bar
Al ¹ :	3/4 in aluminum bar
Al ² :	3/4 in aluminum tube thickness 1/8 in.
Lexan ¹ :	3/4 in lexan bar
Lexan ² :	3/4 in lexan tube thickness 1/8 in.

Figure 75 shows typical strain gage signals when using a solid transmitted bar in comparison with a hollow transmitted bar. A hollow transmitted bar increases the amplitude of the transmitted pulse significantly.

Figure 75 - Typical pulse signals of a solid and hollow bar transmitted bar [61]



Also, both the incident and reflected pulse show some noise (see *Figure 68*) indicating insufficient pulse shaping by the applied clay. A different pulse shaping technique should be applied to slow down dynamic loading of the specimen enough to achieve quasi-static loading, to ensure homogenous deformation, and to reach stress equilibrium in the low-impedance specimen. The author suggests using thin copper plates for pulse shaping instead of clay.

The author recommends cutting the cylindrical Iron Carbonate samples solely with the QEP 4 in. diamond blade on the JET vertical milling machine in the DPML machine shop instead of using the RYOBI circular saw with DIABLO 10 in. saw blade. Thus, the surfaces of the samples could be significantly smoother and more accurate and level. Misalignment between the specimen and the bars could be reduced.

At last, the author thinks it would be important to test specimens made of ordinary Portland cement with the same exact experimental set-up to truly compare the material properties of Iron Carbonate with properties of commonly used OPC-based binders.

7 Conclusive Summary

Conventional concrete is commonly made with ordinary Portland cement (OPC) and has two major issues that make it unsustainable: a high carbon footprint and restricted durability under extreme dynamic loading conditions that makes frequent repair and replacement necessary. Manufacture of 1 ton of Portland cement results in emitting about the same amount of CO₂.

The use of iron carbonated binders has strong environmental benefits because it consumes and sequesters CO₂ from GHG-emitting industries. The sequestration is permanent as opposed to often leaking physical trapping methods. Iron Carbonate could replace cementitious binders and thus reduce the overall production of Portland cement, resulting in a significant reduction of the carbon footprint of the cement and building industry.

The author expected an enhanced performance under dynamic compression testing for the Iron Carbonate binder in the split Hopkinson pressure bar (SHPB) experiment. The performance of Iron Carbonate, under extreme dynamic loading conditions, will potentially establish exceptional dynamic load mitigation characteristics for the carbon-negative sustainable binder under extreme combined environments. Enhanced durability of the novel sustainable concrete through better resistance against dynamic loading would prolong its lifetime, make it even more sustainable and would help to establish Iron Carbonate as a serious alternative for ordinary Portland cement.

Other material properties of Iron Carbonate that have been already tested have shown to be equal or better in comparison to conventional OPC-based binders. Main reason for that is the metallic particulate phase incorporated in the novel binders'

microstructure that increases the toughness of Iron Carbonate because of energy dissipation by plastic deformation of the unreacted and elongated, strong and ductile iron particles. In addition, the matrix of Iron Carbonate contains other additives including harder fly ash particles, softer limestone particles, and ductile clayey phases which significantly influence the overall fracture performance of the novel sustainable binder.

Objective of the carried out dynamic compression tests in a split Hopkinson pressure bar (SHPB) experiment was the determination of the stress equilibrium, true stress-strain plots and strain-rate for Iron Carbonate specimens. Building up of the split Hopkinson pressure bar (SHPB) system in the Dynamic Photomechanics Laboratory (DPML) proved to be extremely difficult and time consuming and analysis of the obtained pulses revealed that the transmitted pulses of the tested Iron Carbonate specimens were of much smaller magnitude than the incident and reflected pulses. As a result, achievement of stress equilibrium and homogeneous deformation of the Iron Carbonate samples was prevented. Thus, the strain gage signals could not be properly interpreted and obtainment of reliable dynamic stress-strain curves was averted. The main reason is believed to be the – in this paper determined – low mechanical impedance of Iron Carbonate.

Testing specimens made of material with low mechanical impedance allows the incident bar-specimen interface to nearly move freely under stress wave loading, so that most of the incident pulse is reflected backward into the incident bar. Only a small portion of the loading pulse is transmitted through the specimen into the transmission bar.

Therefore, the conventionally used experimental standard set-up of the split Hopkinson pressure bar using steel bars has to be modified in order to determine accurate dynamic stress-strain responses for Iron Carbonate. To increase the magnitude of the transmitted pulses, the author recommends using a softer material, such as aluminum, as transmitted bar material instead of steel. Furthermore, the author suggests using a hollow transmitted bar instead of a solid bar. The lower Young's modulus of an aluminum alloy and the smaller cross-section of the hollow bar would increase the amplitude of the transmitted strain signals by at least an order of magnitude as compared to a conventional steel bar.

Although proper interpretation of the strain gage signals was not possible and reliable dynamic stress-strain curves could not be determined, the present paper is suitable to be used as helpful guide for future SHPB experiments on Iron Carbonate. By implementing the modifications described in detail in the present paper, the author believes that successful dynamic tests on Iron Carbonate can be carried out that eventually help to establish exceptional dynamic load mitigation characteristics for the carbon-negative sustainable binder under extreme combined environments.

8 Bibliography

- [1] M. S. Imbabi, C. Carrigan and S. McKenna, "Trends and developments in green cement and concrete technology," *International Journal of Sustainable Built Environment*, pp. 194-216, 2012.
- [2] J. W. Phair, "Green chemistry for sustainable cement production and use," *Green Chemistry*, pp. 763-780, 2006.
- [3] C. Shi, A. F. Jiménez and A. Palomo, "New cements for the 21st century: The pursuit of an alternative to Portland cement," *Cement and Concrete Research*, pp. 750-763, 2011.
- [4] I. Amato, "Concrete Solutions," *Nature*, pp. 300-301, 21 February 2013.
- [5] P.-C. Aïtcin, *Binders for durable and sustainable concrete*, Oxon: Taylor & Francis, 2008.
- [6] N. Winter, "Understanding Cement," 2005. [Online]. Available: <http://www.understanding-cement.com/history.html>. [Accessed 29 December 2016].
- [7] O. Bowles, "Rock Quarrying for Cement Manufacture," *Bulletin 160 - Mineral Technology 22 (U.S. Dept of the Interior)*, 1918.
- [8] Portland Cement Association, "Concrete Thinking for a Sustainable World," 2016. [Online]. Available: <http://www.concretethinker.com/detail/History-Portland-Cement.aspx>. [Accessed 29 December 2016].
- [9] IEA (International Energy Agency), "Technology Roadmap: Cement," 2009. [Online]. Available: <http://www.iea.org/publications/freepublications/publication/technology-roadmap-cement.html>. [Accessed 3 January 2017].

- [10] H. Jennings and J. Thomas, "The Science of Concrete," Northwestern University (Evanston, IL), 2014. [Online]. Available: http://iti.northwestern.edu/cement/monograph/Monograph5_4_3.html. [Accessed 31 December 2016].
- [11] National Energy Information Center (NEIC), "eia.doe.gov," 2004. [Online]. Available: <http://www.eia.gov/oiaf/1605/ggcebro/chapter1.html>. [Accessed 31 December 2016].
- [12] U.S. Environmental Protection Agency (EPA), "Greenhouse Gas Emissions," 2014. [Online]. Available: <https://www.epa.gov/ghgemissions/overview-greenhouse-gases>. [Accessed 31 December 2016].
- [13] E. Dlugokencky and P. Tans, "Trends in Atmospheric Carbon Dioxide," NOAA/ESRL, 2016. [Online]. Available: <https://www.esrl.noaa.gov/gmd/ccgg/trends/>. [Accessed 2 January 2017].
- [14] L. Barcelo, J. Kline, G. Walenta and E. Gartner, "Cement and carbon emissions," *Materials and Structures* 47, pp. 1055-1065, 2014.
- [15] V. M. John, "On the sustainability of concrete," *UNEP Industry and Environment*, pp. 62-63, April-September 2003.
- [16] F.-J. Ulm, *Breaking the Wall of Concrete Pollution @FallingWalls*, Berlin, 2009.
- [17] T. R. Naik, F. Canpolat and Y.-m. Chun, "Limestone powder use in cement and concrete," CBU - University of Wisconsin, Milwaukee, 2003.
- [18] M. Juenger, F. Winnefeld, J. Provis and J. Ideker, "Advances in alternative cementitious binders," *Cement and Concrete Research* 41, pp. 1232-1243, 2011.
- [19] E. Worrel, L. Price, N. Martin, C. Hendriks and L. O. Meida, "Carbon dioxide emissions from the global cement industry," *Annu. Rev. Energy Environ.*, pp. 303-329, 2001.

- [20] F. Rodrigues and I. Joekes, "Cement industry: sustainability, challenges and perspectives," Springer, 2010.
- [21] EPA, "Persistent Organic Pollutants: A Global Issue, A Global Response," 2016. [Online]. Available: <https://www.epa.gov/international-cooperation/persistent-organic-pollutants-global-issue-global-response>. [Accessed 2 January 2017].
- [22] T. Naik, "Sustainability of the cement and concrete industries," Dundee (Scotland), 2005.
- [23] CEMBUREAU, "World cement production 2014," 2014. [Online]. Available: http://www.cembureau.be/sites/default/files/World%20Cement%20production_2.pdf. [Accessed 3 January 2017].
- [24] U.S. Geological Survey, "Cement Statistics and Information," 2016. [Online]. Available: <https://minerals.usgs.gov/minerals/pubs/commodity/cement/>. [Accessed 3 January 2017].
- [25] United Nations, "Our common future, report of the World Commission on Environment and Development," United Nations, Geneva, 1987.
- [26] International Energy Agency, "Cement Technology Roadmap 2009," 2009.
- [27] F.-J. Ulm, "What's the matter with concrete?," *Convegno Nazionale IGF XX, Torino*, pp. 3-10, 24-26 June 2009.
- [28] M. Bauchy, M. Abdolhosseini Qomi, F.-J. Ulm and R. Pellenq, "Gorilla cement: Tougher, yet greener," MIT Concrete Sustainability Hub, Cambridge, 2014.
- [29] Portland Cement Association, "Chemical Admixtures," 2016. [Online]. Available: <http://www.cement.org/cement-concrete-basics/concrete-materials/chemical-admixtures>. [Accessed 21 January 2017].

- [30] K. Majcher, "What Happened to Green Concrete?," 2015. [Online]. Available: <https://www.technologyreview.com/s/535646/what-happened-to-green-concrete/>. [Accessed 16 January 2017].
- [31] greenspec, "Concrete: Cement Substitutes," 2017. [Online]. Available: <http://www.greenspec.co.uk/building-design/concrete-cement-substitutes/>. [Accessed 18 January 2017].
- [32] M. Aguayo, S. Das, V. Dey, R. Kachala, B. Mobasher, G. Sant and N. Neithalath, "The fracture response of blended formulations containing limestone powder [...]," *Cement & Concrete Composites* 53, pp. 316-326, 2014.
- [33] J. Ideker, K. Folliard and M. Thomas, "Early-age properties of calcium aluminate cement concrete with rigid cracking and free shrinkage frames: isothermal testing, Calcium Aluminate Cements: Proceedings of the Centenary Conference," Avignon, France, 2008.
- [34] F. Winnefeld and B. Lothenbach, "Hydration of calcium sulfoaluminate cements - experimental findings and thermodynamic modelling," *Cement and Concrete Research* 40, pp. 1239-1247, 2010.
- [35] C. Yip, G. Lukey, J. Provis and J. van Deventer, "Effect of calcium silicate sources on geopolymerisation," *Cement and Concrete Research* 38, pp. 554-564, 2008.
- [36] W. Shen, L. Cao, Q. Li, Z. Wen, J. Wang, Y. Liu, R. Dong, Y. Tan and R. Chen, "Is magnesia cement low carbon? Life cycle carbon footprint comparing with Portland cement," *Journal of Cleaner Production* 131, pp. 20-27, 2016.
- [37] P. Krivenko, "Alkaline cements: terminology, classification, aspects of durability, Proceedings of the 10th International Congress of the Chemistry of Cements," Goeteborg, 1997.
- [38] J. Davidovits, Geopolymer. Chemistry and Applications, Saint-Quentin, France: Institut Geopolymere, 2008.
- [39] A. Gruskovnjak, B. Lothenbach, F. Winnefeld, R. Figi, S.-C. Ko, M. Adler and U. Mäder, "Hydration mechanisms of super sulphated slag cements," *Cement and Concrete Research* 38, pp. 983-992, 2008.

- [40] D. Bradley, "MIT Technology Review (TR10)," 2010. [Online]. Available: <http://www2.technologyreview.com/news/418542/tr10-green-concrete/>. [Accessed 16 January 2017].
- [41] D. Biello, "Cement from CO₂: A Concrete Cure for Global Warming? (Scientific American)," 2008. [Online]. Available: <https://www.scientificamerican.com/article/cement-from-carbon-dioxide/>. [Accessed 16 January 2017].
- [42] Calera Corporation, "Calera - The Process," 2017. [Online]. Available: <http://www.calera.com/beneficial-reuse-of-co2/process.html>. [Accessed 16 January 2017].
- [43] P. De Silva, L. Bucea, D. Moorehead and V. Sirivivatnanon, "Carbonate binders: Reaction kinetics, strength and microstructure," *Cement & Concrete Composites* 28, pp. 613-620, 2006.
- [44] S. Das, B. Souliman, D. Stone and N. Neithalath, "Synthesis and Properties of a Novel Structural Binder Utilizing the Chemistry of Iron Carbonation," *ACS Applied Materials & Interfaces* 6, pp. 8295-8304, 2014.
- [45] L. Mo, F. Zhang, D. K. Panesar and M. Deng, "Development of low-carbon cementitious materials via carbonating Portland cement - fly ash - magnesia blends under various curing scenarios: a comparative study," *Journal of Cleaner Production*, pp. 1-10, 2016.
- [46] K. Xia and W. Yao, "Dyanmic rock tests using split Hopkinson (Kolsky) bar system - A review," *Journal of Rock Mechanics and Geotechnical Engineering*, no. 7, pp. 27-59, 2015.
- [47] S. Das, D. Stone, B. Mobasher and N. Neithalath, "Strain energy and process zone based fracture characterization of a novel iron carbonate binding material," *Engineering Fracture Mechanics*, no. 156, pp. 1-15, 2016.

- [48] S. Das, A. Hendrix, D. Stone and N. Neithalath, "Flexural fracture response of a novel iron carbonate matrix – Glass fiber composite and its comparison to Portland cement-based composites," *Construction and Building Materials*, no. 93, pp. 360-370, 2015.
- [49] S. Das, D. Stone, D. Convey and N. Neithalath, "Pore- and micro-structural characterization of a novel structural binder based on iron carbonation," *Materials Characterization* 98, pp. 168-179, 2014.
- [50] Dynamic Photomechanics Laboratory, "Steel-SHPB Matlab Code," 2017. [Online]. Available: <http://web.uri.edu/dpml/files/Steel-SHPB-Matlab-Code.txt>. [Accessed 6 June 2017].
- [51] D. Grote, S. Park and M. Zhou, "Dynamic behavior of concrete at high strain rates and pressures: I. experimental characterization," *International Journal of Impact Engineering*, no. 25, pp. 869-886, 2001.
- [52] W. Chen and B. Song, Split Hopkinson (Kolsky) Bar: Design, Testing and Applications, New York: Springer, 2011.
- [53] X. Chen, S. Wu and J. Zhou, "Experimental and modeling study of dynamic mechanical properties of cement paste, mortar and concrete," *Construction and Building Materials*, no. 47, pp. 419-430, 2013.
- [54] W. Riley and L. Zachary, Introduction to Mechanics of Materials, New York: John Wiley & Sons, 1989.
- [55] A. Shukla and J. Dally, "17.7 Split Hopkinson (Kolsky) Bar Technique," in *Experimental Solid Mechanics*, Knoxville, College House Enterprises, LLC., 2010, pp. 554-560.
- [56] B. Hopkinson, "A Method of Measuring the Pressure Produced in the Detonation of High Explosives or by the Impact of Bullets," *Philosophical Transactions of the Royal Society of London. Series A, Containing Papers of Mathematical or Physical Character*, no. 213, pp. 437-456, 1914.

- [57] H. Kolsky, "An investigation of the mechanical properties of materials at very high rates of loading," *Proceedings of the Royal Society A: Mathematical, Physical and Engineering Sciences*, vol. B62, no. 11, pp. 676-700, 1949.
- [58] J. Krafft, A. Sullivan and C. Tipper, "The effect of static and dynamic loading and temperature on the yield of stress of iron and mild steel in compression," *Proceedings of the Royal Society of London Series A: Mathematical and Physical Sciences*, no. 221, pp. 114-270, 1954.
- [59] Z. Li and J. Lambros, "Determination of the dynamic response of brittle composites by the use of the split Hopkinson pressure bar," *Composites Science and Technology* 59, pp. 1097-1107, 1999.
- [60] Dynamic Photomechanics Laboratory, "Standard Operating Procedures - Split Hopkinson Pressure Bar/ Kolsky Bar," 2017. [Online]. Available: <http://web.uri.edu/dpml/standard-operating-procedures/>. [Accessed 28 February 2017].
- [61] A. Shukla, Writer, *Split-Hopkinson (Kolsky) Bar Technique (Lecture)*. [Performance]. Dynamic Photo-Mechanics Laboratory, University of Rhode Island, 2017.
- [62] T. Tang and H. Saadatmanesh, "Behaviour of concrete beams strengthened with fibre-reinforced polymer laminates under impact loading," *Compos Constr ASCE*, no. 7, pp. 209-218, 2003.
- [63] Y.-Q. Zhang, H. Hao and Y. Lu, "Anisotropic dynamic damage and fragmentation of rock materials under explosive loading," *Int J Eng Sci*, no. 41, pp. 917-929, 2003.
- [64] K. Xia, "Status of characterization of strength and fracture properties of rocks under dynamic loading," *Rock fragmentation by blasting: proceedings of the 10th international symposium of rock fragmentation by blasting*, pp. 41-51, 2012.

- [65] E. Davies and S. Hunter, "The dynamic compression testing of solids by the method of the split Hopkinson pressure bar," *Journal of the Mechanics and Physics of Solids*, no. 11, pp. 155-179, 1963.
- [66] C. A. Ross, P. Thompson and J. Tedesco, "Split-Hopkinson Pressure-Bar Tests on Concrete and Mortar in Tension and Compression," *ACI Materials Journal*, no. 86-M43, pp. 475-481, 1990.
- [67] Z. Bieniawski and M. Bernede, "Suggested methods for determining the uniaxial compressive strength and deformability of rock materials," *International Journal of Rock Mechanics and Mining Sciences and Geomechanics Abstracts*, no. 16, pp. 138-140, 1979.
- [68] Q. Li and H. Meng, "About the dynamic strength enhancement of concrete-like materials in a split Hopkinson pressure bar test," *International Journal of Solids and Structures*, no. 40, pp. 343-360, 2003.
- [69] D. Grady and M. Kipp, "The micromechanics of impact fracture of rock," *Int J Rock Mech Min Sci Geomechan Abstr*, no. 16, pp. 293-302, 1979.
- [70] C. Ross, D. Jerome, J. Tedesco and M. Hughes, "Moisture and strain rate effects in concrete strength," *ACI Mater J*, no. 93, pp. 293-300, 1996.
- [71] D. Kim, K. Sirijaroonchai, S. El-Tawil and A. Naaman, "Numerical simulation of the split Hopkinson pressure bar test technique for concrete under compression," *Int J Impact Eng*, no. 37, pp. 141-149, 2010.
- [72] D. Watstein, "Effect of straining rate on the compressive strength and elastic properties of concrete," *ACI Journal*, vol. 49, no. 8, pp. 729-744, 1953.
- [73] J. Takeda and H. Tachikawa, "Deformation and fracture of concrete subjected to dynamic load," in *Proceedings of Int. Conf. on Mechanical Behavior of Materials*, Kyoto, Japan, 1971.

- [74] O. Kvirikadze, "Determination of the ultimate strength and modulus of deformation of concrete at different rates of loading," in *RILEM International Symposium on Testing In-Situ Concrete Structures*, Budapest, 1977.
- [75] T. Hatano and H. Tsutsumi, "Dynamical compressive deformation and failure of concrete under earthquake load," in *Second World Conference on Earthquake Engineering*, Tokyo, Japan, 1960.
- [76] W. Cowell, "Dynamic properties of plain Portland cement concrete, Technical Report No. R447," US Naval Civil Engineering Laboratory, Port Hueneme, CA, 1966.
- [77] B. Hughes and A. Watson, "Compressive strength and ultimate strain of concrete under impact loading," *Magazine of Concrete Research*, vol. 30, no. 105, pp. 189-199, 1978.
- [78] P. Bischoff and S. Perry, "Compression behavior of concrete at high strain-rates," *Materials and Structures*, no. 24, pp. 425-450, 1991.
- [79] D. Yan and G. Lin, "Dynamic properties of concrete in direct tension," *Cem Concr Res*, no. 36, pp. 1331-1338, 2006.
- [80] O. Miller, L. Freund and A. Needleman, "Modeling and simulation of dynamic fragmentation in brittle solids," *Int J Fract*, no. 96, pp. 101-125, 1999.
- [81] Mirco-Measurements, "Strain Gage Installations with M," 2014. [Online]. Available: <http://www.vishaypg.com/docs/11127/11127B127.pdf>. [Accessed 9 July 2017].
- [82] N. McCormick and J. Lord, "Digital Image Correlation," *Materials today*, vol. 13, no. 12, pp. 52-54, 2010.
- [83] Engineering Archives, "True Stress, True Strain, Engineering Stress, and Engineering Strain," [Online]. Available: http://www.engineeringarchives.com/les_mom_truestresstruestrainengstresse ngstrain.html. [Accessed 5 July 2017].
- [84] S. Acharya, R. Gupta, J. Ghosh, S. Bysakh, K. Ghosh, D. Mondal and A. Mukhopadhyay, "High strain rate dynamic compressive behaviour of Al6061-T6 alloys," *Materials Characterization*, no. 127, pp. 185-197, 2017.

- [85] L. Ninan, J. Tsai and C. Sun, "Use of split Hopkinson pressure bar for testing off-axis composites," *International Journal of Impact Engineering*, no. 25, pp. 291-313, 2001.
- [86] W. Chen, F. Lu and B. Zhou, "A Quartz-crystal-embedded Split Hopkinson Pressure Bar for Soft Materials," *Experimental Mechanics*, vol. 40, no. 1, pp. 1-6, 2000.
- [87] D. Mohr, "Dynamic Behavior of Materials and Structures," 2015. [Online]. Available: <https://www.ethz.ch/content/dam/ethz/special-interest/mavt/virtual-manufacturing/ivp-dam/Studium/Vorlesungsunterlagen/Dynamic%20Behavior%20of%20Materials%20and%20Structures/Downloads/Lecture2/Lecture%202.pdf>. [Accessed 9 July 2017].
- [88] Y. Lu and K. Xu, "Modelling of dynamic behavior of concrete materials under blast loading," *Int. Journal of Solids and Structures*, no. 41, pp. 131-143, 2003.
- [89] W. Chen, B. Zhang and J. Forrestal, "A Split Hopkinson Bar Technique for Low-impedance Materials," *Experimental Mechanics*, vol. 39, no. 2, pp. 81-85, 1999.
- [90] ASME, "Split-Hopkinson Pressure Bar Apparatus," 2017. [Online]. Available: <https://www.asme.org/about-asme/who-we-are/engineering-history/landmarks/242-split-hopkinson-pressure-bar-apparatus>. [Accessed 7 February 2017].
- [91] J. Weiss, "Stress-Strain Behavior of Concrete," The Concrete Portal, [Online]. Available: http://www.theconcreteportal.com/cons_rel.html. [Accessed 19 June 2017].
- [92] A. Manes, L. Peroni, M. Scapin and M. Giglio, "Analysis of strain rate behavior of an Al 6061 T6 alloy," *Procedia Engineering*, no. 10, p. 3477–3482, 2011.